

AD-A125-815

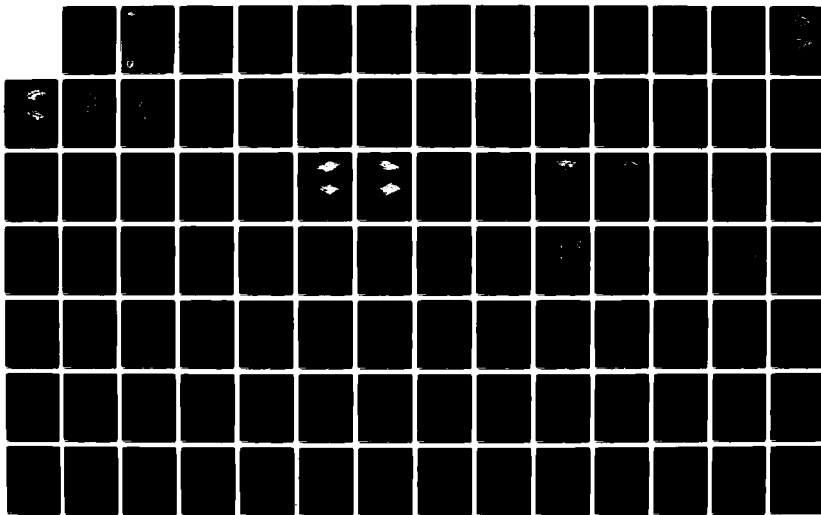
IMPROVED SIMULATIONS OF MESOSCALE METEOROLOGY(U)
SCIENCE APPLICATIONS INC LA JOLLA CA
P C PATNAIK ET AL. JAN 83 SAI-093-82-005LJ

1/2

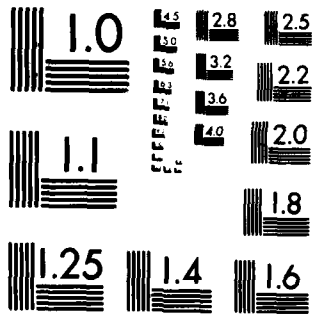
UNCLASSIFIED

ERADCOM/ASL-CR-83-0127-1 DAEA18-73-A-0127 F/G 4/2

NL



M-2



MICROCOPY RESOLUTION TEST CHART
NATIONAL BUREAU OF STANDARDS 1963-A

ADA 125815

12



CR-83-0127-1

AD

Reports Control Symbol
OSD - 1366

IMPROVED SIMULATIONS OF MESOSCALE METEOROLOGY

January 1983

By

**Purna C. Patnaik
Burton E. Freeman
Richard M. Traci
Gary T. Phillips**

**Science Applications, Inc.
1200 Prospect Street
PO Box 2351
La Jolla, California 92038**

DTC
A

DTC FILE COPY

**Under Contract: DAEA18-73-A-0127, Task 13
Contract Monitor: Ronald M. Cionco**

Approved for public release; distribution unlimited.



US Army Electronics Research and Development Command

Atmospheric Sciences Laboratory

White Sands Missile Range, NM 88002

83 03 18 003

NOTICES

Disclaimers

The findings in this report are not to be construed as an official Department of the Army position, unless so designated by other authorized documents.

The citation of trade names and names of manufacturers in this report is not to be construed as official Government indorsement or approval of commercial products or services referenced herein.

Disposition

Destroy this report when it is no longer needed. Do not return it to the originator.

REPORT DOCUMENTATION PAGE		READ INSTRUCTIONS BEFORE COMPLETING FORM
1. REPORT NUMBER ASL-CR-83-0127-1	2. GOVT ACCESSION NO. AD-A12-5815	3. RECIPIENT'S CATALOG NUMBER
4. TITLE (and Subtitle) IMPROVED SIMULATIONS OF MESOSCALE METEOROLOGY		5. TYPE OF REPORT & PERIOD COVERED Contractor Report
		6. PERFORMING ORG. REPORT NUMBER SAI-093-82-005LJ
7. AUTHOR(s) Purna C. Patnaik Richard M. Traci Burton E. Freeman Gary T. Phillips		8. CONTRACT OR GRANT NUMBER(s) DAEA18-73-A-0127
9. PERFORMING ORGANIZATION NAME AND ADDRESS Science Applications, Inc. 1200 Prospect Street, PO Box 2351 La Jolla, California 92038		10. PROGRAM ELEMENT, PROJECT, TASK AREA & WORK UNIT NUMBERS DA Task No. 1L161102B53A-A0
11. CONTROLLING OFFICE NAME AND ADDRESS US Army Electronics Research and Development Command Adelphi, MD 20783		12. REPORT DATE January 1983
		13. NUMBER OF PAGES 172
14. MONITORING AGENCY NAME & ADDRESS (if different from Controlling Office) US Army Atmospheric Sciences Laboratory White Sands Missile Range, NM 88002		15. SECURITY CLASS. (of this report) UNCLASSIFIED
		15a. DECLASSIFICATION/DOWNGRADING SCHEDULE
16. DISTRIBUTION STATEMENT (of this Report) Approved for public release; distribution unlimited.		
17. DISTRIBUTION STATEMENT (of the abstract entered in Block 20, if different from Report)		
18. SUPPLEMENTARY NOTES Contract Monitor: Ronald M. Cionco		
19. KEY WORDS (Continue on reverse side if necessary and identify by block number)		
Meteorology	Complex terrain	PASS data base
Mesoscale	Theoretical models	Computer codes
Simulations	Variational analysis	SIGMET
Mesoscale models	Linearized model	LINMET
Wind fields	Terrain following coordinates	YARMET
20. ABSTRACT (Continue on reverse side if necessary and identify by block number)		
<p>Research has been performed contributing to the improved description of mesoscale meteorology in regions of complex terrain. The investigation is primarily theoretical with the emphasis being placed on the development of several computer models that balance accuracy against economy of use.</p> <p>A major goal of this program is the selection and formulation of suitable simplified physics models. This has been done through</p>		

20. ABSTRACT (cont)

review of recent literature, discussion with mesoscale modeling experts, and a few analytic studies during the first phase of the study. On the basis of these studies, two different classes of models have been identified for development and implementation. A mass-consistent wind-field (or variational analysis) model has been formulated that employs a terrain conformal coordinate system. The technique relies heavily on observational data and is most suited to a data rich region. A computer program, VARMET, has been written, tests of the method have been performed, and several comparisons with field data were carried out. Very satisfactory model performance was found in these comparisons. The second class of model developed adheres more closely to first principles and thereby is applicable to data-poor regions. Based on the linearized steady-state Navier-Stokes equation, model LINMET is written, and the model performance is tested against field data. In addition, the primitive equation hydrostatic code SIGMET, which was developed at SAI for application to a number of meteorological programs, has been adapted to the present program. Enriched with sophisticated model physics, SIGMET simulations form the baseline case for two other simplified physics models.

With cooperation of personnel at the US Army Atmospheric Sciences Laboratory on White Sands Missile Range (WSMR), New Mexico, data were obtained from a comprehensive field observational program, PASS, which was carried out at WSMR in late 1974. These data, together with supporting terrain height and synoptic weather data, have been analyzed and interpolated for comparison with corresponding calculations. A second source of comparison data is the output of calculations that take into account more physical phenomena and which, hopefully, are in substantial agreement with field data. Limited meteorological and terrain data from Fulda, West Germany, were also obtained through WSMR and are used in a few simulations.

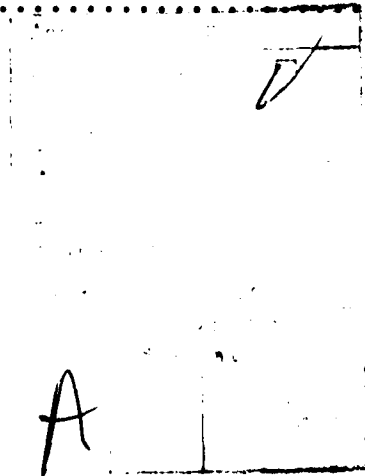
ACKNOWLEDGMENT

This report was prepared for the US Army Atmospheric Sciences Laboratory, White Sands Missile Range, New Mexico, under Contract No. DAEA18-73-A-0127/0013 during the period March 1977-December 1978. The study was carried out in two phases, and the accomplishments were published in two reports, SAI-77-915LJ and SAI-78-948LJ. These two reports are consolidated here to produce this single ERADCOM report.

Science Applications, Inc. (SAI) is pleased to acknowledge the assistance and cooperation of Messrs. William Ohmstede and Ronald Cionco of the US Army Atmospheric Sciences Laboratory, without whose help this study would not have materialized.

CONTENTS

1. INTRODUCTION..... 1
 1.1 ROLE OF SIGMET IN MESOSCALE MODELING..... 2
 1.2 SIMPLE PRESCRIPTIONS FOR OROGRAPHICALLY
 INDUCED FLOWS..... 3
2. DATA ACQUISITION AND REDUCTION..... 5
 2.1 PASS DATA OVER WHITE SANDS REGION..... 5
 2.2 WEST GERMAN DATA..... 17
3. PRIMITIVE EQUATION MODEL SIGMET..... 34
 3.1 SIGMET FORMULATION..... 35
 3.2 SIGMET SIMULATIONS..... 41
4. LINEAR MODEL LINMET..... 50
 4.1 LINMET FORMULATION..... 51
 4.2 LINMET SIMULATIONS..... 63
5. OBJECTIVE ANALYSIS MODEL VARMET..... 75
 5.1 VARMET FORMULATIONS..... 75
 5.2 VARMET SIMULATIONS..... 81
6. SUMMARY AND CONCLUSION..... 96
REFERENCES..... 98
APPENDIX A - SIGMET ORGANIZATION..... A-1
APPENDIX B - LINMET ORGANIZATION..... B-1
APPENDIX C - VARMET ORGANIZATION..... C-1



1. INTRODUCTION

Meteorological forecasting of mesoscale modifications of synoptic weather regimes is still far from operational status. However, within this domain (by "mesoscale" we refer to distance scales of 20.-200. km) takes place most of human activities. The weather that people experience is affected by their specific location: within reach of the land-sea breeze, sheltered or exposed by terrain, subject to katabatic winds, etc. Consequently, the ability to perform accurate simulations on this distance scale would be highly beneficial to many activities that are affected by weather. These include the dispersion of pollutants, transportation, siting of facilities, and the modification of weather through the inadvertent or purposeful intervention of man. Military operations are affected by most of these weather-dependent processes also. In addition are the effects of winds on the dispersion of fallout and CB agents, and on the ballistics of projectiles. Finally, military installations in day-to-day operations are dealing with the many pollution and energy conservation problems that are specific to each site. Mesoscale weather affects these through pollutant dispersion, climatological factors in heating or cooling of buildings, and evaluation of renewable energy sources such as wind and sun.

As the applications discussed above indicate, many (perhaps most) of the uses of the mesoscale simulation involve regions of complex terrain. While there is a substantial history of mesoscale modeling research, this topic has been neglected until recently. However, recently there have been several investigations in these fields. Aided by the growth in computer capability, mesoscale models are now approaching the prototype application stage.

To make further progress toward usable simulation tools, it is now necessary to consider several problems affecting the accuracy and economy of mesoscale computer models. This is being done under Contract DAEA18-73-A-0127/0013 entitled "Improved Simulations of Mesoscale Meteorology," the first phase of which was performed during the period March-October 1977, and the second phase was performed during March-December 1978.

The research program has the objective of advancing the technology of performing accurate and verified mesoscale calculations at a reasonable cost in computer usage. To do so, we have reviewed the recent literature extensively. As an advanced starting point, the SAI SIGMET primitive equation code has been used as the benchmark tool for mesoscale simulation. SIGMET is an advanced and sophisticated meteorological mesoscale code based on three-dimensional hydrostatic equations in primitive form. The mesoscale experiments performed by the Atmospheric Sciences Laboratory of WSMR constitute a valuable data base for the verification of model calculations. These data have been obtained and put to use. A search was made for simpler computer codes applicable to flow over complex terrain, which have greatly reduced computing requirements. Two such codes have been selected. One, requiring considerable local data for initialization, has been implemented and tested. The second formulation, using less data and having more physical content, is developed during the second phase.

1.1 ROLE OF SIGMET IN MESOSCALE MODELING

The SIGMET code will be used in two major capacities. First, the code will be applied to mesoscale flow over complex terrain. Calculations will be compared with field data to indicate how accurately these simulations can be made. Second, the SIGMET code will be compared with simplified physics code in an effort to reduce the expense of mesoscale simulations. The comparisons will permit trade-offs to be made between computing speed and simulation accuracy. The comparisons will also provide

data for the "tuning" of the simpler codes through the adjustment of parameters.

1.2 SIMPLE PRESCRIPTIONS FOR OROGRAPHICALLY INDUCED FLOWS

The presence of terrain in a region of meteorological interest may have large and complicated effects on the local wind field. The regional meteorological forecaster is presented with the problem of inferring the effects of the terrain from a limited number of observations in the vicinity, from synoptic data, and from previous experience in the region. In the case of military operations, the amount of information and experience may be markedly less.

For almost every region of interest, however, in contrast to the sparseness of meteorological data, there are data on terrain height in great detail. These available data are the basic ingredient in improving the objective analysis of the meteorological observations over complex terrain. The location of mountains near an observation site should be taken into account when those data are used, and perhaps more importantly, mountains between observation points should be permitted to influence the estimated wind field in their vicinity.

As we shall consider in the following discussion, several reduced-physics models of wind perturbations by mountains have been developed. If these simple models are able to provide sufficiently accurate representations of the perturbation to the wind field attributable to the complex terrain, a correction or constraint can be imposed on the analysis of the observational data.

In the following report, we describe in some detail the work that has been performed under the contract. Data obtained from the Atmospheric Sciences Laboratory of WSMR have been processed for use in comparisons and for calibration; this work is reported in Section 2. The primitive equation code, SIGMET, was adapted to the investigation and calculations were performed with

it as described in Section 3. In Section 4, a new 3-D linear non-hydrostatic model is described, and some simulation results using the new code, LINMET, are presented. In Section 5, we report on a simplified physics model of flow over complex terrain. The characteristics of the simplified physics computer code, VARMET, derived from this study, are reported in this section together with extensive simulations using this model over the White Sands region. Section 6, summarizes the findings of the study along with some future work. Documentations on the codes SIGMET, VARMET and LINMET, providing details on code organization, subroutine description, input requirement, and sample setups are given in Appendix A, B, and C, respectively.

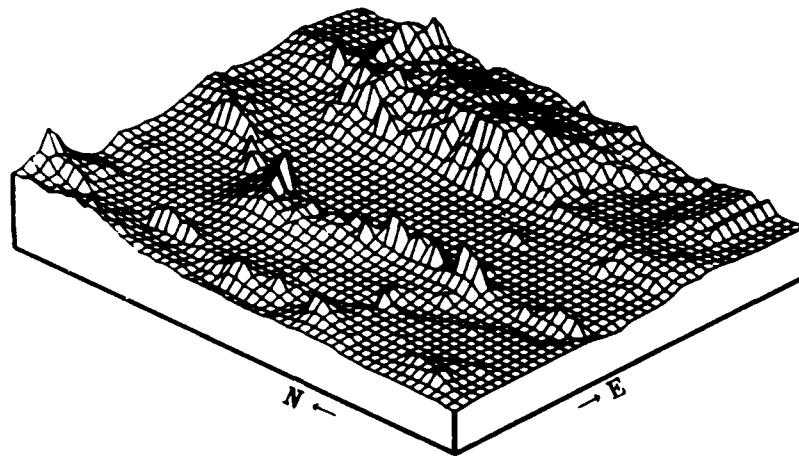
2. DATA ACQUISITION AND REDUCTION

A major task of the program is to validate the computer models using available field data and to simulate the detailed wind field using limited field data. Both the validation and the simulation work require intensive field data having assured quality. The Atmospheric Science Laboratory at White Sands Missile Range has provided us such data, which are the result of the PASS experiment conducted during November-December 1974. During this intensive measurement program, rawinsonde data were gathered at nine different ground stations in the region of White Sands Missile Range over a period of 20 days. The reduced data were made available in a readily usable form through magnetic tape. In addition, terrain data were provided for the region on a 41 x 51 grid of points with 5 km grid interval.

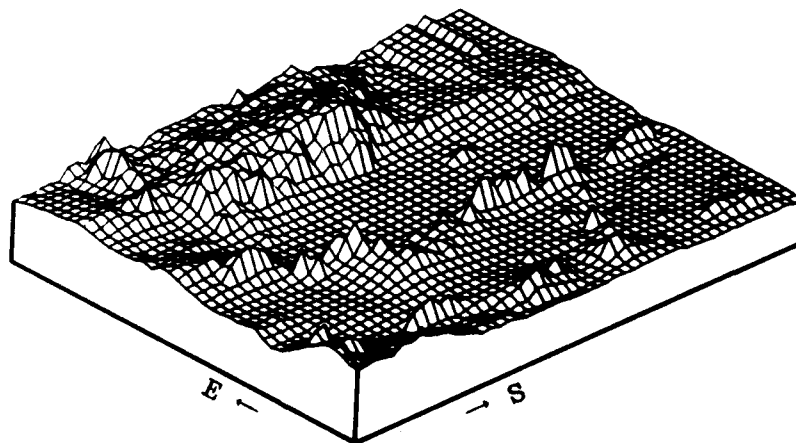
2.1 PASS DATA OVER WHITE SANDS REGION

Figures 2.1(a) to (d) show the four prospective views of the WSMR region using the terrain data. Figure 2.2 shows the contour plot of the same. The graphs display the Tularosa Valley in the center with the San Andres Mountains in the west and the Sacramento Mountains in the east, both running approximately north-south. These two mountain ranges have peaks up to 2600 m in height with the valley floor averaging about 1200 m above sea level. Figure 2.3 shows the ground locations of the nine measuring stations, and Table 2.1 shows the UTM coordinates and station elevation (MSL) for all the stations. The meteorological data include the pressure, temperature, moisture, magnitude of the horizontal velocity components, and the location of the drifting balloon with respect to the release point. Table 2.2 shows these values for a typical station TSX taken at/after 0515 MST on 19 November 1974.

These data have been suitably interpolated both vertically and horizontally to the grid points used by the finite difference

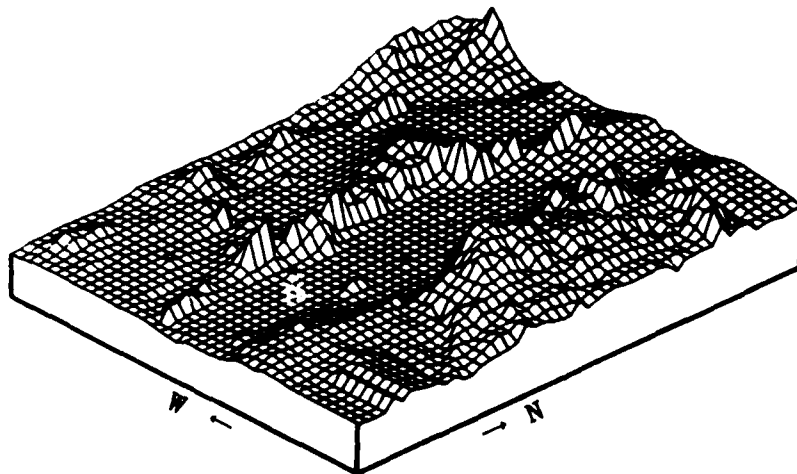


(a)

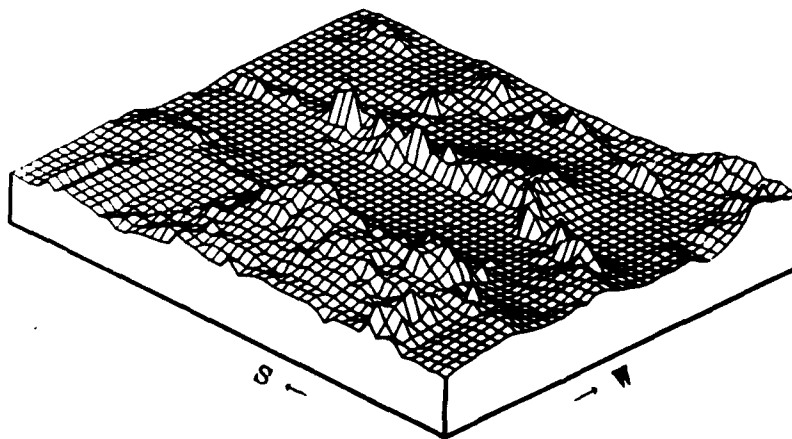


(b)

Figure 2.1 Prospective Views of the Terrain in the White Sands Missile Range Region. The South-West Corner has the UTM Coordinates (280 km, 3510 km).



(c)



(d)

Figure 2.1
(cont'd.)

Prospective Views of the Terrain in the White Sands Missile Range Region. The South-West Corner has the UTM Coordinates (280 km, 3510 km).



Figure 2.2 Contour Plot of White Sands Terrain
on a 41x51 Grid of Points and 5 km
Grid Interval.

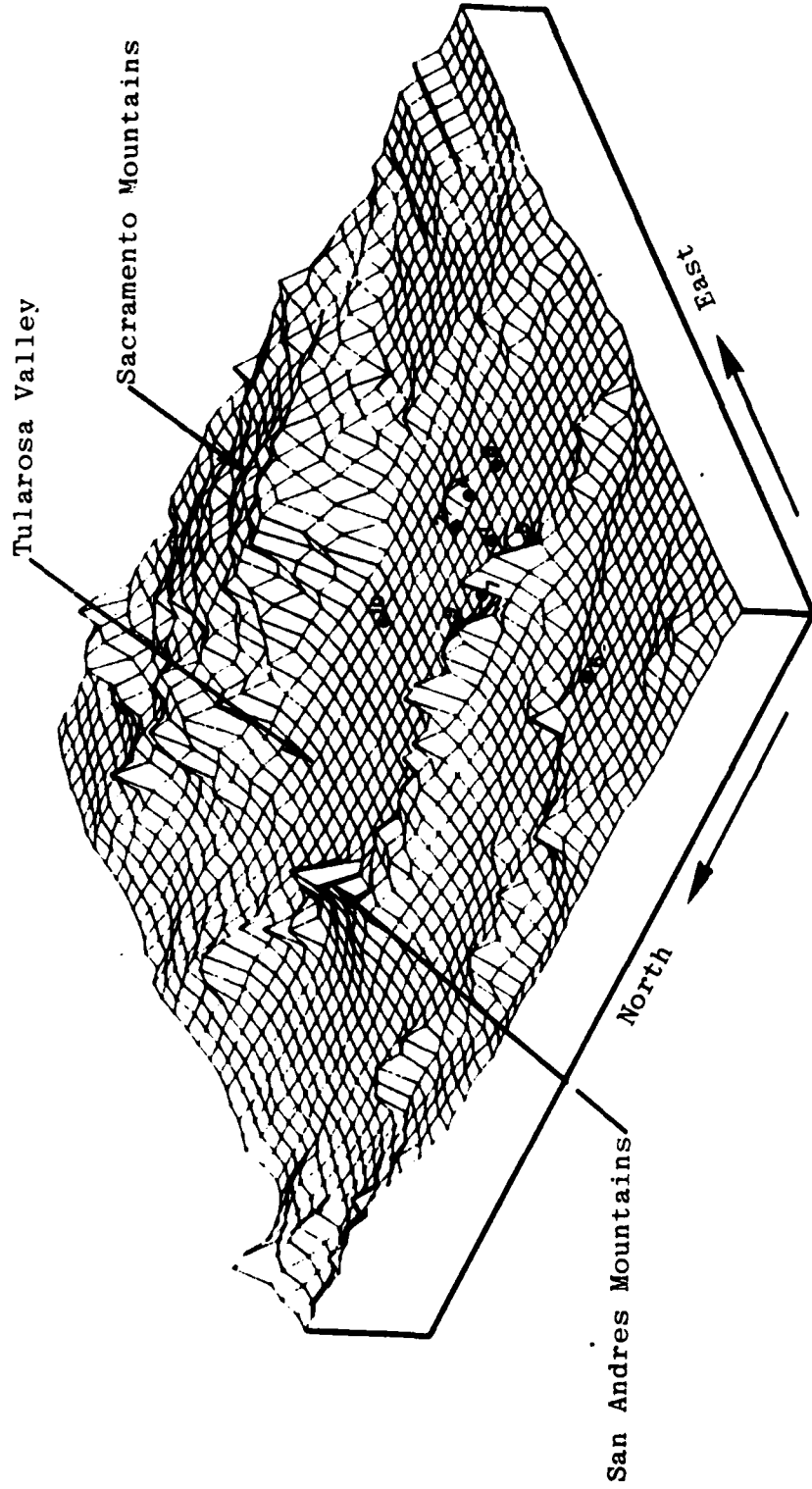


Figure 2.3 Data Gathering Stations During PASS Experiment in White Sands Region.
(For names and exact location, see Table 2.1.)

Table 2.1
 Locations of Rawinsonde Stations Participating
 in PASS Experiment.

Station Index	Station Name	UTM x-coord (km)	UTM y-coord (km)	Elevation MSL (m)
1	TSX	375.57	3586.84	1232.0
2	ORO	392.11	3586.57	1274.0
4	MCG	387.76	3571.64	1247.0
5	WAR	366.96	3572.82	1216.0
6	LSC	319.80	3572.70	1347.0
7	SMR	366.36	3594.73	1218.0
8	RAM	390.66	3597.13	1230.0
9	APA	369.57	3610.63	1204.0
10	HMS	397.69	3635.88	1247.0

Table 2.2
 Rawinsonde Data Taken at Station TSX at 0515 on 11/19/74.

STATION=TSX	DATE=11/19/74	TIME= 515	UTMX= 373.57	UTMY= 3586.84	ZMSL= 1232.00		
P (MB)	Z (M)	X (M)	Y (M)	U (MPS)	V (MPS)	T (DC K)	Q
8.7620E+02	0.0000E+00	1.9300E+02	-2.4400E+02	4.1000E+00	0.0000E+00	2.8600E+02	6.1100E-03
8.5600E+02	2.5500E+02	5.6200E+02	-1.7500E+02	1.1430E+01	1.6600E+00	2.8510E+02	5.2100E-03
7.8900E+02	8.7200E+02	2.0490E+03	-6.6000E+01	1.7010E+01	2.3400E+00	2.8920E+02	4.5900E-03
7.4400E+02	1.3530E+03	3.4490E+03	6.6000E+01	1.6800E+01	-2.3000E-01	2.7770E+02	2.8900E-03
7.0000E+02	1.8460E+03	4.6340E+03	-8.4000E+01	1.3210E+01	-2.3600E+00	2.7400E+02	1.8400E-03
6.9100E+02	1.9490E+03	4.8470E+03	-1.2600E+02	1.3970E+01	-2.2200E+00	2.7400E+02	1.1100E-03
6.3900E+02	2.5750E+03	6.4450E+03	-4.9900E+02	1.7580E+01	-3.7200E+00	2.7190E+02	9.7400E-04
6.1100E+02	2.9300E+03	7.6510E+03	-6.5300E+02	1.9270E+01	-5.3000E-01	2.6930E+02	1.5900E-03
5.9000E+02	3.2060E+03	8.6280E+03	-5.4000E+02	2.0610E+01	-1.4000E+00	2.6910E+02	9.5200E-04
5.3600E+02	3.9580E+03	1.1010E+04	-8.4500E+02	1.9780E+01	-2.8100E+00	2.6630E+02	6.7700E-04
5.0000E+02	4.4960E+03	1.2581E+04	-1.0190E+03	1.8100E+01	-1.5400E+00	2.6210E+02	5.2200E-04
4.4200E+02	5.4260E+03	1.5508E+04	-1.4690E+03	1.7110E+01	-4.5700E+00	2.5360E+02	4.6200E-04
3.9000E+02	6.1580E+03	1.8434E+04	-2.9990E+03	1.5790E+01	-1.1470E+01	2.4720E+02	2.9800E-04
3.2800E+02	7.5670E+03	2.5361E+04	-6.5850E+03	2.1000E+01	-2.6900E+00	2.3800E+02	1.2800E-04
3.0000E+02	8.1810E+03	2.8216E+04	-6.4570E+03	1.8770E+01	3.2500E+00	2.3270E+02	0.0000E+00

model for initialization. We have made use of simple linear interpolation in the vertical and $1/r^2$ weighting in the horizontal (r is the radial distance from the point in question to the data location). Interpolation is done in the transformed vertical coordinate σ , which is defined by

$$\sigma(z) = \frac{z_T - z}{z_T - z_S}$$

where z_T is the constant elevation of the top surface of the model, and z_S is the elevation of the terrain. While such a transformation is appropriate for the simplified time-independent models, an alternate definition of σ is more suitable for the more sophisticated dynamic model:

$$\sigma(p) = \frac{p - p_T}{p_S - p_T}$$

Here, p_T is the constant pressure at the top of the model, and p_S is the surface pressure. In both definitions $0 \leq \sigma \leq 1$. Table 2.3 shows the same measurements as Table 2.2, but has two additional entries $\sigma(z)$ and $\sigma(p)$, with z_T chosen to be 6152 m and $p_T = 500$ mbar. Since the balloon drifts laterally while rising, the appropriate z_S or p_S , which are the terrain height and the surface pressure vertically below the balloon position, have to be interpolated. Since the lateral drift with respect to the release point is known, this interpolation is readily carried out.

The next step is to construct tables similar to Table 2.3 but containing values interpolated to the same σ - levels as used by the models. We use the following log-linear formula for generating σ in the models, which results in fine vertical resolution near the surface and coarse resolution away from the surface.

Table 2.3
 Rawinsonde Data Taken at Station TSX at 0515 on 11/19/74
 Including Calculated Values for $\sigma(z)$ and $\sigma(p)$

STATION=TSX	DATE=11/19/74	TIME= 515	UTRX= 375.57	UTRY= 3586.84	ZMSL= 1232.00				
P (MB)	Z (MB)	X (MB)	Y (MB)	U (MPS)	V (MPS)	T (DC K)	Q	SIGMA (Z)	SIGMA (P)
8.7620E+02	0.0000E+00	1.9300E+02	-2.4400E+02	4.1000E+00	0.0000E+00	2.8600E+02	6.1100E-03	1.0000E+00	1.0000E+00
8.5000E+02	2.5500E+02	5.0200E+02	-1.7500E+02	1.1430E+01	1.6600E+00	2.8510E+02	5.2100E-03	9.4661E-01	9.2830E-01
7.8900E+02	8.7200E+02	2.0490E+03	-6.6000E+01	1.7010E+01	2.3400E+00	2.8020E+02	4.5900E-03	0.2155E-01	7.6660E-01
7.4400E+02	1.3530E+03	3.4490E+03	6.6000E+01	1.6800E+01	-2.3000E-01	2.7770E+02	2.0900E-03	7.2400E-01	6.4730E-01
7.0000E+02	1.8460E+03	4.6340E+03	-3.4000E+01	1.3210E+01	-2.3600E+00	2.7400E+02	1.0400E-03	6.2409E-01	5.3001E-01
6.9100E+02	1.9490E+03	4.0470E+03	-1.2600E+02	1.3970E+01	-2.2200E+00	2.7400E+02	1.1100E-03	6.0323E-01	5.0699E-01
6.3900E+02	2.5750E+03	6.4450E+03	-4.9900E+02	1.7500E+01	-3.7200E+00	2.7190E+02	9.7400E-04	4.7645E-01	3.6929E-01
6.1100E+02	2.9300E+03	7.6510E+03	-6.5300E+02	1.9270E+01	-5.3000E-01	2.6930E+02	1.5900E-03	4.0450E-01	2.9507E-01
5.9000E+02	3.2060E+03	8.6250E+03	-5.4000E+02	2.0610E+01	-1.4000E+00	2.6910E+02	9.5200E-04	3.4047E-01	2.3931E-01
5.3600E+02	3.9580E+03	1.1010E+04	-3.4500E+02	1.9780E+01	-2.8100E+00	2.6630E+02	6.7700E-04	1.9585E-01	9.5095E-02
5.0000E+02	4.4960E+03	1.2531E+04	-1.0190E+03	1.8100E+01	-1.5400E+00	2.6210E+02	5.2200E-04	0.6416E-02	0.0000E+00
4.4200E+02	5.4260E+03	1.5500E+04	-1.4690E+03	1.7110E+01	-4.5700E+00	2.5560E+02	4.0200E-04	-1.0367E-01	-1.5529E-01
4.0000E+02	6.1580E+03	1.8434E+04	-2.9990E+03	1.5790E+01	-1.1470E+01	2.4720E+02	2.9800E-04	-2.5543E-01	-2.7128E-01
3.2800E+02	7.5670E+03	2.5361E+04	-6.5850E+03	2.1090E+01	-2.6900E+00	2.3800E+02	1.2000E-04	-5.4045E-01	-4.6600E-01
3.0000E+02	8.1010E+03	2.8216E+04	-6.4370E+03	1.8770E+01	3.2500E+00	2.3270E+02	0.0000E+00	-6.6706E-01	-5.3027E-01

$$\xi = (1-\sigma) + a_2 \ln(1-\sigma+a_1)$$

Here, values for σ are calculated corresponding to equal increments in ξ . The constant a_1 controls the first increment in σ near the surface, and a_2 controls the log domain. If there are N grid intervals ($N+1$ grids) in the vertical, then the increment in ξ will be

$$\Delta\xi = \frac{\xi(0)-\xi(1)}{N} = \frac{1+a_2 \ln[(1+a_1)/a_1]}{N}$$

Tables 2.4 and 2.5 show the same data as Table 2.1 but interpolated to the σ levels used by the models. Table 2.4 is to be used by the objective model and Table 2.5 by the predictive model. In these tables, 15 vertical levels are generated, and a_1 , a_2 are set at 0.01 and 0.20, respectively.

The last step in the procedure is to make a horizontal interpolation in σ -surfaces to initialize the values at the grid points. This is done by utilizing the $1/r^2$ weighting formula, which assigns maximum relative weight to the data nearest to the grid point and diminishing weights to the ones farther away. In order to initialize the meteorological variable v at grid point $(x_{ijk}, y_{ijk}, \sigma_k)$ using data from m stations, we therefore use

$$v_{ijk} = \frac{\sum_{n=1}^m v_{nk}/r_{ijk,nk}^2}{\sum_{n=1}^m 1/r_{ijk,nk}^2}$$

where $r_{ijk,nk}$ is the radial distance between the grid point and data point in the same σ -level. This is readily done since the UTM coordinates of the ground stations, coordinates of the data points with respect to the ground stations, and the coordinates of the computing mesh with respect to the stations are all known.

Table 2.4
 Rawinsonde Data Interpolated at Specific $\sigma(z)$ Levels to be Used by
 the Objective Analysis Models.

SICHA (Z)	STATION=TSX	DATE=11/19/74	TIME= 515	UTWX= 375.57	UTMY= 3586.84	ZMSL= 1232.00
			U (MPS)	V (MPS)		
9.9589E-01	2.1679E+02	-2.3869E+02	4.6643E+00	1.2779E-01		
9.8477E-01	2.8116E+02	-2.2431E+02	6.1914E+00	4.7363E-01		
9.6652E-01	3.8677E+02	-2.6073E+02	8.6965E+00	1.0410E+00		
9.3867E-01	6.0030E+02	-1.6807E+02	1.1785E+01	1.7032E+00		
8.9943E-01	1.0856E+03	-1.3388E+02	1.3535E+01	1.9165E+00		
8.4833E-01	1.7177E+03	-8.9340E+01	1.5315E+01	2.1944E+00		
7.8611E-01	2.5577E+03	-1.0040E+01	1.6934E+01	1.4063E+00		
7.1422E-01	3.5650E+03	5.1313E+01	1.6448E+01	-4.3856E-01		
6.3429E-01	4.5130E+03	-6.8683E+01	1.3577E+01	-2.1423E+00		
5.4782E-01	5.5454E+03	-2.8903E+02	1.5548E+01	-2.8756E+00		
4.5605E-01	6.7869E+03	-5.4266E+02	1.8059E+01	-2.8157E+00		
3.5999E-01	8.4271E+03	-5.6323E+02	2.0335E+01	-1.2211E+00		
2.6041E-01	1.0002E+04	-7.1598E+02	2.0131E+01	-2.2136E+00		
1.5792E-01	1.1554E+04	-9.0530E+02	1.9198E+01	-2.3699E+00		
5.3011E-02	1.3095E+04	-1.0981E+03	1.7926E+01	-2.0723E+00		

Table 2.5
 Rawinsonde Data Interpolated at Specific $\sigma(p)$ Levels to be Used by
 the Primitive Equation Models.

SIGMA (Z)	X (M)	Y (M)	U (MPS)	V (MPS)	W (MPS)	T (TC K)	Q
9.9589E-01	2.1671E+02	-2.4604E+02	4.5262E+00	9.5152E-02	2.8595E+02	6.0584E-03	
9.8477E-01	2.5865E+02	-2.2934E+02	5.6573E+00	3.5267E-01	2.8581E+02	5.9188E-03	
9.6652E-01	3.3728E+02	-2.1178E+02	7.5236E+00	7.7611E-01	2.8558E+02	5.6798E-03	
9.3867E-01	4.3733E+02	-1.8497E+02	1.0370E+01	1.4200E+00	2.8523E+02	5.3401E-03	
8.9943E-01	7.7835E+02	-1.5553E+02	1.2427E+01	1.7815E+00	2.8422E+02	5.0992E-03	
8.4833E-01	1.2675E+03	-1.2107E+02	1.4191E+01	1.9965E+00	2.8268E+02	4.9032E-03	
7.8611E-01	1.6631E+03	-7.9101E+01	1.6339E+01	2.2583E+00	2.8079E+02	4.6645E-03	
7.1422E-01	2.6647E+03	-7.9489E+00	1.6918E+01	1.2090E+00	2.7910E+02	3.8424E-03	
6.3429E-01	3.5821E+03	4.9151E+01	1.6397E+01	-4.6926E-01	2.7758E+02	2.7721E-03	
5.4782E-01	4.4611E+03	-6.2117E+01	1.3734E+01	-2.0493E+00	2.7454E+02	1.9032E-03	
4.5605E-01	5.4381E+03	-2.6397E+02	1.5305E+01	-2.7748E+00	2.7322E+02	1.0598E-03	
3.5999E-01	6.5961E+03	-5.1830E+02	1.7792E+01	-3.3202E+00	2.7157E+02	1.0512E-03	
2.6041E-01	8.2583E+03	-5.8276E+02	2.0103E+01	-1.0708E+00	2.6918E+02	1.1934E-03	
1.5792E-01	9.9798E+03	-7.1309E+02	2.0139E+01	-2.2002E+00	2.6751E+02	7.9594E-04	
5.3011E-02	1.1713E+04	-9.2281E+02	1.9029E+01	-2.2421E+00	2.6442E+02	6.0768E-04	

STATION=TSX DATE=11/19/74 TIME= 515 UTMX= 375.57 UTMY= 3586.84 ZMSL= 1232.00

It should be mentioned that there is a time-lag between the measurements at different levels, which is inherent in rawinsonde type of observations. This lag is about 10 to 15 min between the ground measurements and measurements at 500 mbar. Moreover, during the experiment the data were gathered at the nine stations in two passes: four stations participating in one pass and the remaining five participating in the second pass, a half-hour later. Therefore, there is an additional 30 min time-lag when one considers the whole data set. In the model initialization, we have ignored these time-lags and considered the entire data as representative of an average state during a 1-hour period.

Figure 2.4 through 2.11 show the velocity and temperature profiles chosen from the PASS experiment data for the simulations over the White Sands region. These data correspond to stations TSX, ORO, WAR, AND SMR taken at 0515, and stations LSC, RAM, APA, and HMS taken at 0545 on 19 November 1974. This day was chosen from the 20 days for which measurements are available, because the NWS weather record at El Paso, Texas, showed that the day was characterized by high wind, very little cloud cover, and near neutral lapse rate.

2.2 WEST GERMAN DATA

During Phase II, additional data were made available by ASL. These included terrain data over a region of West Germany in Hessen State (bordering East Germany), and upper air data from Meiningen, East Germany (east of the above region). The terrain data are on a 55 x 40 grid with 1 km grid interval with the southwest corner at (516.2 km, 5584.3 km) UTM coordinate with respect to 9° East Meridian. Figures 2.12(a) to (d) show the four perspective views of this region. Figure 2.13 shows the contour plot of the terrain data. The graphs display the mountainous and hilly terrain around Fulda in the state of Hessen, which is typical of the Central Upland District of West Germany.

STATION = TSX TIME = 515 DATE = 11-19-74

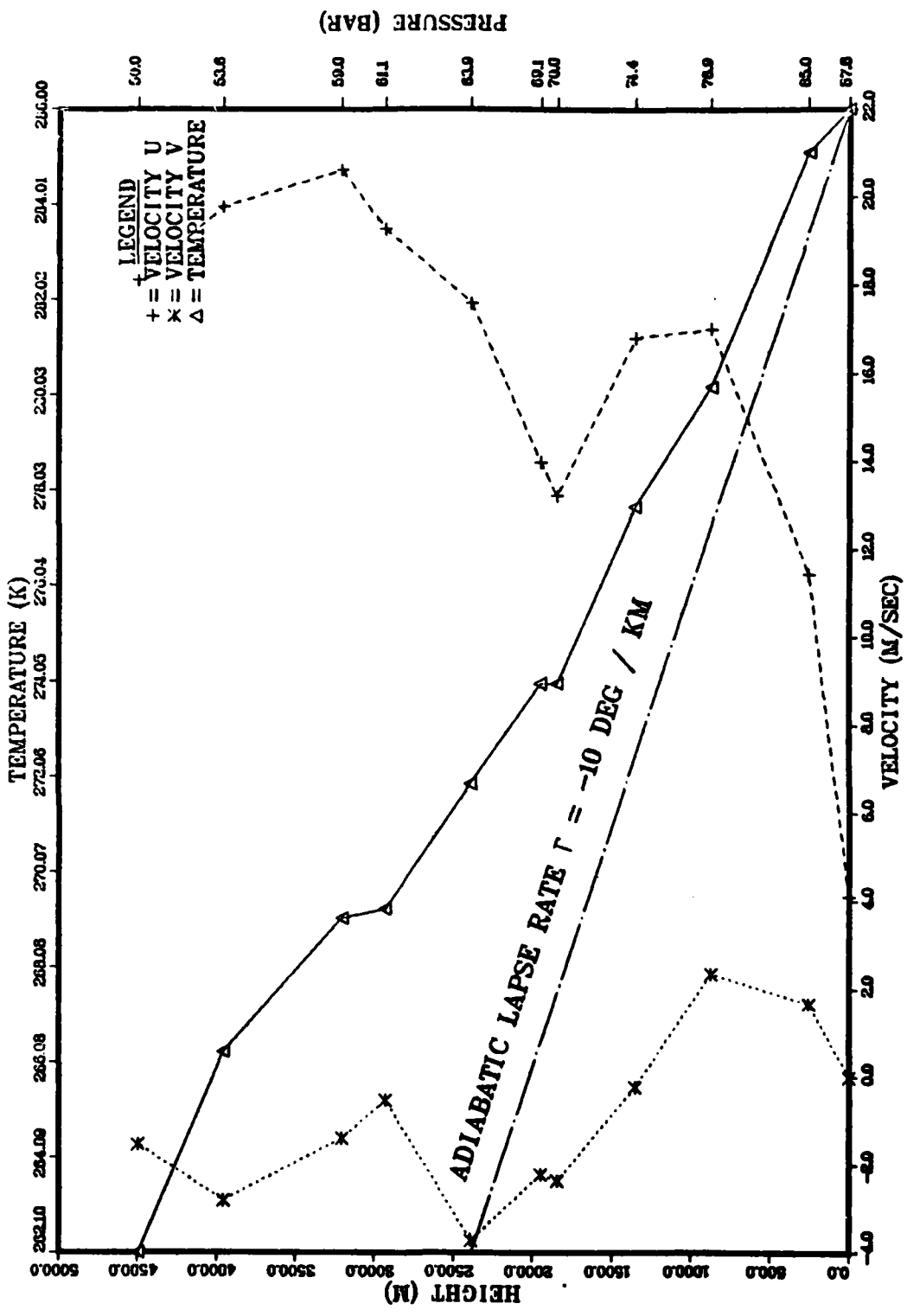


Figure 2.4 WSMR PASS Experiment Upper Air Measurements, 11/19/74, Station TSX.

STATION = ORO TIME = 515 DATE = 11-19-74

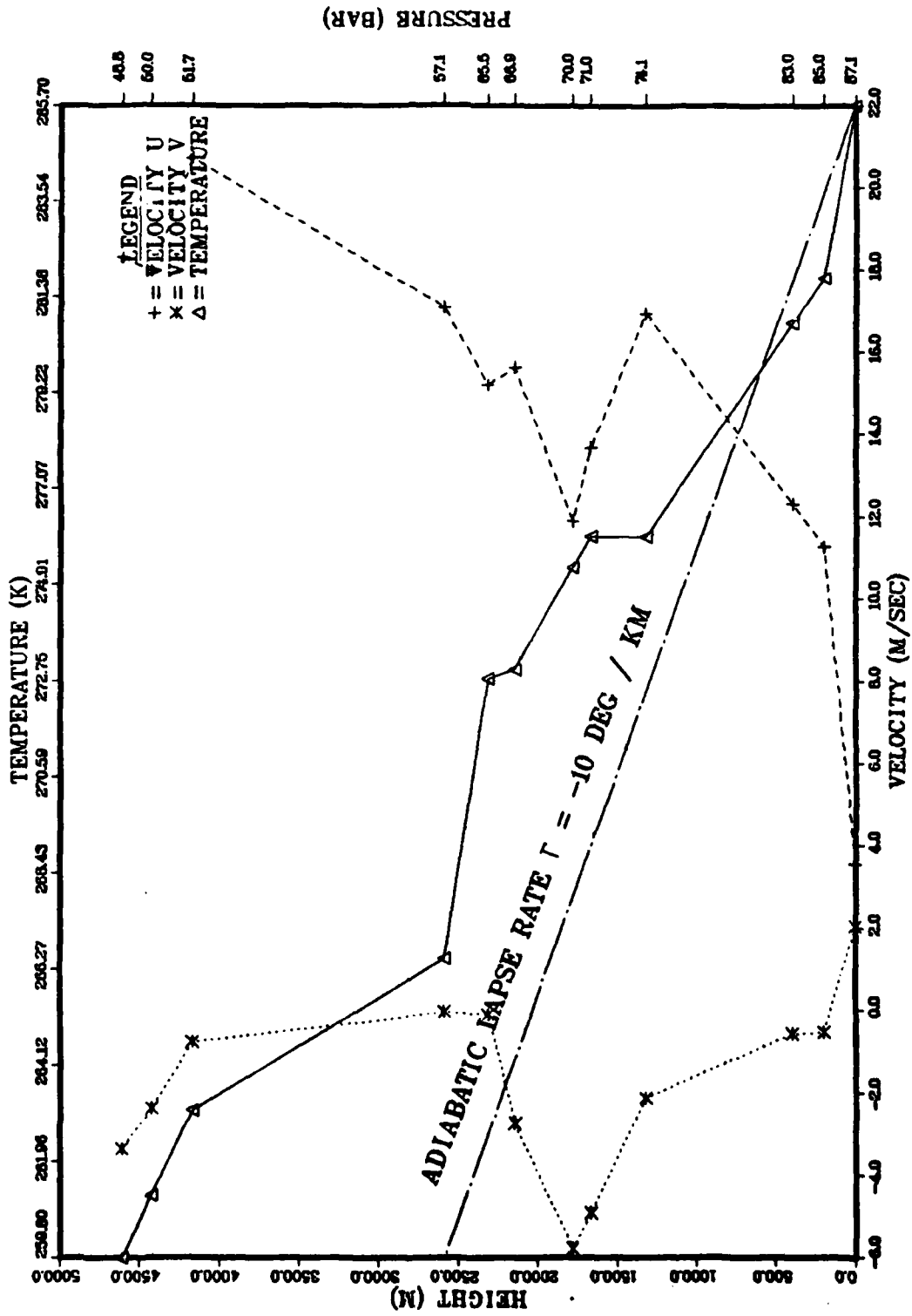


Figure 2.5 WSMR PASS Experiment Upper Air Measurements, 11/19/74, Station ORO.

STATION = WAR TIME = 515 DATE = 11-19-74

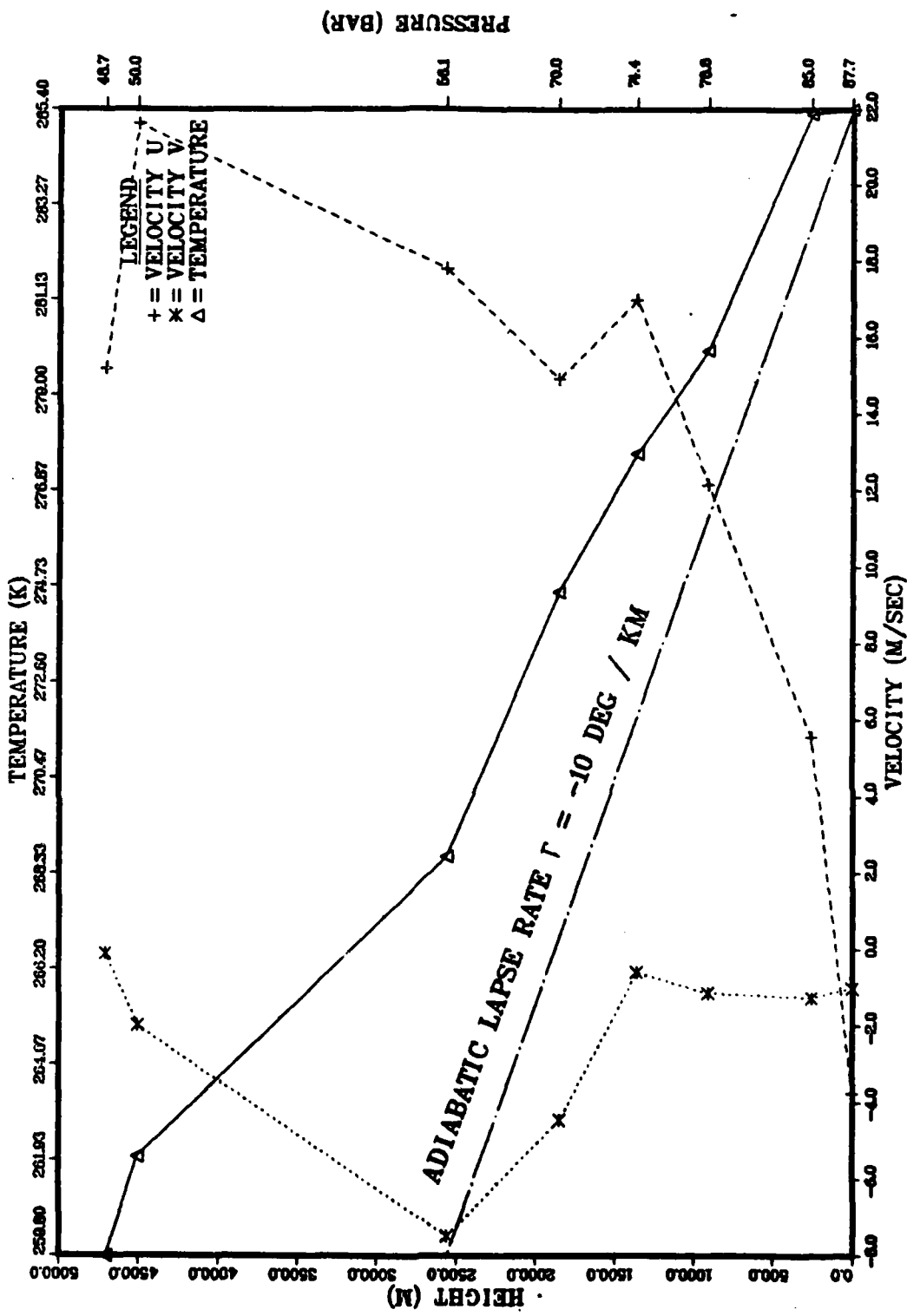


Figure 2.6 WSMR PASS Experiment Upper Air Measurements, 11/19/74, Station WAR.

STATION = SMR TIME = 515 DATE = 11-19-74

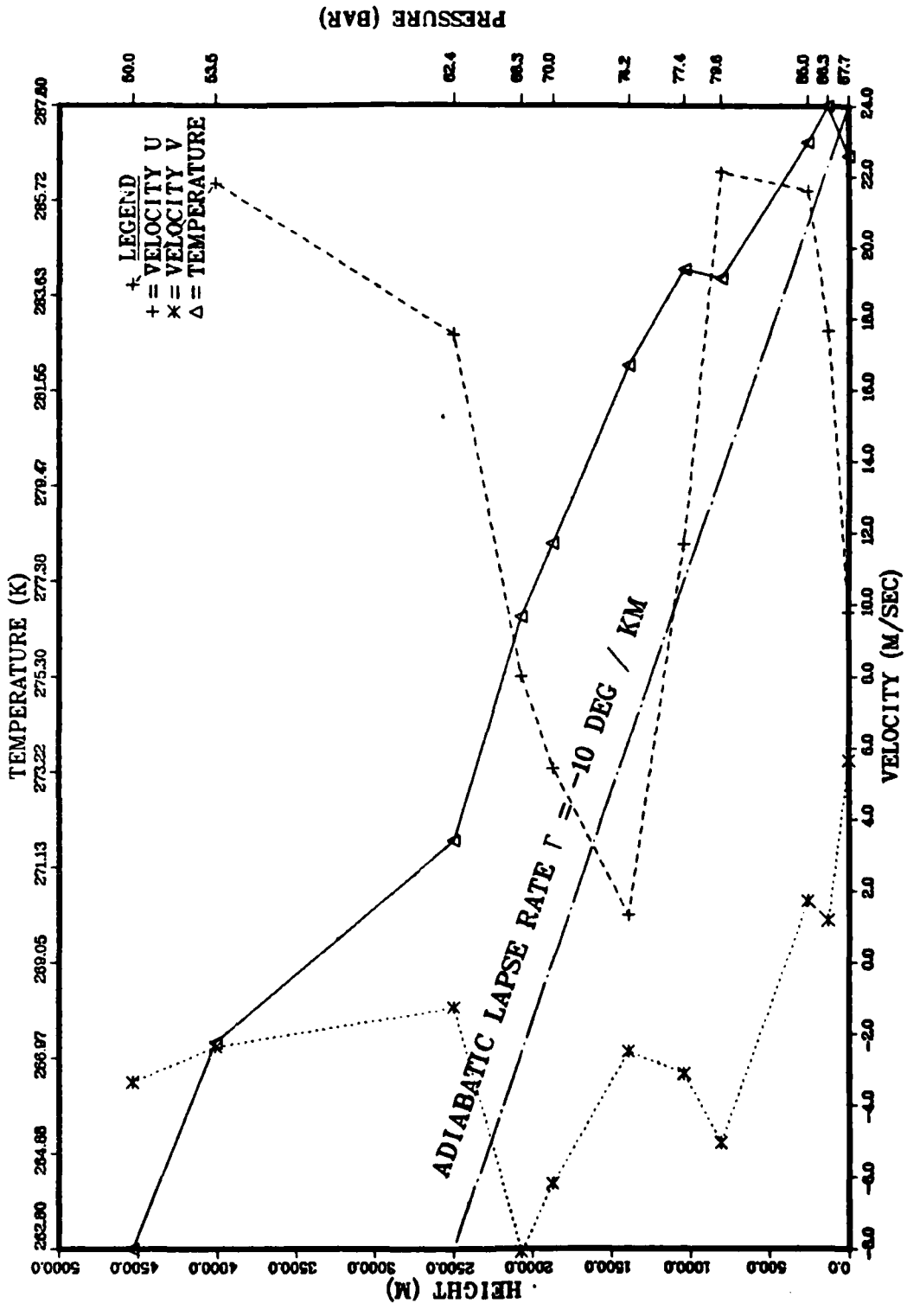


Figure 2.7 WSMR PASS Experiment Upper Air Measurements, 11/19/74, Station SMR.

STATION = LSC TIME = 545 DATE = 11-19-74

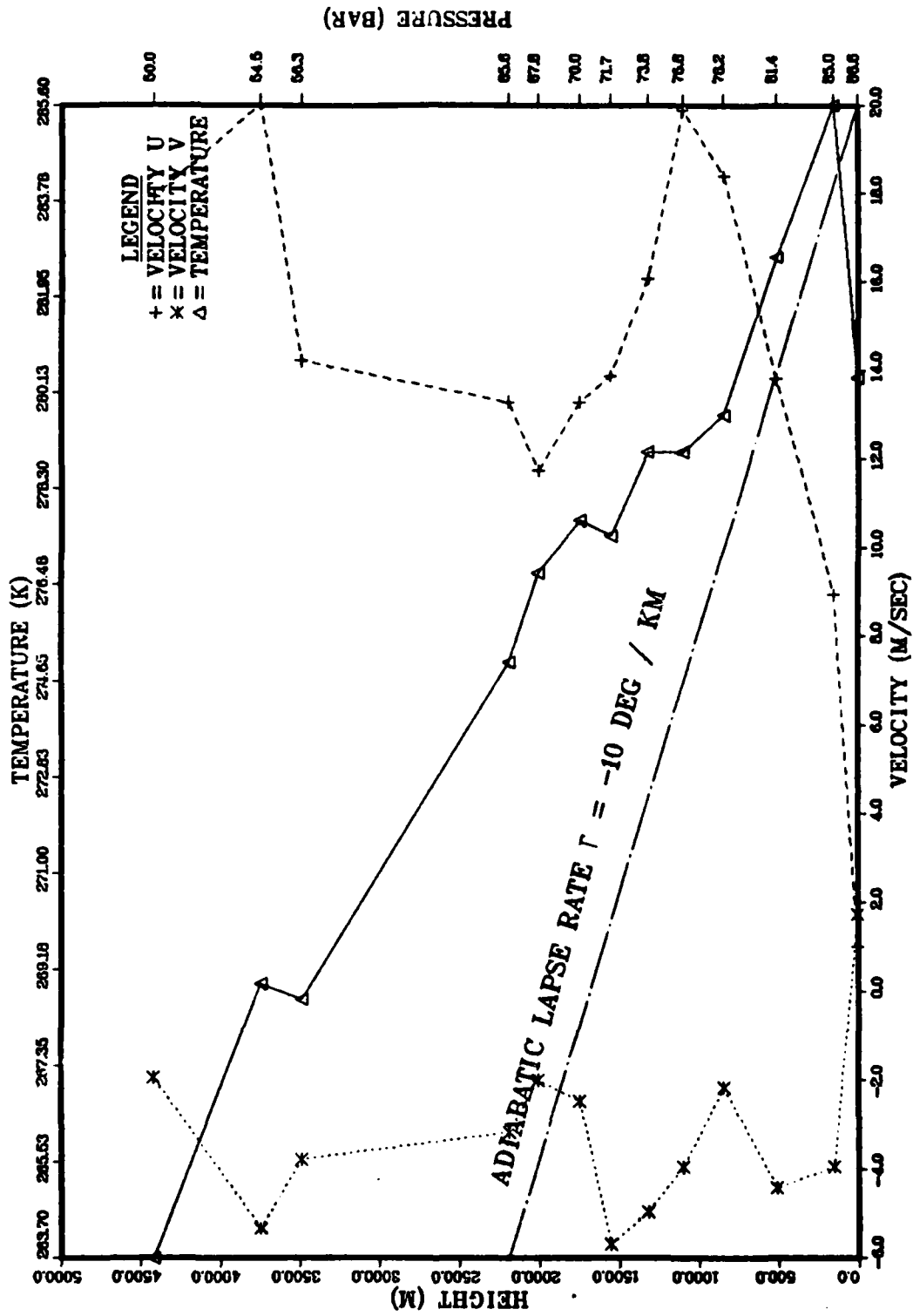


Figure 2.8 WSMR PASS Experiment Upper Air Measurements, 11/19/74, Station LSC.

STATION = RAM TIME = 545 DATE = 11-19-'74

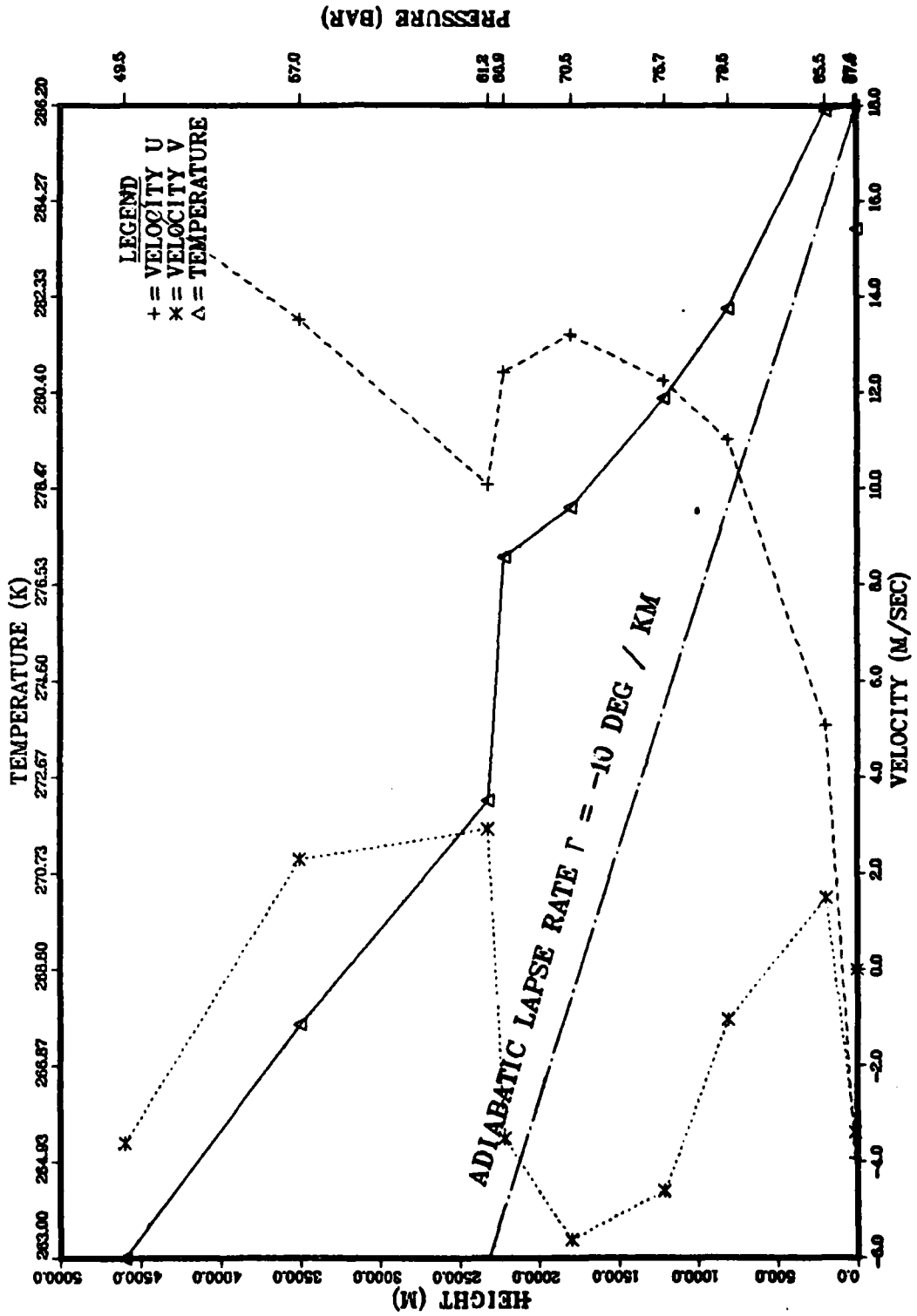


Figure 2.9 WSMR PASS Experiment Upper Air Measurements, 11/19/74, Station RAM.

STATION = APA TIME = 545 DATE = 11-19-74

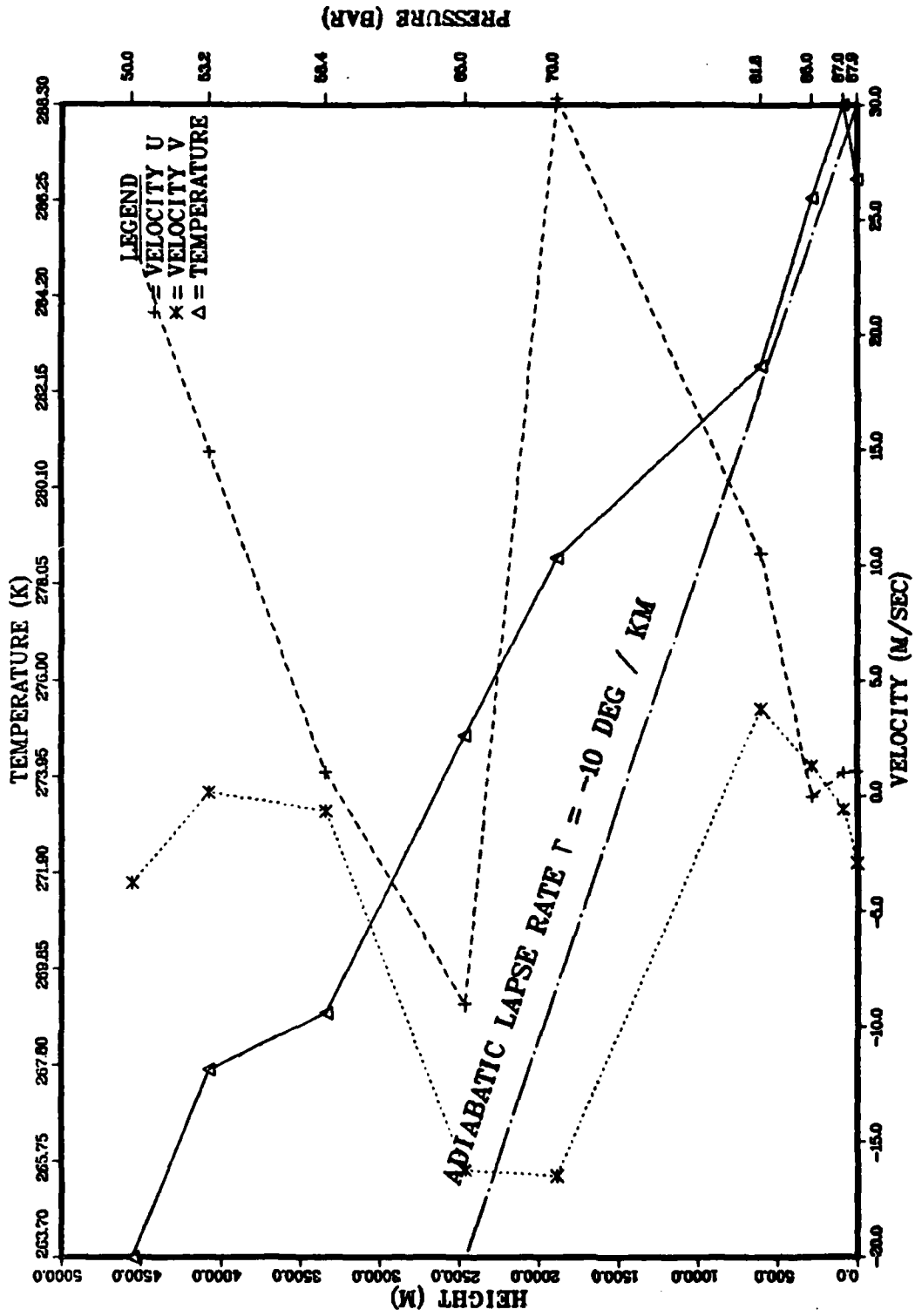


Figure 2.10 WSMR PASS Experiment Upper Air Measurements, 11/19/74, Station APA.

STATION = HMS TIME = 545 DATE = 11-19-74

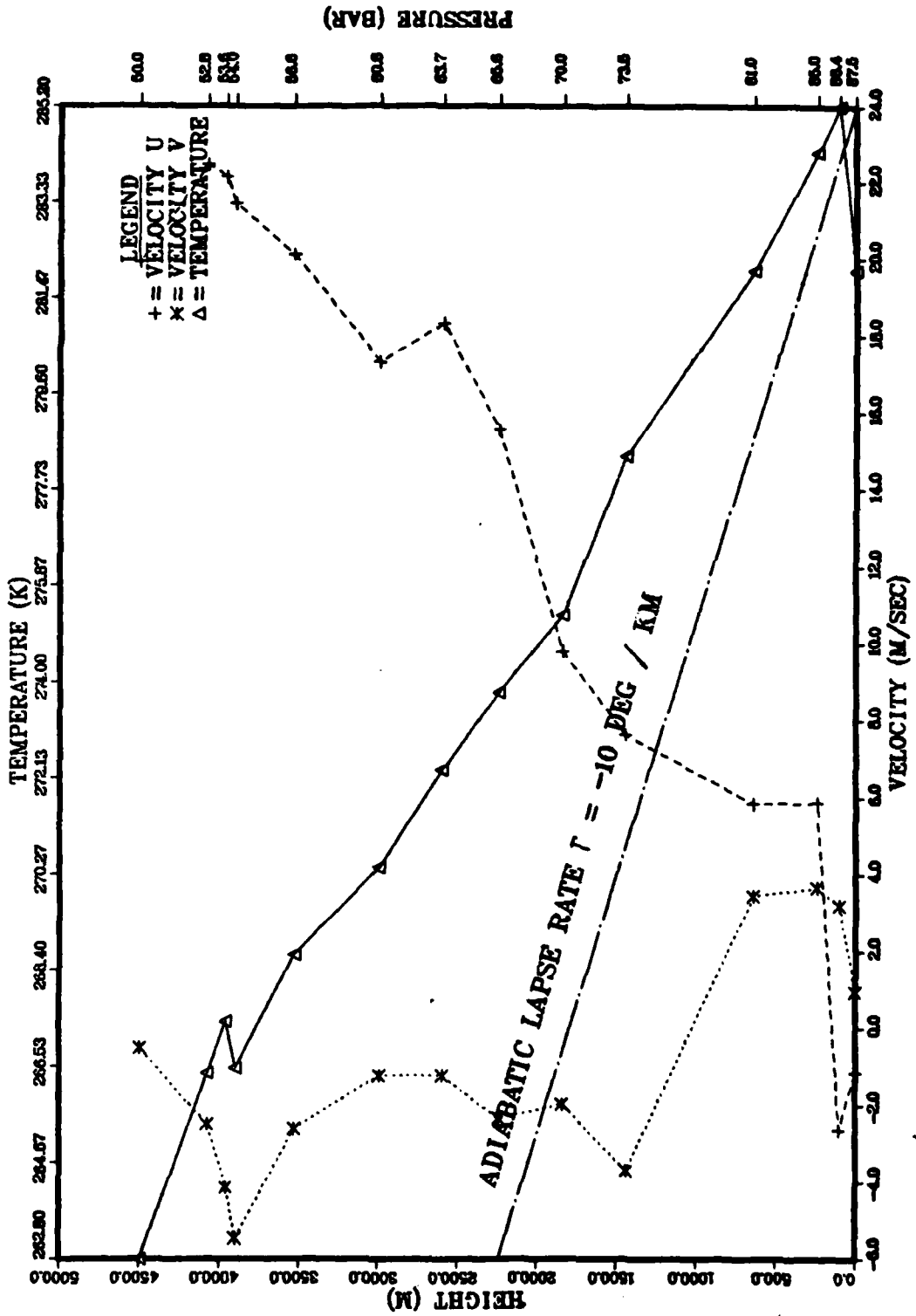
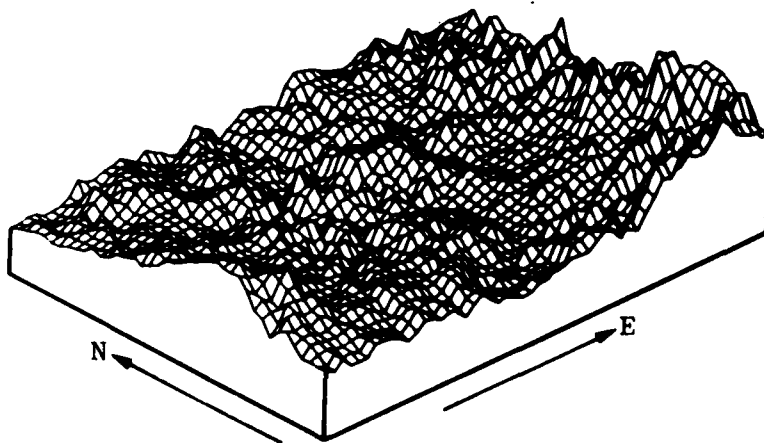
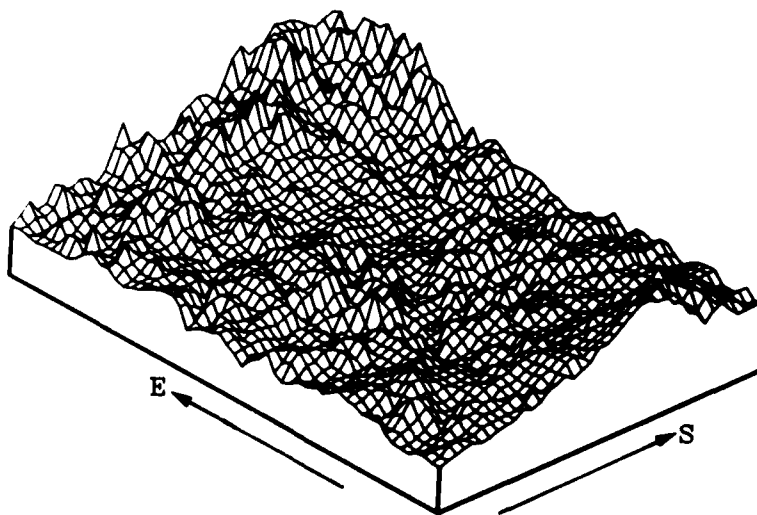


Figure 2.11 WSMR PASS Experiment Upper Air Measurements, 11/19/74, Station HMS.

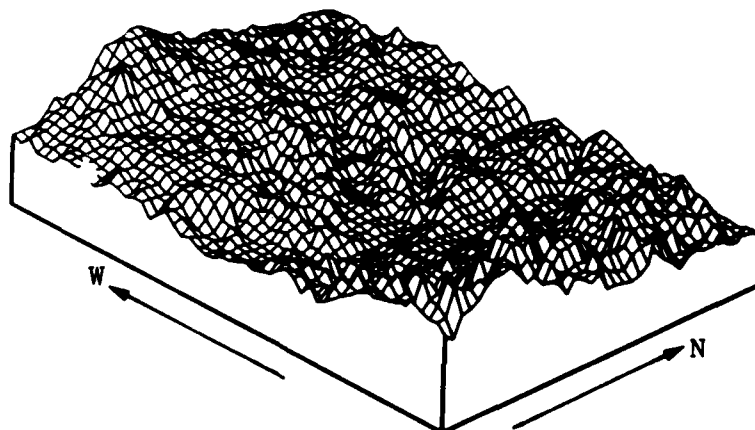


(a)

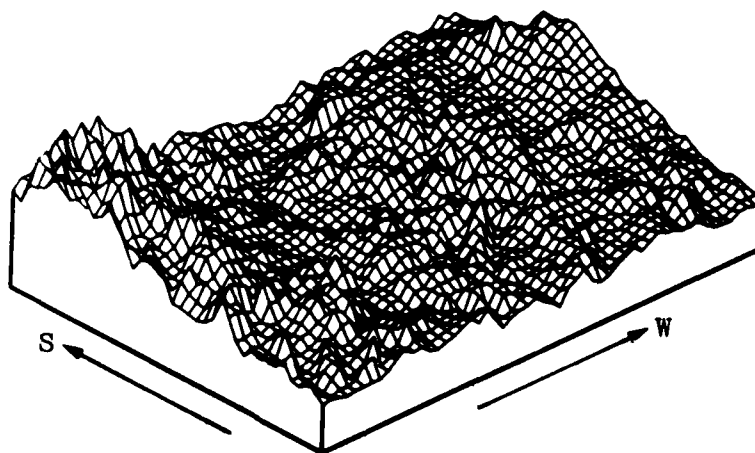


(b)

Figure 2.12 Perspective Views of the Terrain Containing Fulda, West Germany. The Southwest Corner has the UTM Coordinates (516.2 km, 5584.3 km) with Respect to 9° East Meridian.



(c)



(d)

Figure 2.12
(cont'd.)

Perspective Views of the Terrain Containing Fulda, West Germany. The Southwest Corner has the UTM Coordinates (516.2 km, 5584.3 km) with Respect to 9° East Meridian.

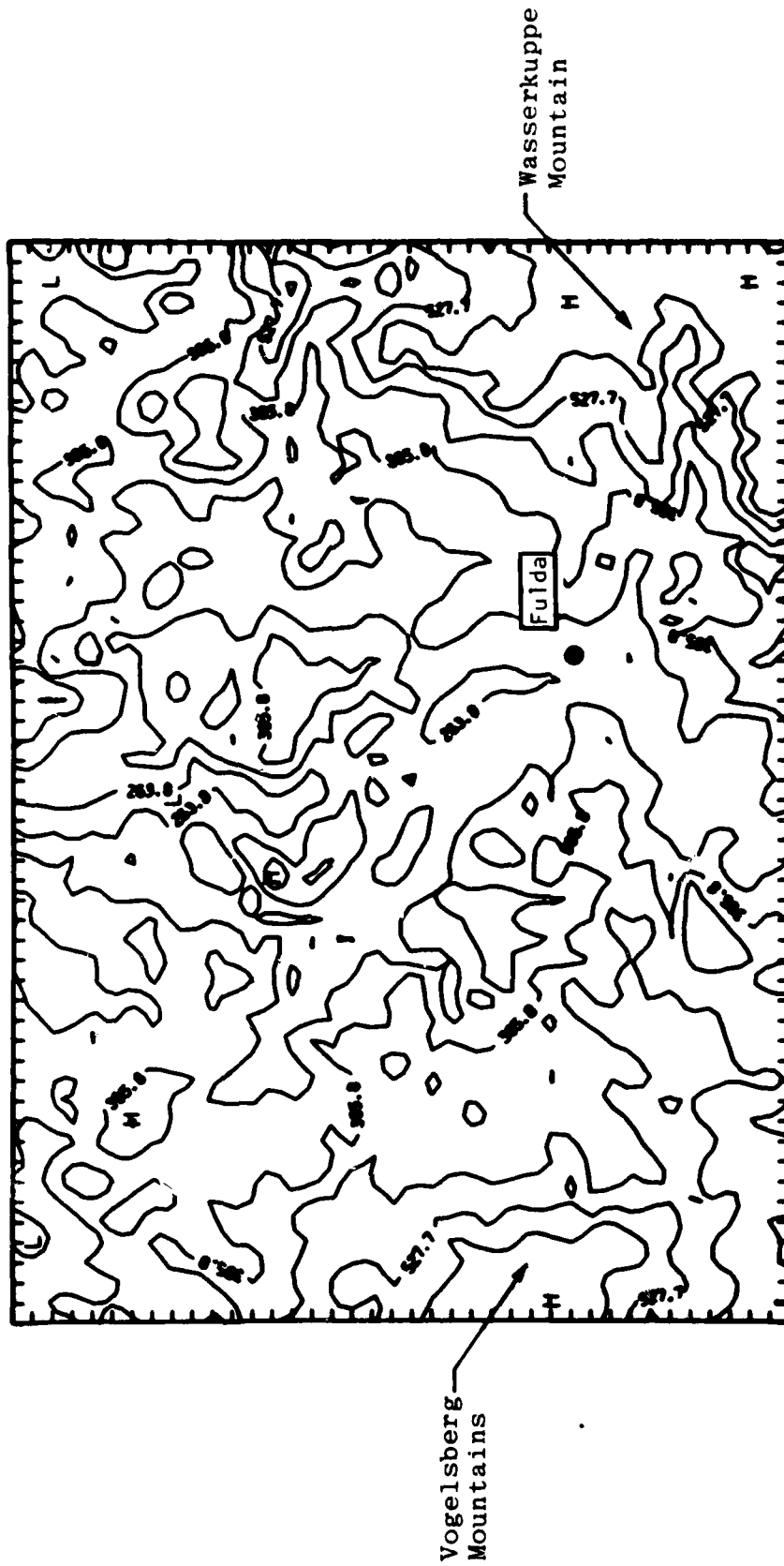
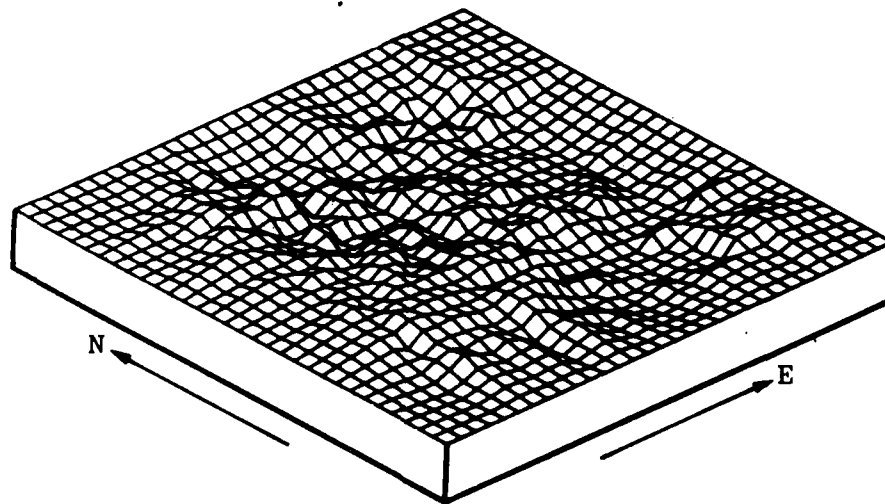


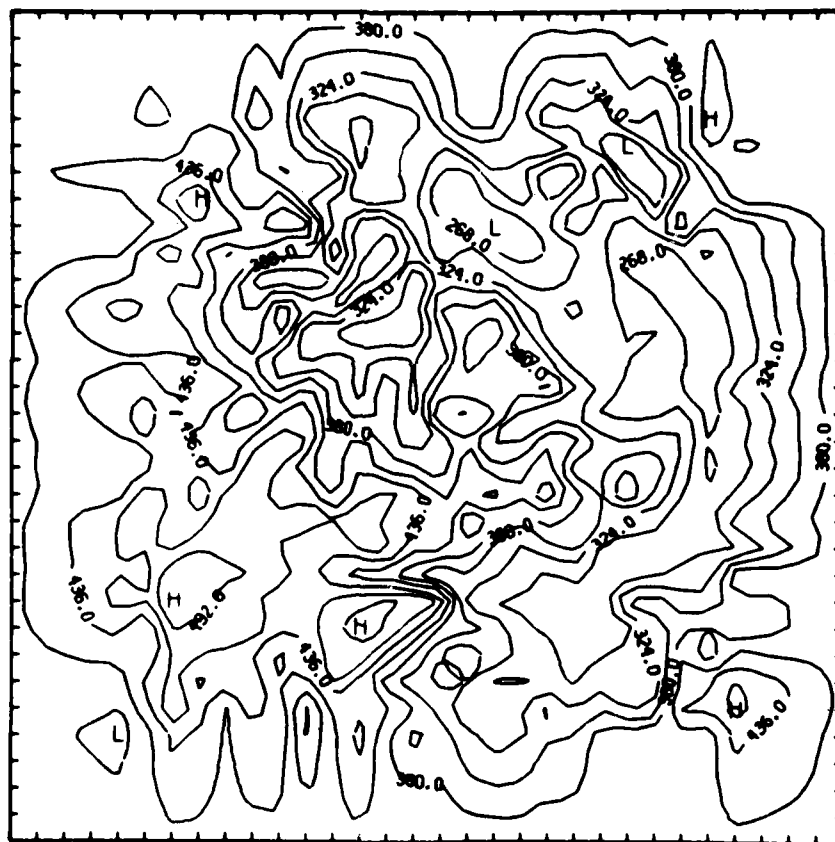
Figure 2.13 Contour Plot of the Region Around Fulda, West Germany, on 55 x 40 Grid of Points with 1 km Grid Interval.

These mountains are small with mild slopes. The highest mountain in this region is Wasserkuppe Mountain on the southeast boundary, with its peak elevation at 950 m above sea level. The Vogelsberg mountain range is in the southwest area of this region, with its highest peak at 774 m, which is outside the region considered. The city of Fulda is in a valley located near the southeast part of this region, with the valley floor elevation ranging from 250 m to 400 m. The Fulda River streams past the city to the north, separating the mountainous regions.

For simulation over this region, as also with the White Sands region, a limited area containing 32 x 32 grid points is chosen. For the West Germany region, an area with its southwest corner at (526.2 km, 5584.3 km), UTM coordinate is taken. Since simulations over this region were carried out using the linear model LINMET which presumes periodic boundary conditions in both lateral directions, a boundary smoother is applied over a 5-grid-wide strip all around the limited area in order to avoid abrupt slopes at the boundaries. This smoother sets the boundary elevation at a constant value of 400 m and then linearly interpolates the elevation between the first and the fifth grid. The elevations at the fifth grid and beyond are left at the original values. This smoother effectively removes the boundary problem and seems to work satisfactorily. Figures 2.14(a) and (b) show the perspective and contour view of this limited area. Figures 2.15(a) and (b) show the same for the limited area in the White Sands region over which some LINMET simulations are carried out. For this region, the boundary elevation is maintained at 1200 m above sea level, and the southwest corner is located at (340 km, 3570 km) UTM coordinates. Figures 2.16 and 2.17 show two upper air measurements taken at Meiningen, East Germany, which are used for a sample simulation over the Fulda region. Meiningen is located east of the Fulda region.

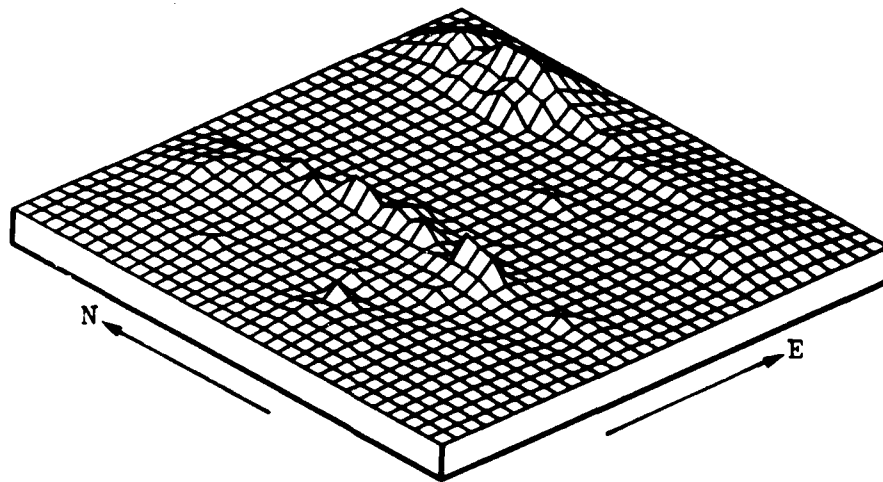


(a)

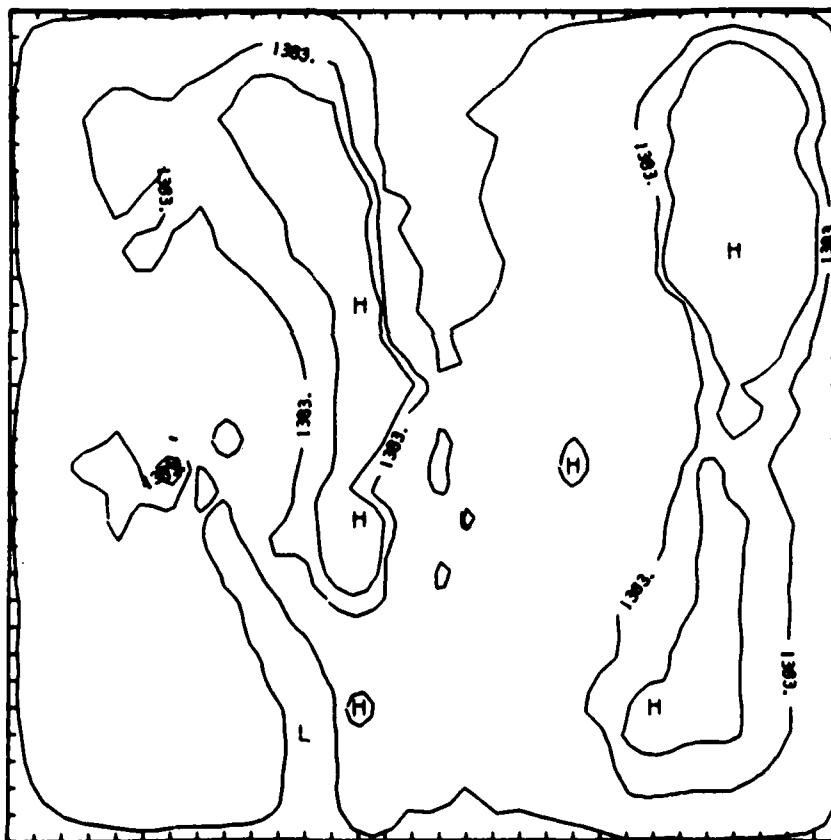


(b)

Figure 2.14 Perspective (a) and Contour (b) Views of the Region Around Fulda, West Germany, on a 32 x 32 Grid with 1 km Grid Interval. The Southwest Corner has UTM Coordinates of (526.2 km, 5584.3 km) and the Boundaries are Smoothed.



(a)



(b)

Figure 2.15 Perspective (a) and Contour (b) Views of the White Sands Region on a 32 x 32 Grid with 5 km Grid Interval. The Southwest Corner has UTM Coordinates of (340 km, 2570 km) and the Boundaries are Smoothed.

STATION = MGN TIME = 0000 DATE = 00-00-00

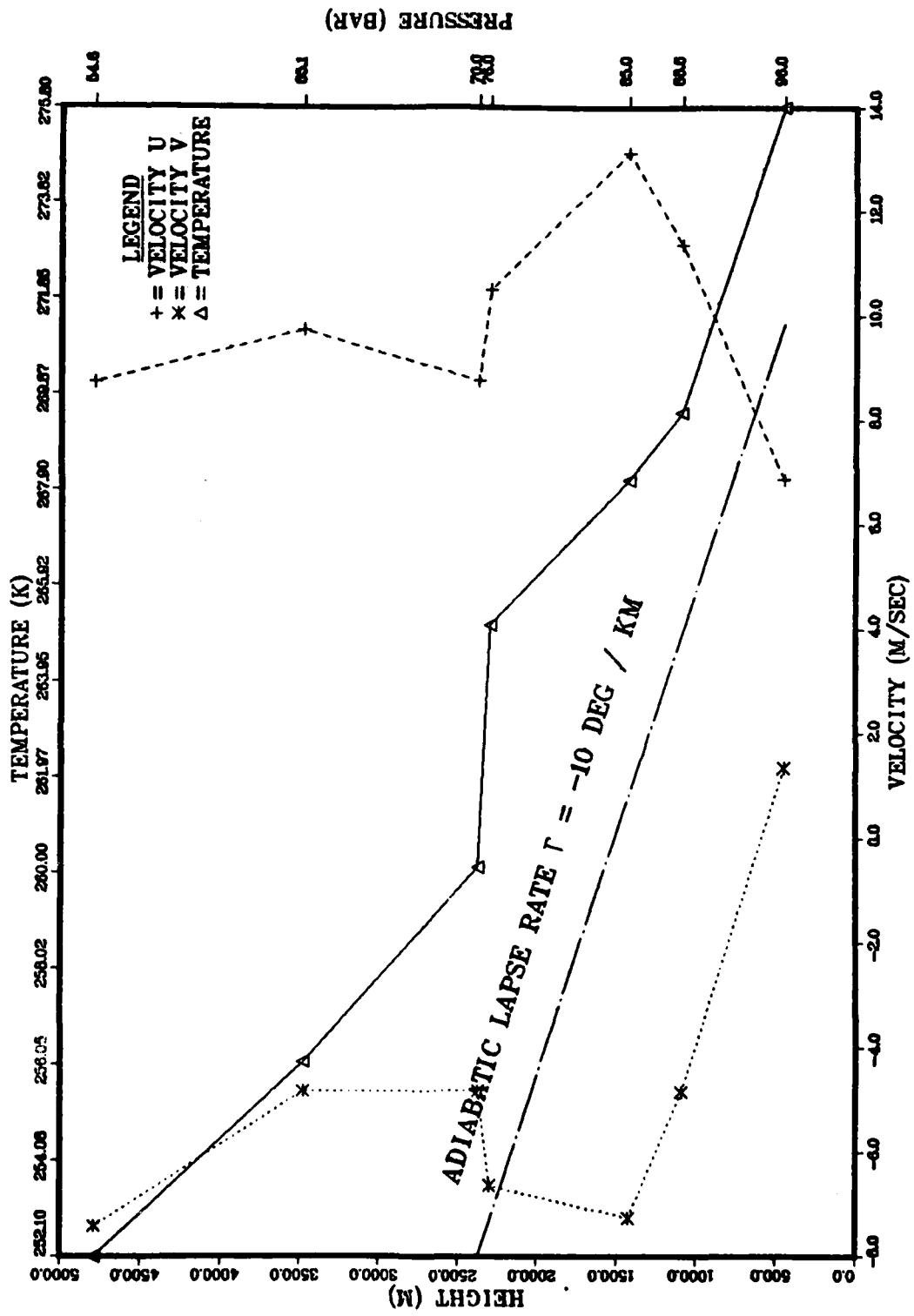


Figure 2.16 Upper Air Measurement at Meiningen, East Germany.

STATION = MGN TIME = 0000 DATE = 00-00-00

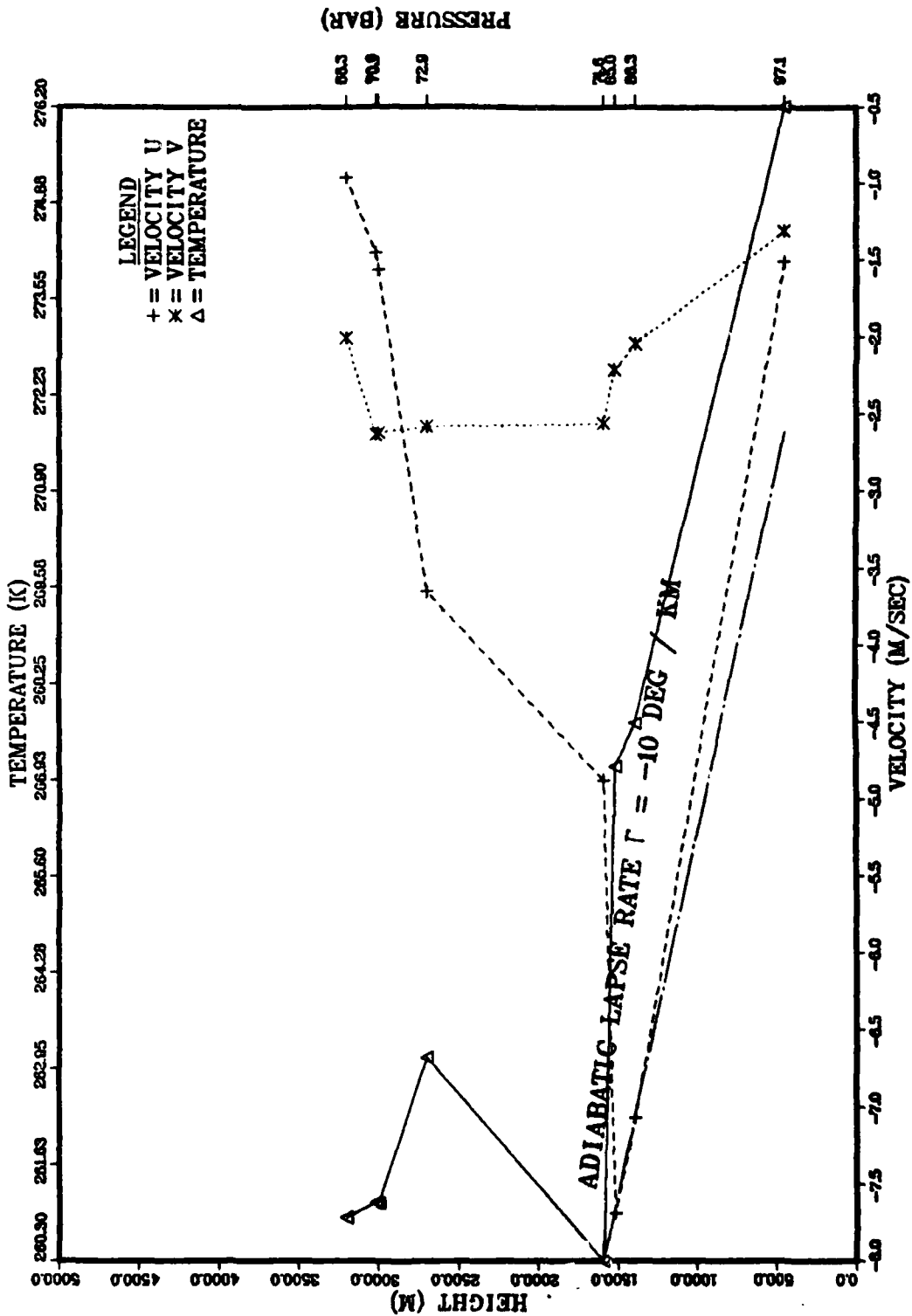


Figure 2.17 Upper Air Measurement at Meiningen, East Germany.

3. PRIMITIVE EQUATION MODEL SIGMET

This class of wind-field calculation is defined as solving the primitive equations. Similar systems of equations are employed for calculations of global circulation, synoptic weather forecasting, mesoscale forecasting, and for research in severe storms and cumulus convection modeling. In this formulation, it is quite straightforward to include the effects of boundary layer turbulence and thermal forcing (as is done in the SIGMET computer code of SAI). These models are applied by performing a 3-D time dependent calculation starting from initial conditions and employing boundary conditions determined by the synoptic or larger-scale weather regime. In the case of diurnally cyclic flow, the calculation should continue for a day or more to determine the distribution of winds at each site. Two different treatments of the vertical velocity can be distinguished, based on the magnitude of the expected vertical acceleration in the flow field. If the vertical acceleration is small, as is the case when the size of zones in the horizontal direction is somewhat greater than 1 km and when the terrain is relatively smooth, the hydrostatic approximation can be employed. This simplifies the calculation and makes the transformation to a terrain-conformal coordinate system (as used in SIGMET) easier. If the horizontal spacing is small, the vertical acceleration equation can be retained. Frequently the resulting equations are solved in the Boussinesq approximation, in which the effects of buoyancy are present only in the equation for the vertical component of momentum.

The primitive equation models are the only class in which all of the physical processes affecting near surface winds are included. Other considerations aside, the primitive equation models are the obvious choice for mesoscale applications. Factors weighing against their use are: complexity, incomplete verifications of the codes, and expense. Presently, the calculation of

one case of a 3-D mesoscale wind field costs a few hundred dollars for a short calculation, but this cost will be reduced by code optimization, faster computers, and the technique of partial implementation. The combination of these could reduce the cost by a factor of 10 or more.

3.1 SIGMET FORMULATION

The SIGMET family of mesoscale (10 +100 km) meteorology simulation codes is based on the work of Anthes (1972) and uses a finite difference technique to solve the so-called primitive equations to describe transient flow in the atmosphere. One- two- and three-dimensional versions of the code have been written, each of which share the same level of physical approximation as well as similar numerical techniques. These common features among the codes have permitted the development and testing of much of the physical and numerical modeling using the more economical 1-D or 2-D versions with subsequent implementation in the 3-D code. Also, although the 3-D version is required ultimately for application to mesoscale simulations of regional meteorology, it is believed that much can be learned with the simpler and more economical codes.

The SIGMET codes solve the conservation equations for the relevant meteorological variables (wind components, temperature, and moisture) and describe both the planetary boundary layer and upper level flow as they are affected by complex terrain. The equations, formulated in an Eulerian framework, account for advection, Coriolis effects, turbulent heat, momentum and moisture transport, and viscosity. In many of the applications of mesoscale simulation, the atmospheric boundary layer winds are of particular interest. Over regions of complex terrain, these low level winds suffer from numerical errors when finite differences are formed in Cartesian Coordinates. In order to avoid this problem, a coordinate transformation has been carried out to a new coordinate system (the sigma, σ , coordinate system) in which the lowest coordinate surface is conformal to the terrain surface. In this

representation, after care is exercised in calculating the transformed pressure gradients, the needed resolution and accuracy near the surface are achieved by concentrating the finite difference grid in the near surface region. Expanding the grid into the upper levels with a non-constant grid distribution satisfies the less stringent accuracy requirements there while minimizing vertical grid points to maintain an economical calculation.

Diurnally varying winds such as the land-sea breeze, slope winds, etc., are important in the regional meteorology. These winds are caused by thermal forcing of the mesoscale flow, and the simulation requires that solar radiation and its related phenomena be included in the model. To do so, subroutines of SIGMET have been developed in which solar and terrestrial radiation are calculated. These affect the winds by inducing thermal pressure gradients across regions of differing albedo and along sloping terrain. These radiation terms are also affected by the amount of atmospheric water vapor and by the conduction and storage of heat in the soil. Consequently, soil temperature and moisture, and atmospheric water vapor mixing ratio, which satisfy prognostic equations, are included in SIGMET. The development and testing of the surface heat and mass transfer balances have resulted in significant improvements in the physical accuracy and numerical economy of their treatment. As a result of recent work, all versions of the SIGMET code are currently at the same level of development in terms of the physical modeling items mentioned.

A very important physical effect, which must necessarily be taken into account in mesoscale calculations, is the transport of momentum, energy, and water vapor by turbulence in the atmospheric boundary layer. This is a field of active current research in fluid dynamics. Several different approaches to the description of turbulent transport have been studied, and the best compromise for meteorological flows seems to be the "level 2" and "level 2½" models of Yamada and Mellor (1975). The algebraic equations designated as a "level 2" model by the authors correspond to a mixing

length, equilibrium turbulence theory in which full account of density stratification effects is retained. Comparison of the level 2 predictions of the atmospheric boundary layer with those of more complicated approximations indicates that they capture many of the features of boundary layer turbulence (Mellor and Yamada, 1974). This purely local theory, however, does not account for turbulence history effects, i.e., nonequilibrium effects caused by flow over terrain, changes in surface roughness, etc. Such effects are contained in the level 2½ model which as used in the present work includes a turbulent energy transport equation. Because of the importance of such effects in complex terrain to the structure of the boundary layer winds, the level 2½ model has recently been studied and incorporated in all versions of the SIGMET code. Barring unforeseen difficulties with the model, this completes the turbulence modeling work, since it is believed that the present model is as detailed as required in the present program.

Strong turbulent diffusion across the small zones required to resolve the planetary boundary layer near the surface may, under some circumstances, limit the time interval to a few seconds if an explicit formulation is used. In order to remove this limitation, a new formulation of the vertical diffusion which is partially implicit has been implemented. This method eliminates the time interval restriction associated with diffusion. As indicated by a linear stability analysis, it also markedly relaxes the stability inequality associated with vertical advection. The partially implicit code contains simultaneous linear equations in each vertical column of zones. These equations are equivalent to a coefficient matrix of the unknown quantities which is tridiagonal and is solved by a forward/backward substitution algorithm. This vertical diffusion subroutine has been incorporated into all versions of SIGMET, and the resulting code has been debugged and tested.

In summary, the SIGMET modeling contains all of the physics required to simulate the time dependent meteorology of a region

based upon minimal weather station data. However, the relative expense of the calculations, together with desire to increase the amount of wind-field modeling possible within a limited budget, has prompted the continuing efforts to increase the numerical efficiency of the codes.

We now outline the equations that are solved in the 3-D SIGMET code. These consist of the equations for the 3-D distributions of the horizontal components of the wind velocity, the potential temperature, and the mixing ratio of the water vapor. In addition, there is an equation for the 2-D distribution of the pressure thickness of the atmosphere. In terms of these quantities the equivalent vertical velocity $\dot{\sigma}$ is obtained as a diagnostic quantity.

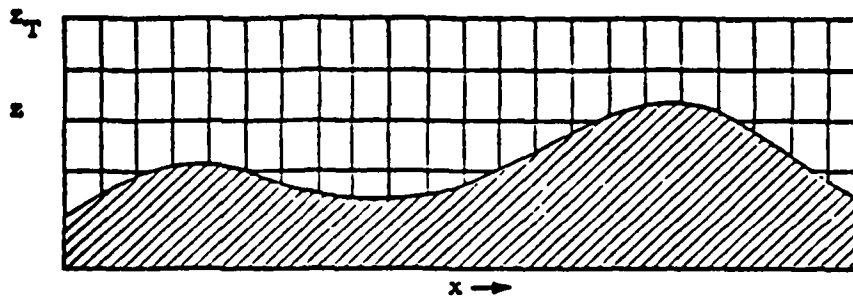
By virtue of the condition of hydrostatic balance, it is possible to simplify the calculation substantially by eliminating the differential equation for the vertical velocity. In addition, it proves useful to transform the vertical coordinate, replacing the altitude with a scaled pressure coordinate. This pressure coordinate, called the sigma coordinate, is defined as follows:

$$\sigma = \frac{P - P_T}{P_S - P_T} \quad (3.1)$$

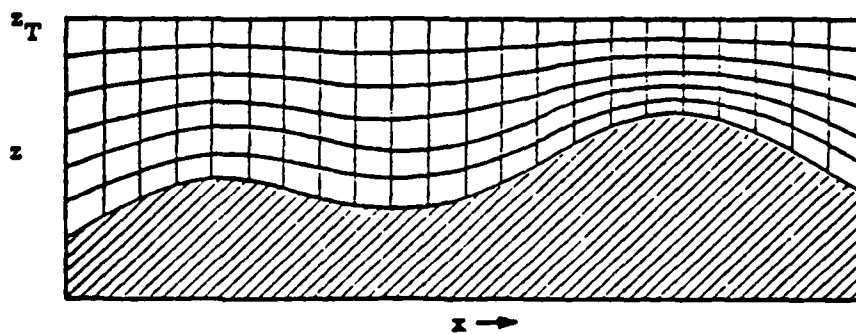
The hydrostatic relation

$$\frac{dz}{d\sigma} = - \frac{\pi}{g\rho} \quad (3.2)$$

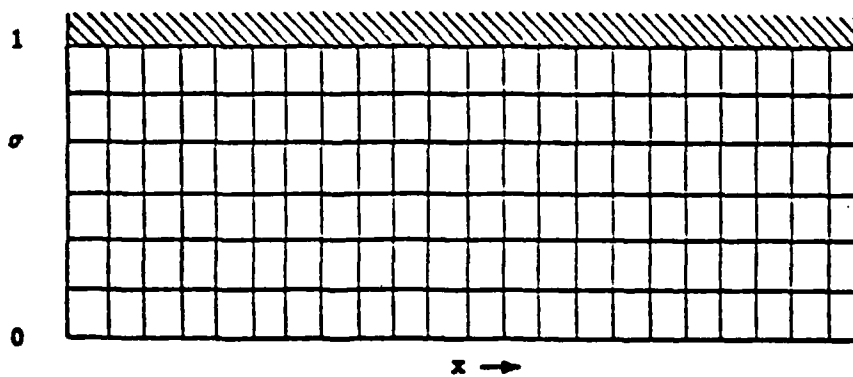
gives the relationship between the altitude and the σ coordinate. The sigma coordinate is in the range $0 \leq \sigma \leq 1$, and takes the value $\sigma = 1$ at the surface. It is applicable to a surface with complex terrain, as illustrated in Figure 3.1.



(a). Two-Dimensional Terrain in x, z Space.



(b). Two-Dimensional Terrain in x, z Space With Contours of Constant σ Superimposed.



(c). Two-Dimensional Terrain in x, σ Space. The Location of the Terrain is Indicated by the Cross-Hatched Region.

Figure 3.1 Terrain Coordinate Transformation.

This transformation is used to eliminate the altitude. After considerable manipulation, the primitive equations take the form

$$\begin{aligned}
 \frac{\partial \pi u}{\partial t} + \frac{\partial u \pi u}{\partial x} + \frac{\partial v \pi u}{\partial y} + \frac{\partial \dot{\sigma} \pi u}{\partial \sigma} - f \pi v + \pi \left(\frac{\partial \phi}{\partial x} + \frac{\sigma}{\rho} \frac{\partial \pi}{\partial x} \right) &= F_V(u) + F_H(u) \\
 \frac{\partial \pi v}{\partial t} + \frac{\partial u \pi v}{\partial x} + \frac{\partial v \pi v}{\partial y} + \frac{\partial \dot{\sigma} \pi v}{\partial \sigma} + f \pi u + \pi \left(\frac{\partial \phi}{\partial y} + \frac{\sigma}{\rho} \frac{\partial \pi}{\partial y} \right) &= F_V(v) + F_H(v) \\
 \frac{\partial \pi \theta}{\partial t} + \frac{\partial u \pi \theta}{\partial x} + \frac{\partial v \pi \theta}{\partial y} + \frac{\partial \dot{\sigma} \pi \theta}{\partial \sigma} &= F_V(\theta) + F_H(\theta) + \pi Q \\
 \frac{\partial \pi C}{\partial t} + \frac{\partial u \pi C}{\partial x} + \frac{\partial v \pi C}{\partial y} + \frac{\partial \dot{\sigma} \pi C}{\partial \sigma} &= F_V(C) + F_H(C) \\
 \frac{\partial \pi}{\partial t} + \frac{\partial u \pi}{\partial x} + \frac{\partial v \pi}{\partial y} + \frac{\partial \dot{\sigma} \pi}{\partial \sigma} &= 0
 \end{aligned} \tag{3.3}$$

The effects of vertical and horizontal turbulent diffusion are contained in the terms F_V and F_H of Eq. (3.3). These are approximated by Fickian diffusion expressions.

$$F_V(\psi) = \left(\frac{g}{\pi} \right)^2 \frac{\partial}{\partial \sigma} \left(K_V \rho^2 \frac{\partial \pi \psi}{\partial \sigma} \right) \tag{3.4}$$

and

$$F_H(\psi) = \pi \left[\frac{\partial}{\partial x} \left(K_H \frac{\partial \psi}{\partial x} \right) + \frac{\partial}{\partial y} \left(K_H \frac{\partial \psi}{\partial y} \right) \right] \tag{3.5}$$

Eqs. (3.4) and (3.5) contain diffusion coefficients for vertical and horizontal transport by turbulent eddies. The horizontal coefficients have been evaluated from empirical data, and the vertical diffusion coefficients are evaluated using Yamada-Mellor turbulence closure theories.

The first two equations of Eq. (3.3), describing the rate of change of the horizontal velocity components, contain terms for the horizontal pressure gradient and the Coriolis force. Each component of the pressure gradient consists of two terms: the first is proportional to the gradient of geopotential height, and the second contains the gradient of the surface pressure. These two terms are evaluated by independent difference approximations which, over complex terrain, will contain truncation errors. We have found that these errors can be appreciable and have devised a scheme for reducing them to a negligible value. The Coriolis parameter $f = 2\Omega \sin\theta$ can be taken to be constant over the meso-scale region. The third of Eq. (3.3) is for the rate of change of the energy. In Q , we take into account at present only the radiative flux divergence, neglecting the liquid water effects.

Difference equations approximating the above differential equations attempt, so far as possible, to retain second-order accuracy in the spatial and time dependence. The spatial difference equations employ a rectangular mesh in which velocity variables are offset from the thermodynamic variables. The time derivatives of the equations employ three levels in the finite difference scheme. This is basically a leapfrog formulation.

3.2 SIGMET SIMULATIONS

Relatively short duration simulations of the wind field around White Sands Missile Range have been performed using the three-dimensional version of SIGMET. The calculations utilized the limited terrain shown in Figures 3.2 and 3.3. This region encompasses all the measurement locations, major parts of the Tularosa Valley and the San Andres Mountains, and parts of the Sacramento Mountains. The finite difference grid design is defined in the following.

$$\begin{aligned} I_{\max} &= 25, J_{\max} = 21, K_{\max} = 15 \\ \Delta x &= \Delta y = 5 \text{ km} \end{aligned}$$

$$\left. \begin{aligned}
 \Delta z_{\min} &= 20 \text{ m} \\
 \Delta z_{\max} &= 1000 \text{ m} \\
 z_{\text{top}} &= 5500 \text{ m ASL (500 mbar)}
 \end{aligned} \right\} \begin{array}{l} \text{geometric progression with} \\ \text{1.25 expansion ratio} \end{array}$$

This results in a solution domain of 125 km (east-west) by 105 km (north-south) around WSMR, which is defined by the borders of the contour plot mentioned above. The relatively coarse 5 km horizontal zoning was chosen in an effort to include as much of the wind field influencing terrain around White Sands as possible, while retaining a relatively economical calculation. The simulation was initialized at 0515 LST using the wind speed components, temperature, and water vapor concentration given by the station TSX upper air sounding at that time on 19 November 1974 (see Figure 2.4).

From this initial state, the equations were integrated with a time step of 3 sec to a total simulation time of 7½ min (or 150 cycles). The 3 sec time step is considerably below the maximum time step allowed by the gravity wave stability limitation of the finite difference scheme in SIGMET, i.e., $\Delta t_c \approx \min(\Delta x, \Delta y) / 2\sqrt{gH}$, where H is the maximum depth of the atmospheric layer being simulated. In order to test the timewise truncation error in the solution (formally second-order), the calculation was repeated with $\Delta t = 9$ sec, which is just under (80 % of) the critical time step Δt_c . At a simulation time of 7½ min, the resulting field variables from each calculation compared to within ~1% indicating the absence of significant timewise truncation error.

The results of the $\Delta t = 3$ sec calculation are presented in Figures 3.4 through 3.7 below. The near surface wind vectors and speed contours shown in Figures 3.4, for ~15.m AGL, and Figure 3.5, ~200.m AGL, illustrate the development of the expected terrain effects. They show the speed-up on the lee side of the San Andres Mountains, near the center of the region, and the turning and flow acceleration due to the higher Sacramento Mountains to the east and northeast. Also shown is the tendency toward low winds in the central valley. Finally, additional details of the simulation

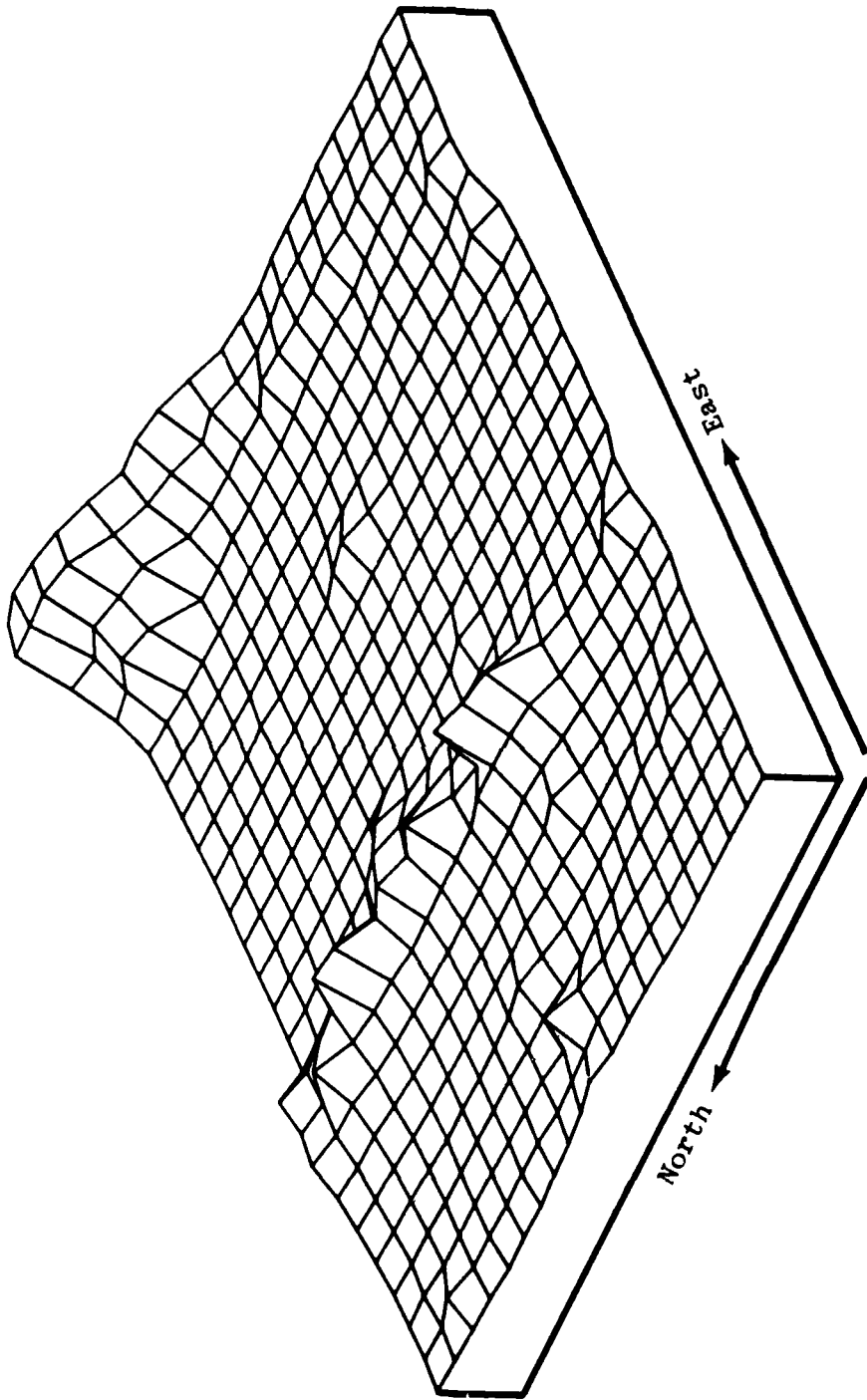


Figure 3.2 Prospective View of Limited White Sands Terrain (120 km x 100 km) on a 5 km grid used for SIGMET Simulation. The South-West corner has the UTM Coordinates (310 km, 3540 km).

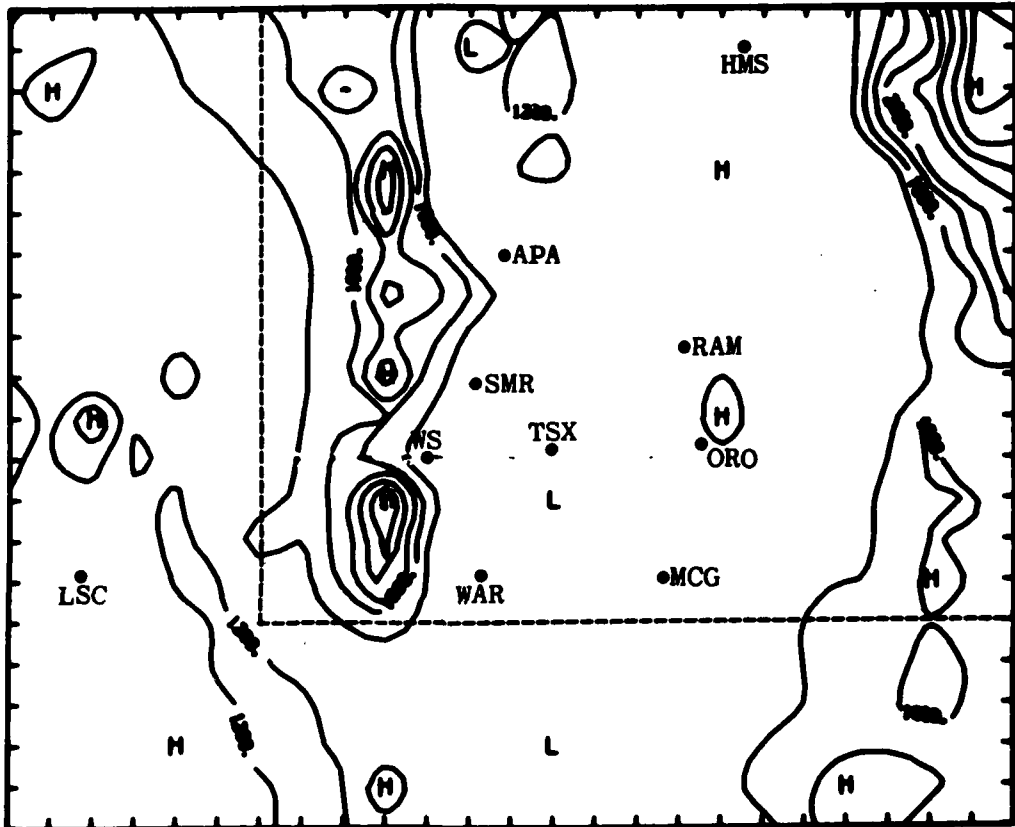


Figure 3.3 Contour Plot of Limited White Sands Terrain Used for SIGMET Simulation. The Rectangle Shown by Dashed Lines is used for VARMET Simulations.

are presented in the near surface temperature contours, Figure 3.6; water vapor, Figure 3.7; and turbulent energy, Figure 3.7. The turbulence energy contours show the high turbulence in the high shear regions of the flow; in addition, they show the relatively low values in the low wind, stable valley floor areas of the flow.

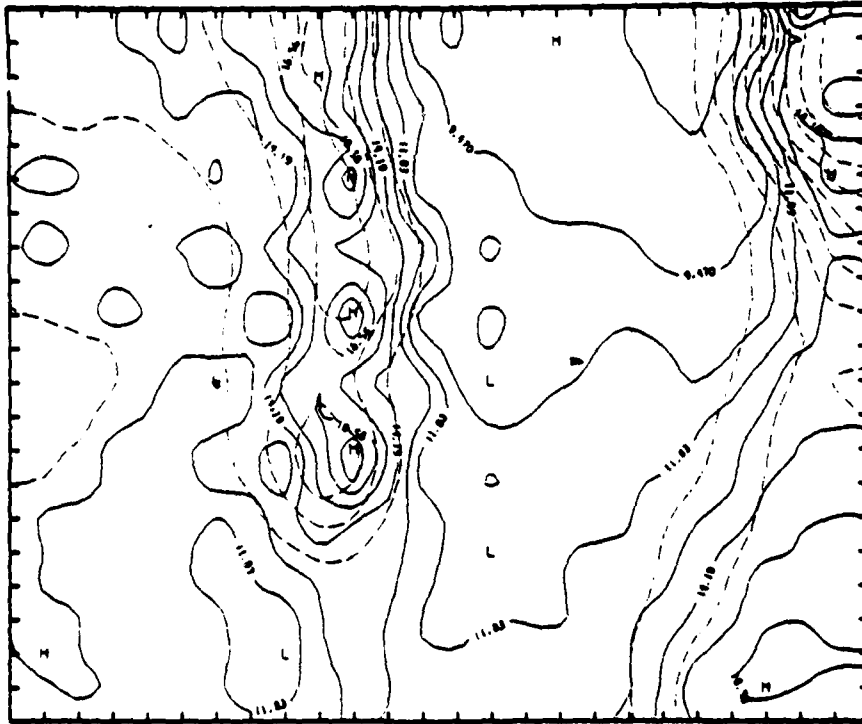
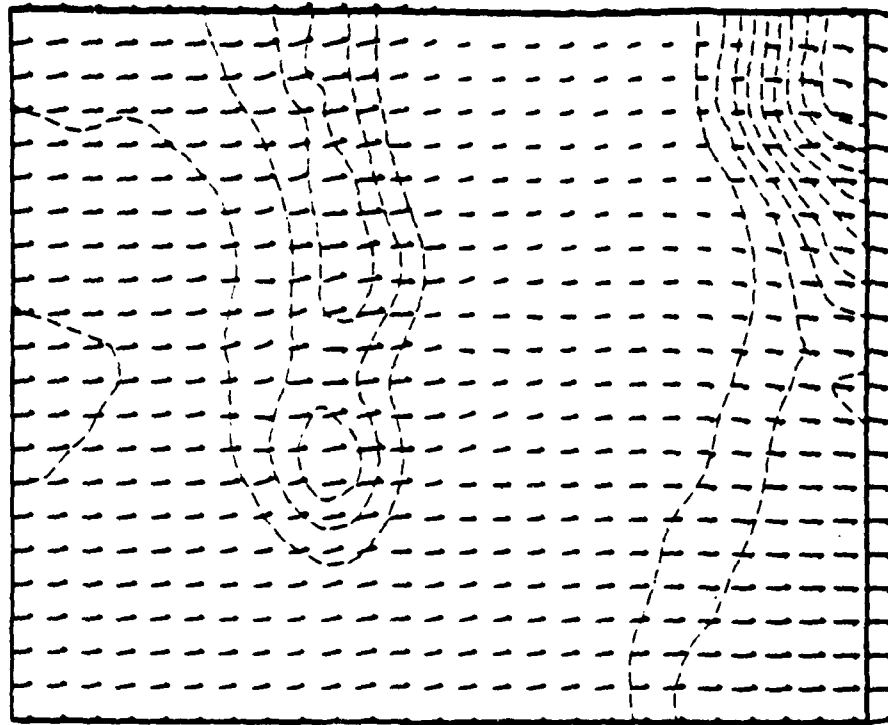
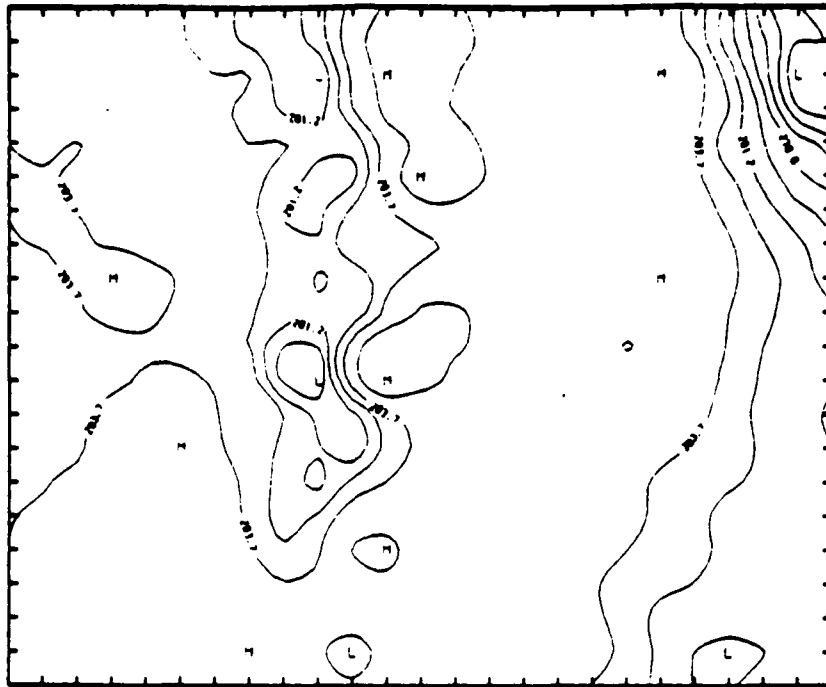
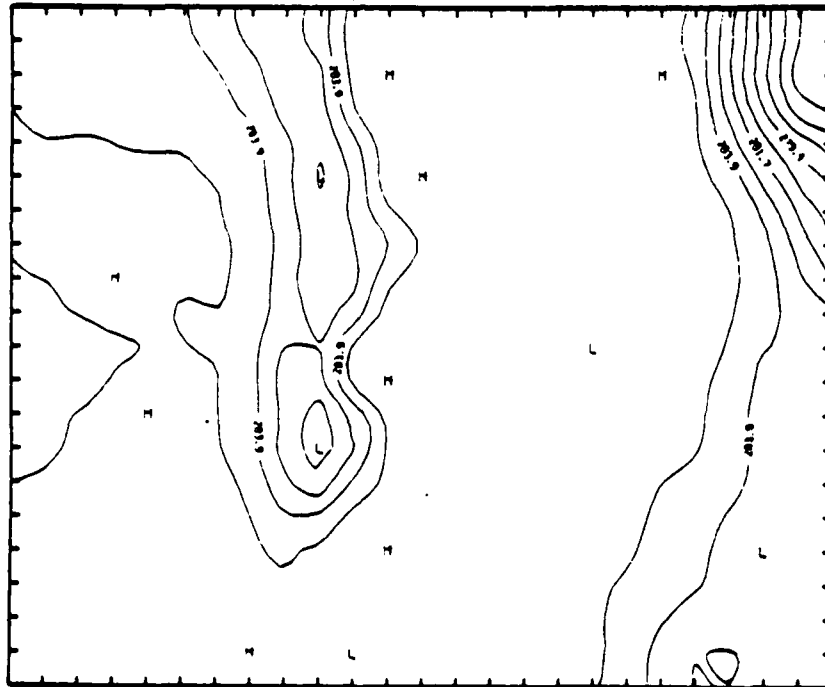


Figure 3.4 Near Surface (~15 m AGL) Wind Field Vectors and Speed Contours: SIGMET Simulation of WSMR, 0515, 11/19/74.



a) ~200.m AGL



b) ~15.m AGL

Figure 3.6 Near Surface Temperature Contours ($^{\circ}$ K)
SIGMET Simulation of WSMR, 0515, 11/19/74.

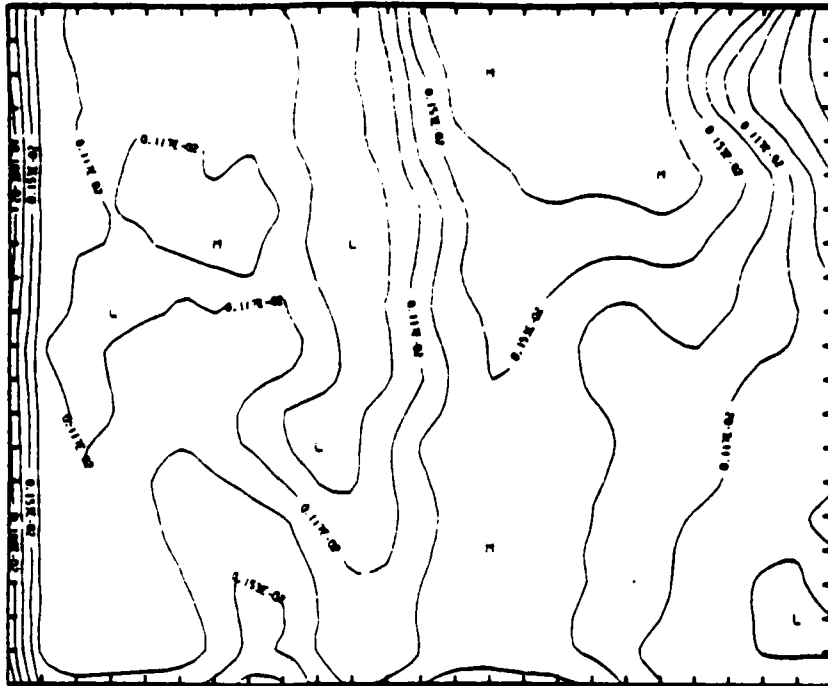


Figure 3.7 Near Surface Water Vapor Mixing Ratio
SIGMET Simulation of WSMR, 0515, 11/19/74

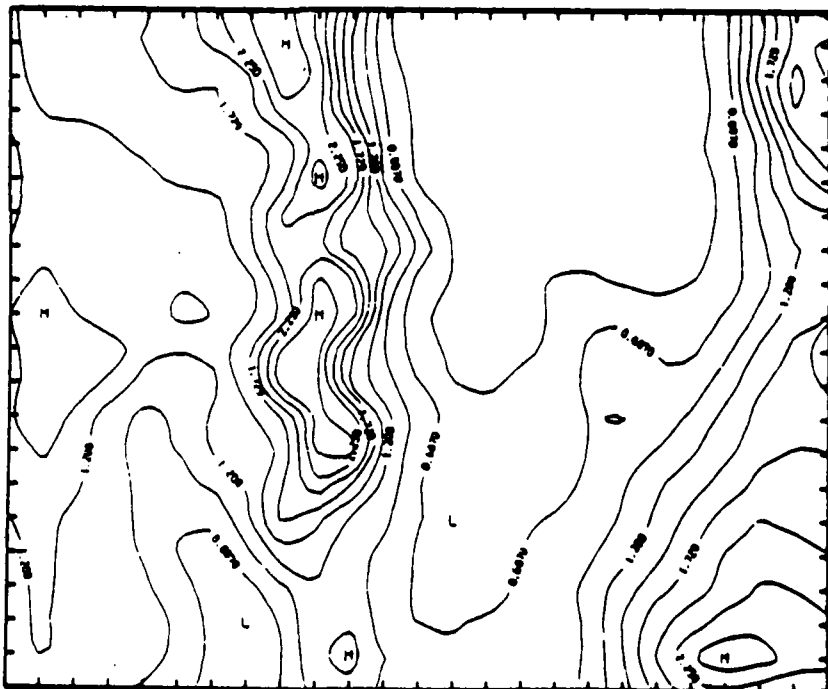


Figure 3.8 Near Surface Mean Square Turbulent Velocity
Fluctuation (m^2/sec^3); SIGMET Simulation of
WSMR, 0515, 11/19/74.

LINEAR MODEL LINMET

Based on steady linearized, inviscid Navier-Stokes equations in three-dimensions, a model is developed to predict wind field in data poor regions with moderate success. While this class of models will not simulate the detailed physics of the flow, like the sophisticated primitive equation models described in the previous chapter, the computational effort will be significantly less. It may thus be possible to use such models in real-time operations. One such model, LINMET, is developed here. The theoretical basis for its formulation and some sample calculations, using the code, are given in the following.

4.1 LINMET FORMULATION

In order to construct a compact and self-consistent set of finite difference equations for LINMET, we discuss both the differential equations of motion and the discretizations of the equations for numerical computation side by side. Extensive use of Fast Fourier Transform (FFT) is contemplated in this model.

We assume that the terrain height H_{ij} is represented at the Cartesian Coordinates $x_i = x_0 + i\Delta x$, $y_j = y_0 + j\Delta y$ ($i = 1, N_1$; $j = 1, \dots, N_2$) separated by constant intervals Δx , Δy . The orientation of x and y axes is arbitrary. Assuming that the boundary conditions are periodic in both x and y , then the finite Fourier transform $\hat{H}_{k\ell}$ can be readily obtained from the data;

$$\hat{H}_{k\ell} = \sum_{i=1}^{N_1} \sum_{j=1}^{N_2} H_{ij} \exp \left\{ 2\pi i \left[(i-1)(k-1)/N_1 + (j-1)(\ell-1)/N_2 \right] \right\} \quad (4.1)$$

$$k = 1, 2 \dots N_1, \ell = 1, 2 \dots N_2 \text{ and } i = \sqrt{-1} .$$

The inverse transform is given by a similar expression;

$$H_{ij} = \frac{1}{N_1 N_2} \sum_{k=1}^{N_1} \sum_{\ell=1}^{N_2} \hat{H}_{k\ell} \exp \left\{ -2\pi i \left[\frac{(i-1)(k-1)}{N_1} + \frac{(j-1)(\ell-1)}{N_2} \right] \right\}. \quad (4.2)$$

Since these finite representations do not admit differentiation, it is necessary ultimately to form difference equations for the atmospheric variables that can be represented in the form indicated in Eqs. (4.1) and (4.2). Consequently, in the following discussion, we derive the equations satisfied by components of the discrete Fourier transform of the fluid dynamic variables.

The linearized steady-state equations for the conservation of mass, momentum and energy of the atmosphere are:

$$\begin{aligned} U\bar{\rho}_x + V\bar{\rho}_y + w\bar{\rho}_z + \bar{\rho}(u_x + v_y + w_z) &= 0 \\ Uu_x + Vu_y + wU_z + \frac{1}{\bar{\rho}} p_x &= 0 \\ Uv_x + Vv_y + wV_z + \frac{1}{\bar{\rho}} p_y &= 0 \\ Uw_x + Vw_y + \frac{1}{\bar{\rho}} p_z &= -\frac{\rho g}{\bar{\rho}} \\ UT_x + VT_y + w(\bar{T}_z + \Gamma) &= \frac{1}{\bar{\rho} C_p} (Up_x + Vp_y) \\ \frac{p}{\bar{p}} &= \frac{\rho}{\bar{\rho}} + \frac{T}{\bar{T}} \end{aligned} \quad (4.3)$$

In the above equations, differentiation with respect to the horizontal coordinates x , y , or the vertical coordinate z , is represented by the corresponding subscript. Unperturbed variables (corresponding to horizontal, steady flow in the absence of terrain) are denoted by U, V , and the overbarred quantities

that depend only on z . The dependent variables are: u, v, w , the wind vector components; and ρ, p, T , the air density, pressure, and temperature. The other quantities appearing in Eq. (4.3) are the adiabatic lapse rate $\Gamma = g/C_p$, the specific heat of air at constant pressure C_p , and the gravitational constant g . The unperturbed atmosphere is in hydrostatic equilibrium with $\bar{p}_z = -g\bar{\rho}$. The above atmospheric variables are related to the terrain height through the linearized boundary condition

$$w(o) = U(o)H_x + V(o)H_y \quad (4.4)$$

In order to reduce Eq. (4.3) to a more compact form, we eliminate T and ρ , obtaining

$$\begin{aligned} w_z + (S-s)w + u_x + v_y + (up_x + vp_y)/(\bar{\rho}C_s^2) = 0 \\ U^2w_{xx} + 2UVw_{xy} + V^2w_{yy} + gSw + (Up_{xz} + Vp_{yz})/\bar{\rho} \\ + g(Up_x + Vp_y)/(\bar{\rho}C_s^2) = 0 \end{aligned} \quad (4.5)$$

where $S = (\bar{T}_z + \Gamma)/\bar{T}$
 $s = -\bar{\rho}_z/\bar{\rho}$

and

$$C_s^2 = (C_p\bar{p})/(C_v\bar{\rho}), \text{ the adiabatic sound speed.}$$

These equations, together with the second and third equations of Eq. (4.3), constitute four equations for the quantities u, v, w , and p . Rather than performing further reduction of the equation in differential form, requiring additional differentiation, we proceed to form difference equations that are subsequently

subjected to discrete Fourier transform. The resulting equations may be solved algebraically. By applying Fourier transform to the discretized equations rather than to the continuous equations, we avoid the negative wave numbers. Moreover, it can be shown that this approach results in more accurate representation of higher wave number modes.

Eqs. (4.3) and (4.4) contain first and second derivative terms, which are to be approximated by central difference expressions. We define each of the variables ϕ_{ij} at the same position x_i, y_i . Forming centered differences, we obtain the following approximations.

$$(\phi_x)_{ij} = \frac{\phi_{i+1,j} - \phi_{i-1,j}}{2\Delta x}$$

$$(\phi_{xx})_{ij} = \frac{\phi_{i+1,j} - 2\phi_{i,j} + \phi_{i-1,j}}{\Delta x^2}$$

$$(\phi_{xy})_{ij} = (\phi_{yx})_{ij} = \frac{\phi_{i+j,j+1} - \phi_{i-1,j+1} - \phi_{i+1,j-1} + \phi_{i-1,j-1}}{4\Delta x\Delta y} \quad (4.6)$$

We now transform these terms using Eq. (4.1) and taking into account that the boundary conditions are cyclic. For example,

$$\begin{aligned} (\hat{\phi}_x)_{ij} &= \frac{1}{2\Delta x} \sum_{i=1}^{N_1} \sum_{j=1}^{N_2} (\phi_{i+1,j} - \phi_{i-1,j}) \\ &\quad \exp 2\pi i \left\{ [(i-1)(k-1)/N_1 + (j-1)(\ell-1)/N_2] \right\} \\ &= \frac{-i \sin |2\pi(k-1)/N_1|}{\Delta x} \hat{\phi}_{k\ell} \\ &= i S_k \hat{\phi}_{k\ell} \end{aligned}$$

Similarly, we obtain

$$(\hat{\phi}_y)_{ij} = i S_\ell \hat{\phi}_{k\ell}$$

$$(\hat{\phi}_{xx})_{ij} = C_k \hat{\phi}_{k\ell}$$

$$(\hat{\phi}_{yy})_{ij} = C_\ell \hat{\phi}_{k\ell}$$

(4.7)

and $(\hat{\phi}_{xy})_{ij} = -S_k S_\ell \hat{\phi}_{k\ell}$.

Where $S_k = -\sin [2\pi (k-1)/N_1]/\Delta x$

$$S_\ell = -\sin [2\pi (\ell-1)/N_2]/\Delta y$$

$$C_k = \frac{2}{\Delta x^2} \left\{ \cos [2\pi(k-1)/N_1] - 1 \right\}$$

and $C_\ell = \frac{2}{\Delta y^2} \left\{ \cos [2\pi(\ell-1)/N_2] - 1 \right\}$.

Using Eq. (4.7), the second and third equations of Eq. (4.3) and both equations of Eq. (4.5) can be transformed to the discretized Fourier space.

$$U_n \hat{u} - iU_z \hat{w} + \frac{S_k}{\rho} \hat{p} = 0$$

$$U_n \hat{v} - iV_z \hat{w} + \frac{S_\ell}{\rho} \hat{p} = 0$$

(4.8)

$$\hat{w}_z + (S-s)\hat{w} + i \left(S_k \hat{u} + S_\ell \hat{v} + \frac{U_n}{\rho C_s^2} \hat{p} \right) = 0$$

$$\left(U^2 C_k - 2S_k S_\ell UV + V^2 C_\ell + gS \right) \hat{w} + i \frac{U_n}{\rho} \left(\hat{p}_z + \frac{g}{C_s^2} \hat{p} \right) = 0$$

where $U_n = US_k + VS_\ell$

and the $k\ell$ subscript has been omitted from each of the transformed variables.

From the first three equations \hat{u} and \hat{v} can be eliminated to give

$$\hat{w}_z + \left(s - s - \frac{U_{nz}}{U_n} \right) \hat{w} - i \frac{U_n}{c} \left(\frac{S_k^2 + S_\ell^2}{U_n^2} - \frac{1}{C_s^2} \right) \hat{p} = 0. \quad (4.9)$$

By elimination of \hat{p} and \hat{p}_z between Eq. (4.8) and (4.9), we obtain a single equation for \hat{w} .

$$\hat{w}_{zz} - \left(s - \frac{\mu z}{\mu} \right) \hat{w}_z + \left(L'^2 - K^2 \right) \hat{w} = 0 \quad (4.10)$$

where

$$L'^2 = \frac{g}{U_s^2} \left(s + \frac{\mu z}{\mu} \right) - \frac{(U_s)_{zz}}{U_s} + \left(s + \frac{\mu z}{\mu} \right) \frac{(U_s)_z}{U_s}$$

$$K^2 = \left(-U^2 C_k + 2S_k S_\ell UV - V^2 C_\ell \right) \frac{\mu}{U_s^2}$$

$$U_s^2 = \frac{U_n^2}{S_k^2 + S_\ell^2}$$

(4.11)

$$\mu = 1 - \frac{U_s^2}{C_s^2}$$

The equations derived above are based on a difference formulation, which, for small wave numbers, would be expected to limit to a more familiar differential expression. Consequently, let us

examine the behavior of the following coefficients when the indices k and l are small.

$$S_k = - \frac{\sin[2\pi(k-1)/N_1]}{\Delta x} \approx \frac{2\pi(k-1)}{N_1 \Delta x} = - k_x$$

$$C_k = \frac{2}{\Delta x^2} \left\{ \cos [2\pi(k-1)/N_1] - 1 \right\} \approx - \left[\frac{2\pi(k-1)}{N_1 \Delta x} \right]^2 = - k_x^2 .$$

Similarly,

$$S_l \approx - k_y$$

(4.12)

$$C_l \approx - k_y^2 .$$

The discrete wave numbers k_x and k_y are defined in terms of the indices k and l and the lengths $x = N_1 \Delta x$ and $y = N_2 \Delta y$. These limiting values can be introduced in Eq. (4.11).

$$U_s^2 = \frac{(k_x^2 + k_y^2)}{k_x^2 + k_y^2} = u_n^2$$

$$\nu = \left(1 - \frac{u_n^2}{C_s^2} \right)$$

(4.13)

$$K^2 = (k_x^2 U^2 + 2k_x k_y UV + k_y^2 V^2) \left(1 - \frac{u_n^2}{C_s^2} \right) / u_n^2$$

$$L'^2 = \frac{g}{u_n^2} \left(s + \frac{\nu z}{\nu} \right) - \frac{(u_n) z z}{u_n} + \left(s + \frac{\nu z}{\nu} \right) \frac{(u_n) z}{u_n} .$$

These terms give the limiting form

$$w_{zz} - \left(s + \frac{\mu z}{\mu}\right) w_z + \left[L'^2 - (k_x^2 + k_y^2) \left(1 - \frac{u_n^2}{C_s^2}\right) \right] \hat{w} = 0. \quad (4.14)$$

In order to place Eq. (4.10) in a form convenient for numerical integration, we eliminate the first derivative term. Introducing the modified vertical velocity term,

$$\hat{W} = \left(\frac{\bar{\rho}}{\rho(0)} \frac{\mu(0)}{\mu} \right)^{1/2} \hat{w} \quad (4.15)$$

we obtain the familiar Scorer equation in canonical form.

$$\hat{W}_{zz} + [L^2 - K^2] \hat{W} = 0 \quad (4.16)$$

where

$$L^2 = L'^2 + \frac{1}{4} \left(s + \frac{\mu z}{\mu} \right)^2 + \frac{1}{2} \left(s + \frac{\mu z}{\mu} \right)_z.$$

In order to find the horizontal components of the perturbed wind velocity, the first two equations of Eq. (4.8) and (4.9) are used. Substituting for pressure, we obtain

$$\begin{aligned} u &= i \left\{ \frac{S_k \hat{w}_z}{\mu (S_k^2 + S_l^2)} + \left[\left(S - s - \frac{(U_s)_z}{U_s} \right) \frac{S_k}{\mu (S_k^2 + S_l^2)} + \frac{U_z}{U_n} \right] \hat{w} \right\} \\ v &= i \left\{ \frac{S_l \hat{w}_z}{\mu (S_k^2 + S_l^2)} + \left[\left(S - s - \frac{(U_s)_z}{U_s} \right) \frac{S_l}{\mu (S_k^2 + S_l^2)} + \frac{V_z}{U_n} \right] \hat{w} \right\}. \end{aligned} \quad (4.17)$$

Consequently, these quantities can be obtained directly when \hat{w} and its vertical derivative \hat{w}_z are known.

Boundary conditions are required at the top and bottom of the computational region. These conditions reflect the physical constraints that are imposed at these locations. At the surface, the flow is assumed to follow the terrain without taking account of dissipation in the boundary layer. In the linear approximation, the boundary condition is applied at $z = 0$. Here the unperturbed horizontal velocity is deflected by the sloping terrain inducing a vertical velocity.

$$w(0) = U(0) H_x + V(0) H_y . \quad (4.18)$$

We need the boundary condition for $\hat{W}(0)$, which is derived from Eq. (4.18) by replacing the derivatives by central difference approximations and performing the discrete Fourier transform

$$\begin{aligned} \hat{W}(0) &= i[U(0)S_k + V(0)S_\ell] \hat{H}_{k\ell} \\ &= iU_n(0) \hat{H}_{k\ell} . \end{aligned} \quad (4.19)$$

At the upper boundary, the physical condition is not understood as well. It is known that certain gravity waves may propagate into the stratosphere where at high altitude (~ 100 km) they are dissipated. Under other circumstances, the gravity waves may be substantially or completely reflected by adverse wind gradients. These two alternatives are crudely incorporated into the formulation by evaluating whether the solution displays exponential or oscillatory behavior at the upper boundary. In the former case, corresponding to the coefficient of \hat{W} in Eq. (4.16)

$$\left(K^2 - L^2 \right)_{z=z_T} > 0 . \quad (4.20)$$

The boundary conditions are given by

$$\hat{W}_z = -\sqrt{K^2 - L^2} \hat{W} .$$

For the second case, when

$$\left(K^2 - L^2 \right)_{z=z_T} < 0$$

the boundary conditions are chosen to correspond to upward propagating waves alone. These conditions are achieved when

$$W_z = i \sqrt{L^2 - K^2} \hat{W} \operatorname{sgn} (U_s) . \quad (4.21)$$

For numerical solution, the second-order ordinary differential Eq. (4.16) is decomposed into a set of four first-order equations (corresponding to real and imaginary parts of \hat{W}) and are solved using sixth-order Adams-Moulton Predictor-Corrector method, with starting procedure based on Roser's formula. The Fourier analysis and synthesis are performed by a version of the Cooley-Tukey algorithm. The one we use requires the dimension of the data in both directions to be an integral power of two. While it is possible to acquire a generalized algorithm for any arbitrary dimension, the computational expense will be higher.

In order to solve the boundary value problem Eq. (4.16), subject to conditions Eqs. (4.19) and (4.20) or (4.21), it is advantageous to reformulate the equation into an initial value problem for the purpose of numerical integration. First we notice that a general solution of

$$\hat{W}_{zz} + (L^2 - K^2) \hat{W} = 0$$

is given by

$$\hat{W} = au_1 + bu_2$$

with $u_1(z_T) = 1, u_{1z}(z_T) = 0$

$$\text{and } u_2(z_T) = 0, u_{2z}(z_T) = 1. \quad (4.22)$$

The quantity \hat{W} is complex and both real part \hat{W}_R and imaginary part \hat{W}_I obey the same equation (since $L^2 - K^2$ is real) and are given by

$$\begin{aligned} \hat{W}_R &= a_R u_1 + b_R u_2 \\ \hat{W}_I &= a_I u_1 + b_I u_2. \end{aligned} \quad (4.23)$$

The lower boundary condition Eq. (4.19) requires

$$\begin{aligned} \hat{W}(0) &= iU_n(0)\hat{H}_{k\ell} \\ &= -U_n(0)\hat{H}_I + iU_n(0)\hat{H}_R \\ &= \hat{W}_R(0) + i\hat{W}_I(0) \end{aligned}$$

$$\text{where } \hat{W}_R(0) = a_R u_1(0) + b_R u_2(0) = -U_n(0)\hat{H}_I \quad (4.24)$$

$$\text{and } \hat{W}_I(0) = a_I u_1(0) + b_I u_2(0) = U_n(0)\hat{H}_R.$$

$$\text{Case A: } \left(K^2 - L^2 \right)_{z_T} > 0.$$

In this case the upper boundary condition is given by Eq. (4.20) where Eq. (4.22) exhibits an exponential solution. Then at $z = z_T$

$$\frac{d\hat{W}}{dz} = -\sqrt{K^2 - L^2} \hat{W}.$$

In terms of coefficients a and b, this boundary condition translates to

$$b_R = -\sqrt{K^2 - L^2} a_R \quad (4.25)$$

$$b_I = -\sqrt{K^2 - L^2} a_I .$$

Both a and b can be evaluated from Eq. (4.24) and (4.25). Substituting in Eq. (4.23), we then get the solution

$$\begin{aligned} \hat{W}_R &= -\bar{u}(z)U_n(o)\hat{H}_I/\bar{u}(o) \\ \hat{W}_I &= \bar{u}(z)U_n(o)\hat{H}_R/\bar{u}(o) \end{aligned} \quad (4.26)$$

where $\bar{u}(z) = u_1(z) - \left(K^2 - L^2\right)^{\frac{1}{2}}_{z=z_T} u_2(z) .$

The quantity $\bar{u}(z)$ is obtained by solving the following initial value problem:

$$\bar{u}_{zz} + \left(K^2 - L^2\right) \bar{u} = 0$$

with $\bar{u}(z_T) = 1$

and $\bar{u}_z(z_T) = -\left(K^2 - L^2\right)^{\frac{1}{2}}_{z=z_T} . \quad (4.27)$

Case B: $\left(K^2 - L^2\right)_{z_T} < 0 .$

For this case the upper boundary condition is given by

$$\frac{d\hat{W}}{dz} = i \operatorname{Sgn}(U_S) \left(L^2 - K^2\right)^{\frac{1}{2}} \hat{W} .$$

In terms of coefficients a and b, this condition can be written as

$$\begin{aligned} b_R &= - \text{Sgn}(U_S) \sqrt{L^2 - K^2} a_I \\ b_I &= \text{Sgn}(U_S) \sqrt{L^2 - K^2} a_R \end{aligned} \quad (4.28)$$

As before, a and b can be evaluated from Eq. (4.24) and (4.28) and then substituted in Eq. (4.23) to give the following solution

$$\begin{aligned} \hat{W}_R &= X_O \left\{ \left[X_T u_2(o) \hat{H}_R - u_1(o) \hat{H}_I \right] u_1(z) \right. \\ &\quad \left. - \left[X_T u_1(o) \hat{H}_R + X_T^2 u_2(o) \hat{H}_I \right] u_2(z) \right\} \\ \hat{W}_I &= X_O \left\{ \left[u_1(o) \hat{H}_R + X_T u_2(o) \hat{H}_I \right] u_1(z) \right. \\ &\quad \left. + \left[X_T^2 u_2(o) \hat{H}_R - X_T u_1(o) \hat{H}_I \right] u_2(z) \right\} \end{aligned}$$

Where

$$\begin{aligned} X_O &= \frac{U_n}{u_1^2 + (L^2 - K^2) u_2^2} \Big|_{z=0} \\ X_T &= \text{Sgn}(U_S) (L^2 - K^2)^{\frac{1}{2}} \Big|_{z=z_T} \end{aligned} \quad (4.29)$$

Unlike Case A, here we have to solve two initial value problems for u_1 and u_2 subject to initial values given by Eq. (4.22). In actual computation z_T is taken at the top of the computational region unless a critical level (where U_S vanishes) is detected at a lower altitude, in which case z_T is taken at the closest vertical mesh below the critical layer and reflection or absorption condition is applied there. Integration of Eq. (4.16) then ranges only between the ground and the critical level.

4.2 LINMET SIMULATIONS

As a first step LINMET calculations are compared to simple analytic solutions of the differential equations Eq. (4.14). Under neutral atmospheric conditions with constant horizontal velocity U_0 , the solution to Eq. (4.14) in two-dimensions subject to boundary conditions similar to those given by Eq. (4.19) and (4.20) can be obtained as:

$$\hat{w}(z) = - ik_x U_0 \hat{H} \exp(-k_x z) \quad (4.30)$$

and the horizontal perturbation velocity can be obtained as

$$\hat{u}(z) = - k_x U_0 \hat{H} \exp(-k_x z) \quad (4.31)$$

Table 4.1 shows the computed vs. the analytic results for the horizontal surface velocity $\hat{u}(0)$ for different modes. The comparison is good, and the difference is mainly because of discretization. Note that the analytic solution is for the differential equation, Eq. (4.14), whereas the LINMET solution is based on the difference equation, Eq. (4.16).

Klemp and Lilly (1975) have obtained an analytic solution of their hydrostatic model with constant stability and constant velocity U_0 (one-layer atmosphere). They have shown that

$$\begin{aligned} \hat{u}(0) &= N\hat{H} \\ &= \left(-\frac{g}{T_0} \frac{\partial T}{\partial z}\right)^{\frac{1}{2}} \hat{H} \end{aligned} \quad (4.32)$$

LINMET, which solves the nonhydrostatic problem, was modified by setting $K = 0$ to compare the results with Eq. (4.32). The computed vs. the analytic values are tabulated in Table 4.2. The agreement is again very close.

Table 4.1 LINMET vs. Analytic Results for $\hat{u}(o)$.

Wave Number	LINMET Result	Analytic Result
2	-63.26	-60.19
3	18.22	17.68
4	- 2.08	- 1.98
5	- 0.72	0.07

Table 4.2 LINMET vs. Analytic Results for $\hat{u}(o)$ for the One-Layer Model.

Wave Number	LINMET Result	Analytic Result
2	-403.87	-401.10
3	60.46	60.05
4	- 4.67	- 4.64
5	- 1.22	- 1.22

As before, the PASS measurement records for the day 19 November 1974 were used for LINMET simulations, since the day was characterized by relatively high winds and a near neutral lapse rate. The structure of the wind field in the area is indicated by the upper air records of east-west and north-south wind components and temperature presented for eight stations in Figures 2.4 through 2.11. The region of the solution domain is indicated in Figure 2.15, which is 155 km wide in both north-south and east-west directions. As shown, the area is approximated by 32 x 32 grids, with 5 km grid spacings in both directions. The southwest corner is located at local UTM coordinates (340 km, 3570 km). A linear boundary smoother is utilized, which sets the boundary of the region at the constant level of 1200 m MSL to avoid abrupt discontinuity from periodic boundary conditions. The top of the computing mesh is set at 5000 m MSL, and the bottom of the computing region is chosen at the mean height of the terrain, which is 1355 m. The vertical zoning utilizes 20 levels with uniform grid size of 192 m. We have not carried out any sensitivity test with respect to vertical zoning and the height of the computing mesh, but we believe that under certain conditions the solution will be sensitive to finer zoning and a larger computing domain.

For the first simulation, LINMET was initialized with the soundings from TSX. The perturbation surface velocity vector plot is shown in Figure 4.28. This is repeated for the 385 m AGL and 3261 m AGL in Figures 4.29 and 4.30, respectively. The contour of normal velocity component (which is not shown here) reflects the zero normal velocity boundary condition, resulting in positive vertical velocity upslope on the San Andres and Sacramento Mountains and negative vertical velocity downslope. At a higher level (395 m above mean height of the terrain), Figure 4.29 shows higher disturbance horizontal velocity on the slopes but almost zero velocity in the valleys where the terrain is flat. This picture remains unchanged even at high levels such as in the ones shown in Figure 4.30, which corresponds to 3261 m AGL. This is because of the atmospheric

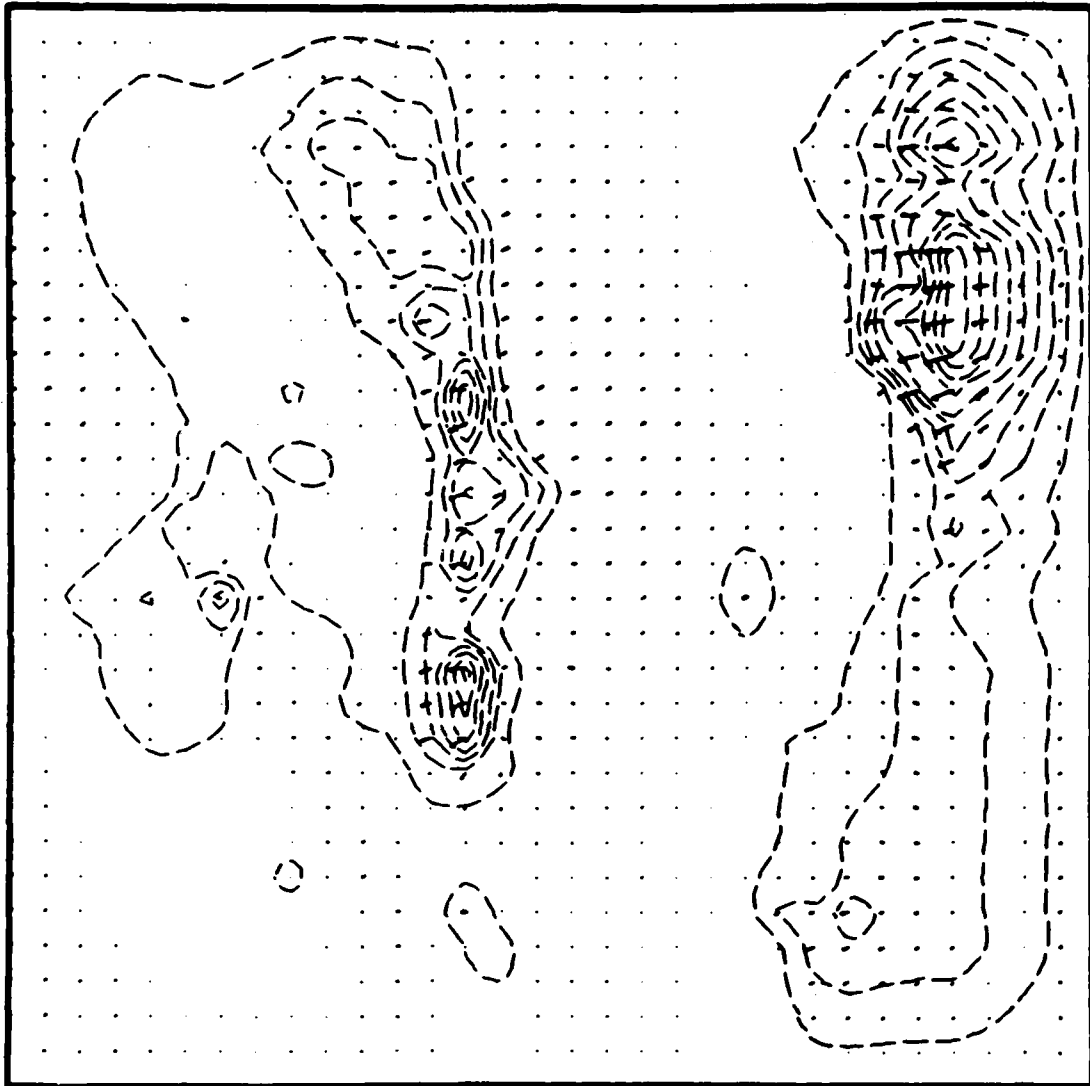


Figure 4.28 Perturbation Surface Horizontal Velocity Vector Plot for the White Sands Region. Flow Field was Initialized using Data from Station TSX on 11/19/74.

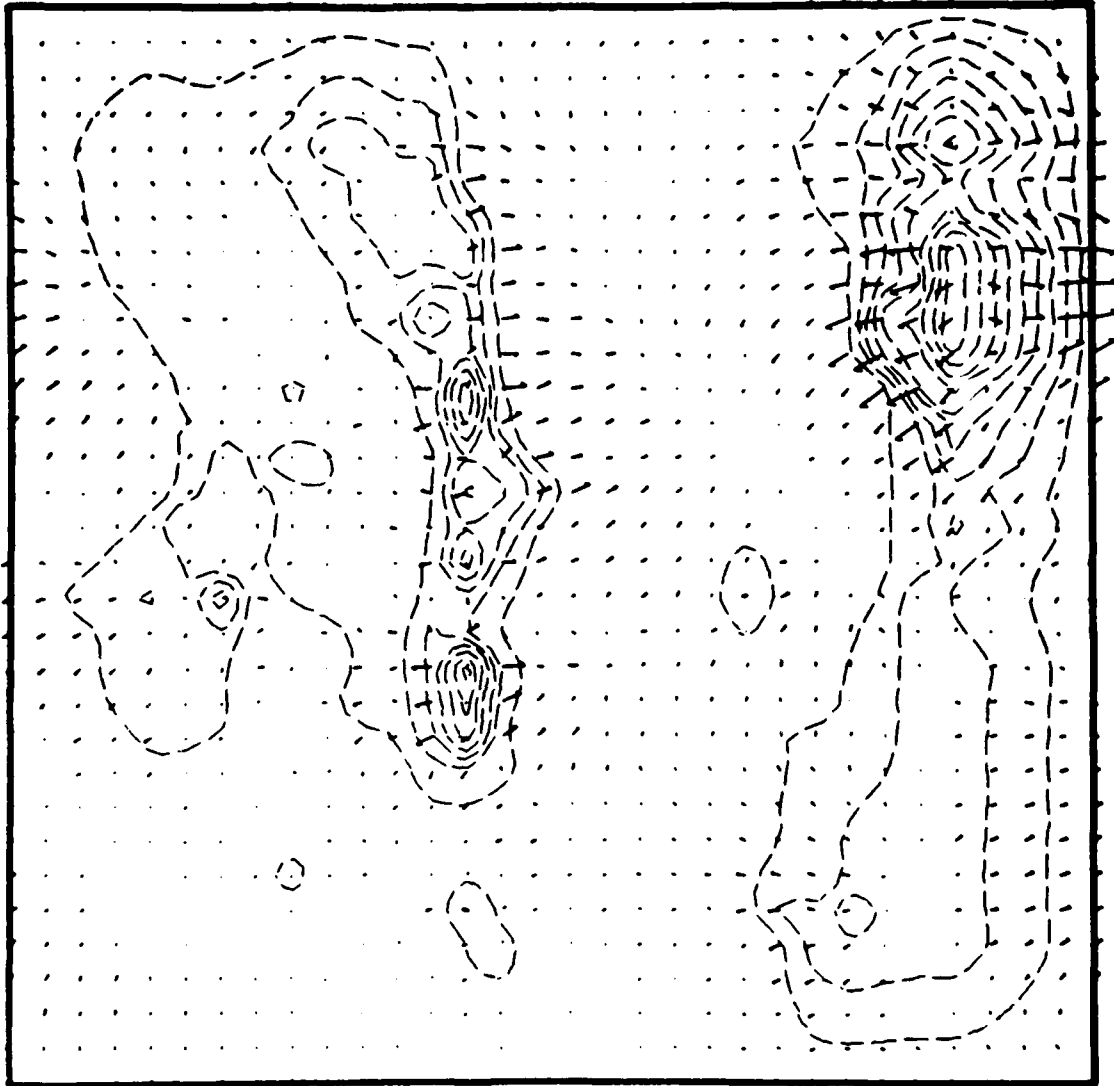


Figure 4.29 Perturbation Horizontal Velocity Vector Plot at 385.m above Mean Terrain over White Sands Region. Flow Field was Initialized using Data from Station TSX on 11/19/74.

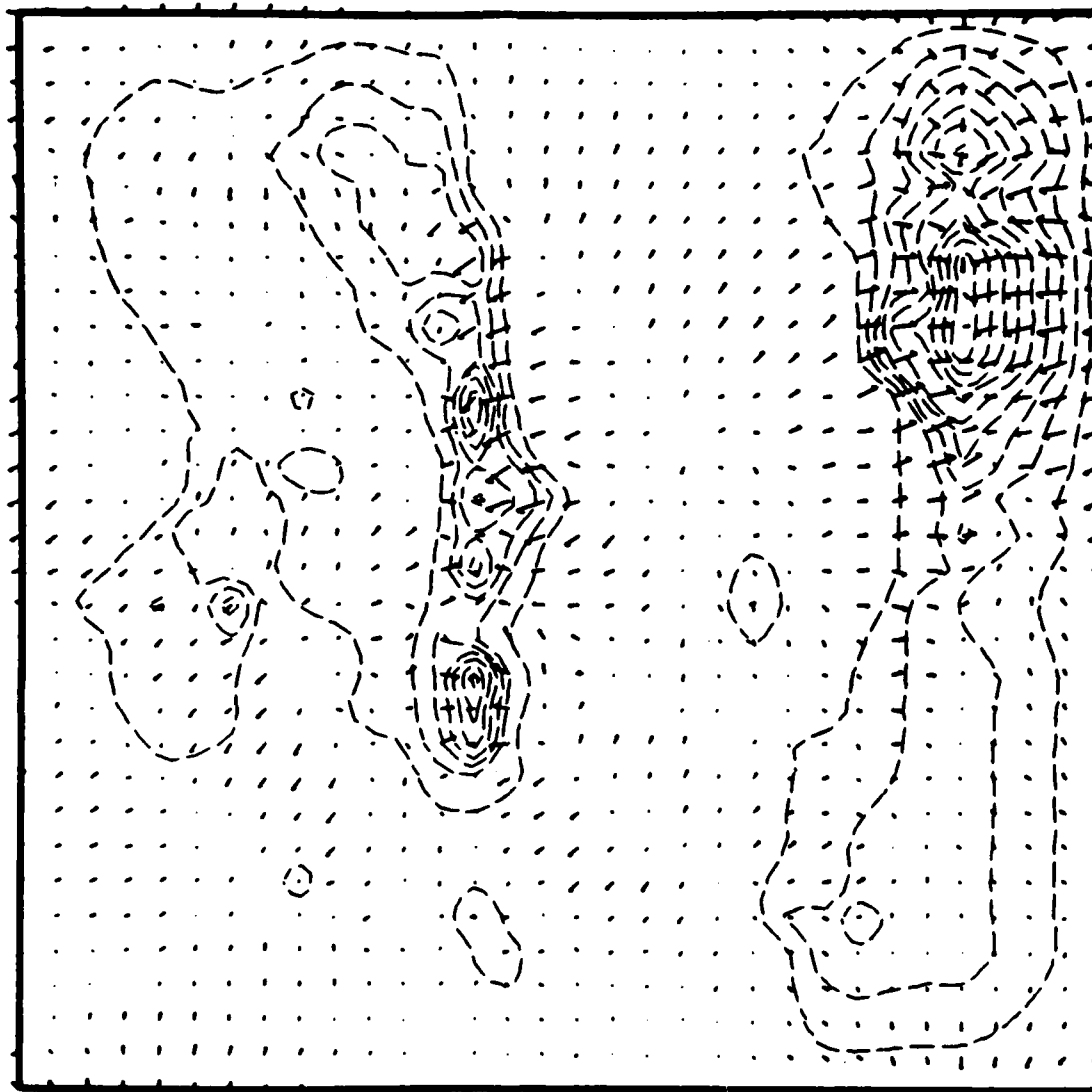


Figure 4.30 Perturbation Horizontal Velocity Vector Plot at 3261.m above Mean Terrain over White Sands Region. Flow Field was Initialized using Data from Station TSX on 11/19/74.

conditions on that day, which permitted outgoing waves at the upper boundary. This causes the disturbance to propagate up without any reflection. The linear model obviously cannot exhibit any low-level turning that could be expected because of early morning low-level inversion (~200 m) as shown by the temperature data at TSX.

The second simulation was made by initializing with measurement data from station ORO. The location of ORO is close to TSX, and both are located in the Tularosa Valley. Wind and temperature at ORO are close to those at TSX, and the simulation did not exhibit any new trend or feature.

The third simulation was made by initializing LINMET with data from station RAM. For this simulation, velocity vector plots are shown for the surface level, 385 m level and 3261 m level in Figures 4.31 through 4.33, respectively. The low level flow in the simulation, when superimposed on the ambient wind, looks very close to the VARMET stable simulation (presented in Chapter 5) using upper air data for all eight stations (Figure 5.2).

We have encountered problems in initializing LINMET with WAR, SMR, and HMS data. Insufficient vertical resolution, along with possible occurrence of resonant modes resulting in large amplitude waves (Klemp and Lilly, 1975) could have caused this. The problem could be resolved by employing finer vertical grid spacings and extending the horizontal domain of computation.

The limited area chosen from the West German region for simulation is shown by Figure 2.14. The area is approximated by 32 x 32 grids with 1 km grid spacing in both directions. The southwest corner of this area is located at local UTM coordinates (526.2 km, 5584.3 km). The linear boundary smoother is applied to a boundary strip 5 km wide, which sets the boundary terrain heights at a constant value of 400 m. The top of the computing region is set at 5000 m MSL and the bottom at 379 m MSL, which is the average height of the region. The vertical zoning utilizes 20 levels with uniform grid size of 243 m.

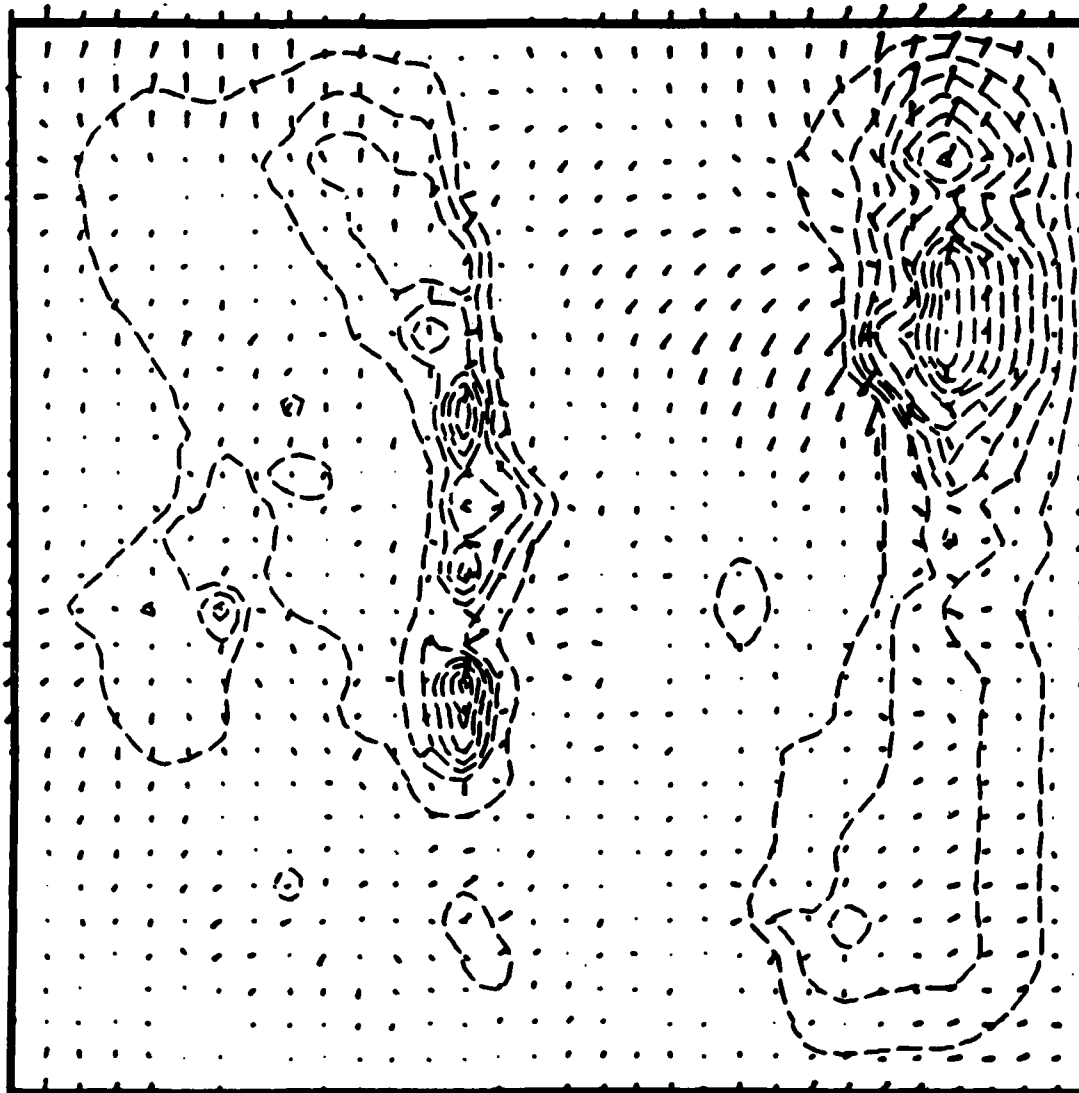


Figure 4.31 Perturbation Surface Horizontal Velocity Vector Plot for the White Sands Region. Flow Field was Initialized using Data from Station RAM on 11/19/74.

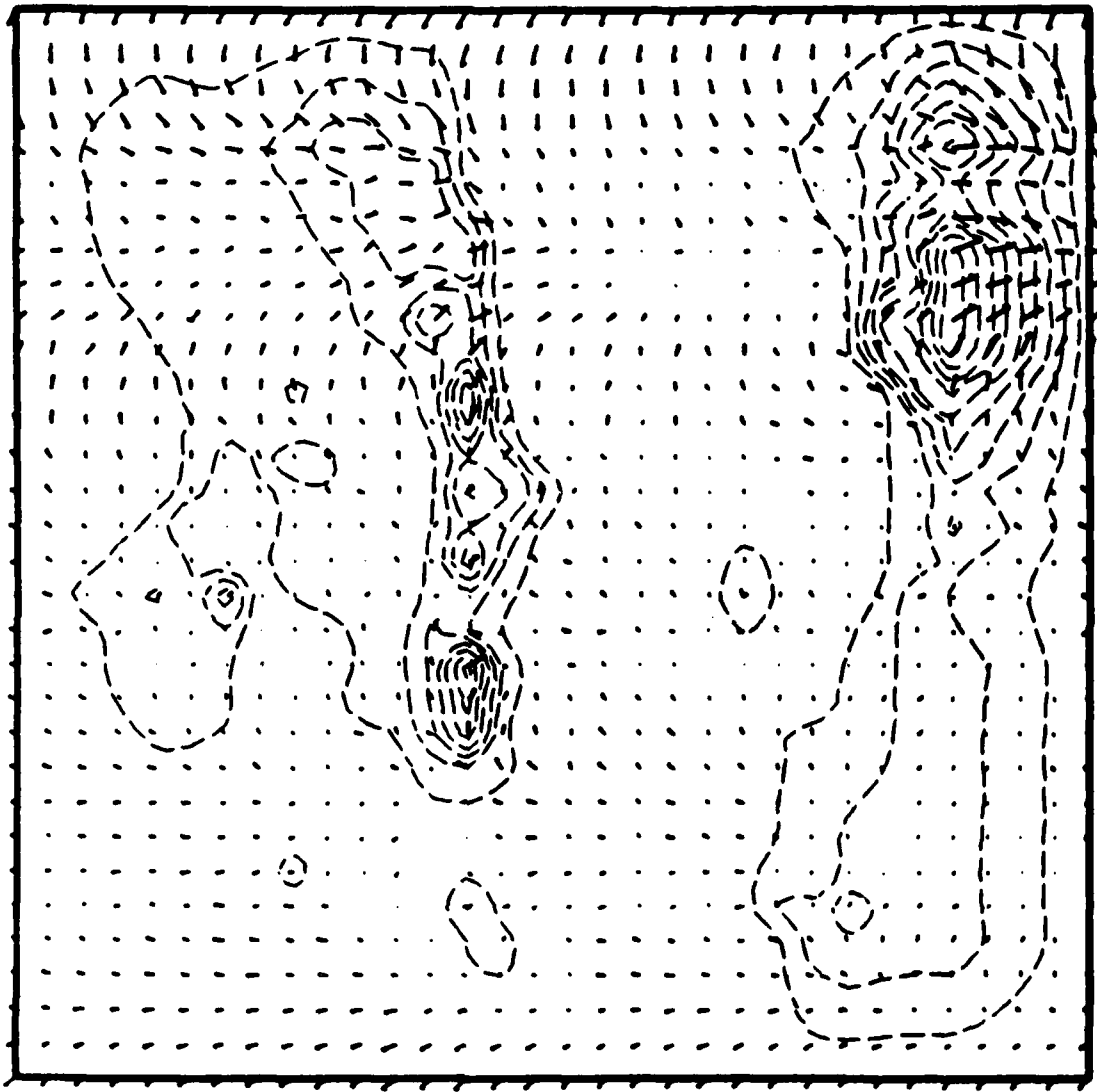


Figure 4.32 Perturbation Horizontal Velocity Vector Plot at 385 m above Mean Terrain over White Sands Region. Flow Field was Initialized using Data from Station RAM on 11/19/74.

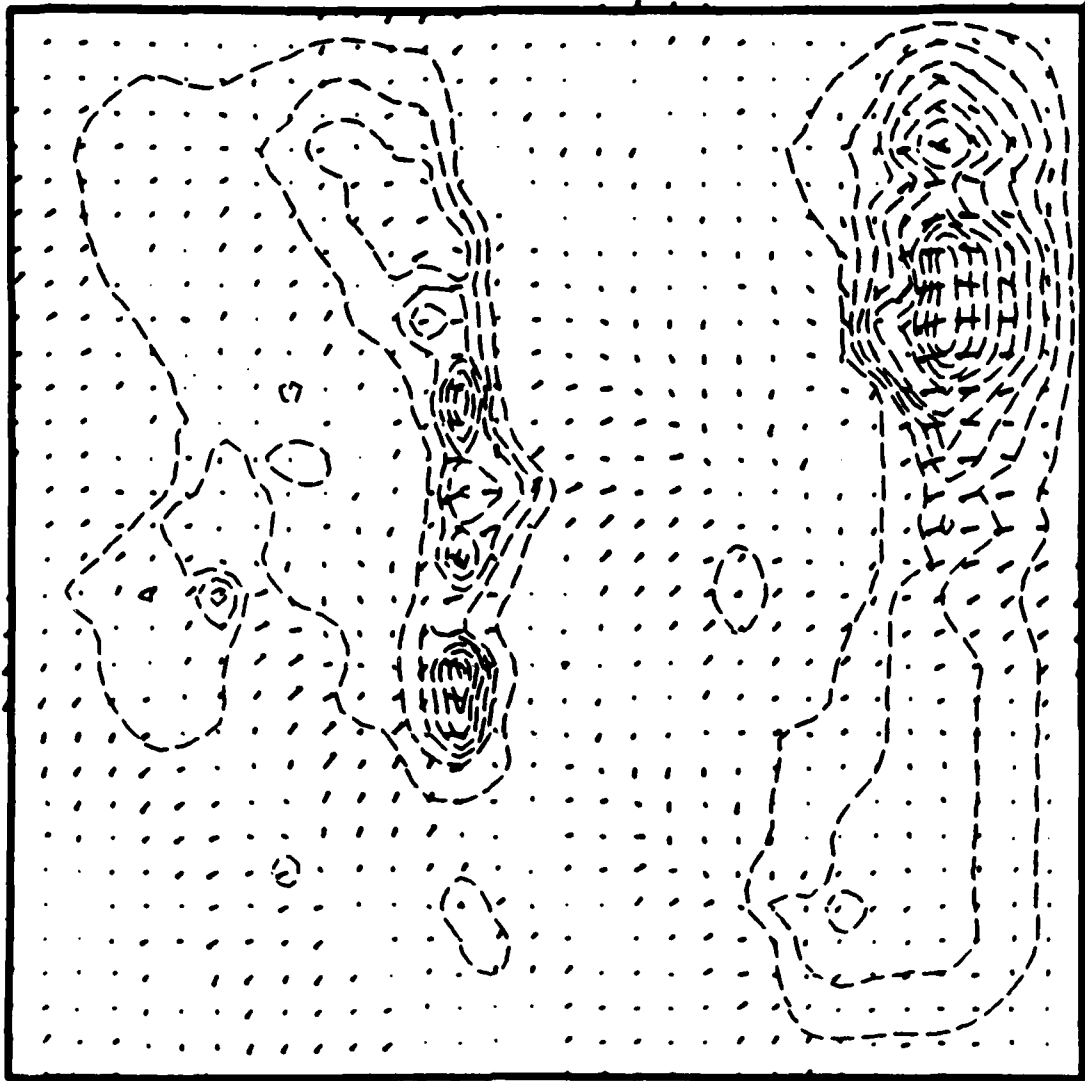


Figure 4.33 Perturbation Horizontal Velocity Vector Plot at 3261 m above Mean Terrain over White Sands Region. Flow Field was Initialized using Data from Station RAM on 11/19/74.

Using the upper air soundings from Meiningen, East Germany (Figure 2.16), which is east of the region of simulation, a LINMET simulation was carried out. Figure 4.34 shows the surface perturbation velocity vector for this simulation. This plot shows some oscillations that are believed to be related to the finite extent of the horizontal domain. Even though the terrain in question is without large gradients, sometimes it is necessary to extend the computing domain to great distance over flat terrain to effectively treat the lee waves, which may otherwise be truncated with periodic boundary conditions over the limited terrain. The smaller horizontal grid size (1000 m) could pose a limitation for hydrostatic models, but as LINMET is a nonhydrostatic model this limitation does not apply. More experiments and sensitivity studies must be carried out before definite conclusions can be reached.

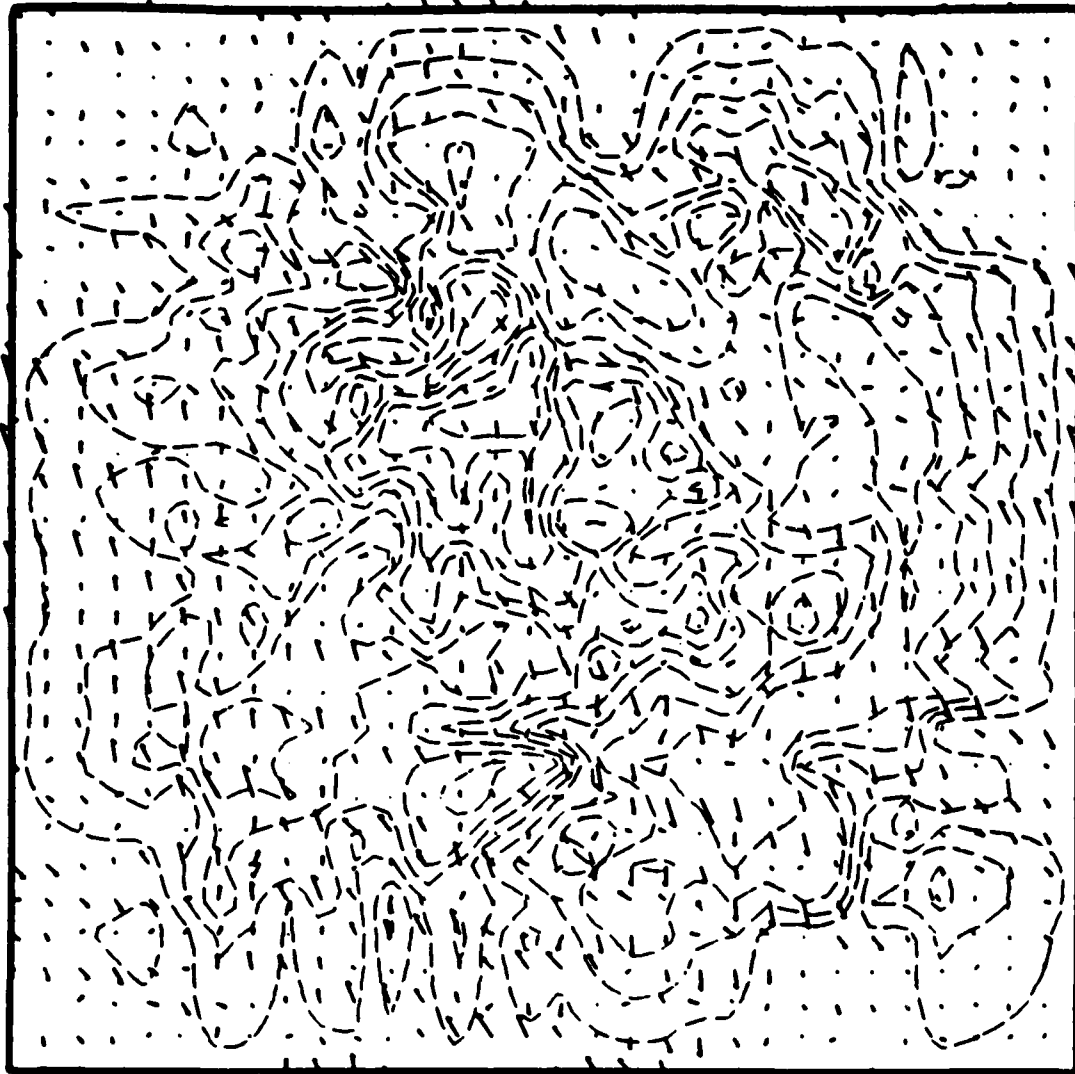


Figure 4.34 Perturbation Surface Horizontal Velocity Vector Plot for the West Germany Region containing Fulda. Flow Field was Initialized using Upper Air Data from Meiningen, East Germany.

5. OBJECTIVE ANALYSIS MODEL VARMET

In this category of simplified models, one follows a procedure of interpolation and extrapolation first to determine an estimated wind field from observed data. This field is then adjusted to account for terrain effects and atmospheric stability considerations constrained by the condition that the resulting wind field be nondivergent. In addition to the mass conservation constraint, one can impose momentum and energy conservation constraints as well, but at the cost of added complication and computing expense. The accuracy so gained may be lost if there is considerable uncertainty in the observed data. In the formulation to follow, we have therefore restricted our work to the mass conserving wind-field models.

5.1 VARMET FORMULATIONS

The theoretical basis for the model was developed by Sasaki (1970) and later used in this context by Sherman (1977). For this model the squared variation of the wind field is minimized subject to the constraint that the adjusted field be non-divergent. The irregular surface boundary $z = z_s(x,y)$ is first removed for computational purposes by a coordinate transformation in which the surface becomes a coordinate surface as well. It is convenient to perform a nonorthogonal transformation in which only the vertical coordinate z is replaced by a function σ , which depends on x, y as well as z . The new coordinate is taken linear in z :

$$\sigma = \frac{z_T - z}{z_T - z_s} = \frac{z_T - z}{\pi} \quad (5.1)$$

where z_T is the constant altitude of the top mesh and z_s is the terrain surface. The values of σ are in the range of

$0 \leq \sigma \leq 1$ ($\sigma=0$ corresponds to the top of the mesh, $\sigma=1$ corresponds to the surface). The variation integral written in the x-y-z frame is

$$I = \iiint \left\{ \alpha_1^2 \left[(u-u_0)^2 + (v-v_0)^2 \right] + \alpha_2^2 (w-w_0)^2 + \lambda \left(\frac{\partial u}{\partial x} + \frac{\partial v}{\partial y} + \frac{\partial w}{\partial z} \right) \right\} dx dy dz , \quad (5.2)$$

where α_1, α_2 are the gauss precision moduli (proportional to $1/(2\beta^2)$, β being observation error and/or deviation of the observed field from the desired adjusted field), and λ is the Lagrange multiplier. The observed field is represented by $u_0, v_0,$ and w_0 . The weights α may be parametrized, that is, constants for a given trial but may vary from trial to trial. More generally, the weights should be a function of position within the region, being large in the vicinity of the actual observation and small in regions remote from observations. The ratio (α_1/α_2) can be viewed as a stability parameter also. Since in a strongly stable flow, the vertical motion is inhibited, (α_1/α_2) should be assigned a low value for stable ambient condition. The ratio equal to one should be chosen for neutral flow condition since there is no preferential direction for motion under those conditions. The associated Euler-Lagrange equations to minimize I can be written as

$$\begin{aligned} 2\alpha_1^2 (u-u_0) - \frac{\partial \lambda}{\partial x} &= 0 , \\ 2\alpha_1^2 (v-v_0) - \frac{\partial \lambda}{\partial y} &= 0 , \\ 2\alpha_2^2 (w-w_0) - \frac{\partial \lambda}{\partial z} &= 0 . \end{aligned} \quad (5.3)$$

From the nature of the coordinate transformation in Eq. (5.1), we can derive expressions for partial derivatives of an arbitrary function f in the two representations.

$$\begin{aligned} \left(\frac{\partial f}{\partial x}\right)_{y,z} &= \left(\frac{\partial f}{\partial x}\right)_{y,\sigma} + \frac{\sigma}{\pi} (z_s)_x \left(\frac{\partial f}{\partial \sigma}\right)_{x,y}, \\ \left(\frac{\partial f}{\partial y}\right)_{x,z} &= \left(\frac{\partial f}{\partial y}\right)_{x,\sigma} + \frac{\sigma}{\pi} (z_s)_y \left(\frac{\partial f}{\partial \sigma}\right)_{x,y}, \\ \left(\frac{\partial f}{\partial z}\right)_{x,y} &= -\frac{1}{\pi} \left(\frac{\partial f}{\partial \sigma}\right)_{x,y}. \end{aligned} \quad (5.4)$$

The subscripts on partial derivatives indicate which variables are being held constant during differentiation, and

$$(z_s)_x = \frac{\partial z_s}{\partial x} \quad \text{and} \quad (z_s)_y = \frac{\partial z_s}{\partial y}.$$

Using this coordinate transformation, the Euler-Lagrange equation, Eq. (5.3), can be rearranged as follows:

$$\begin{aligned} u &= u_0 + \frac{1}{2\alpha_1^2} \left[\frac{\partial \lambda}{\partial x} + \frac{\sigma}{\pi} (z_s)_x \frac{\partial \lambda}{\partial \sigma} \right] \\ v &= v_0 + \frac{1}{2\alpha_1^2} \left[\frac{\partial \lambda}{\partial y} + \frac{\sigma}{\pi} (z_s)_y \frac{\partial \lambda}{\partial \sigma} \right] \\ w &= w_0 - \frac{1}{2\alpha_2^2} \left[\frac{1}{\pi} \frac{\partial \lambda}{\partial \sigma} \right]. \end{aligned} \quad (5.5)$$

Also using the transformation, the divergence-free condition $\nabla \cdot \underline{u} = 0$, or

$$\frac{\partial u}{\partial x} + \frac{\partial v}{\partial y} + \frac{\partial w}{\partial z} = 0$$

takes the form in σ - coordinate

$$\frac{\partial \pi u}{\partial x} + \frac{\partial \pi v}{\partial y} + \frac{\partial \pi \tilde{w}}{\partial \sigma} = 0 \quad (5.6)$$

where,

$$\pi \tilde{w} = \sigma (z_{S_x} u + z_{S_y} v) - w \quad (5.7)$$

The Eq. (5.6) is written in the so-called "conservative form," in which flux analogy can be directly applied. This form is useful in forming difference equations which are more accurate through being constrained to conserve mass in the difference equations.

We now can eliminate u , v , and w in Eq. (5.6) by using Eq. (5.5) and (5.7) to arrive at the following equation in λ .

$$\begin{aligned} & \frac{\partial}{\partial x} \left[\pi \frac{\partial \lambda}{\partial x} + \sigma z_{S_x} \frac{\partial \lambda}{\partial \sigma} \right] + \frac{\partial}{\partial y} \left[\pi \frac{\partial \lambda}{\partial y} + \sigma z_{S_y} \frac{\partial \lambda}{\partial \sigma} \right] \\ & + \frac{\partial}{\partial \sigma} \left\{ \left(\frac{\alpha_1}{\alpha_2} \right)^2 + \sigma^2 (z_{S_x}^2 + z_{S_y}^2) \right\} \frac{1}{\pi} \frac{\partial \lambda}{\partial \sigma} \\ & + \sigma \left\{ z_{S_x} \frac{\partial \lambda}{\partial x} + z_{S_y} \frac{\partial \lambda}{\partial y} \right\} \Big] = -2\alpha_1^2 \left[\frac{\partial \pi u_0}{\partial x} + \frac{\partial \pi v_0}{\partial y} + \frac{\partial \pi \tilde{w}_0}{\partial \sigma} \right] \quad (5.8) \end{aligned}$$

The boundary conditions for the above consistent with minimization of I are given by

$$\lambda \delta(u_n) = 0 \quad (5.9)$$

where $\delta(u_n)$ is the variation of the velocity component normal to the boundary. When λ is zero on the boundary, its normal derivative, in general, is not zero and results in a new normal

boundary velocity different from the initial guessed value. Therefore $\lambda = 0$ is appropriate for "open boundaries." On the other hand, when u_n is held fixed, the Euler-Lagrange equations imply that the normal derivative of λ should vanish. This may be appropriate for "no-flow-through" boundaries. Clearly, the latter is applicable to top and bottom boundaries where $\tilde{w} = 0$. On the lateral sides, either kind of boundary conditions may apply, largely depending on the density of observation data near the boundaries. Observation data are usually available at a few stations. These values should be judiciously used to estimate u_0 , v_0 , and w_0 at all grid points through a process of interpolation/extrapolation. One such method, which is presently being used, is described in Section 2.

At present on all four lateral sides

$$\lambda = 0 \tag{5.10}$$

is used. At top and bottom $\tilde{w} = 0$ or $w = \sigma(z_{Sx}u + z_{Sy}v)$ condition is used. Using Eq. (5.5) and (5.7), this translates to

$$\frac{\partial \lambda}{\partial \sigma} = 0 \quad \text{at the top, and}$$

$$\frac{\partial \lambda}{\partial \sigma} = -\pi \left[2\alpha_1^2 \pi \tilde{w}_0 + z_{Sx} \frac{\partial \lambda}{\partial x} + z_{Sy} \frac{\partial \lambda}{\partial y} \right] / \left[\left(\frac{\alpha_1}{\alpha_2} \right)^2 + z_{Sx}^2 + z_{Sy}^2 \right] \tag{5.11}$$

at the bottom.

The Eq. (5.8), which is a Helmholtz's equation for λ along with the boundary conditions Eq. (5.10) and (5.11), completes formulation of the problem. In practice, iterative methods

making use of over-relaxation technique are employed to solve the system. The numerical procedure is described below.

A staggered grid network is used to discretize the Helmholtz Equation, Eq. (5.8), for numerical solution. In a cube with sides Δx , Δy , and $\Delta \sigma$, the u , v , and w components of the velocity are defined at the center of the faces normal to x , y , and σ directions, respectively. The Lagrange multiplier λ is defined at the geometric center of the cube. With this staggering, one can write a very compact finite difference equation approximating Eq. (5.8) with minimum truncation. The equation can be solved by the method of Successive-Point-Over-Relaxation with an optimum value for successive parameter ω . The rate of convergence strongly depends on the aspect ratio of the mesh, modified by α_1 and α_2 , namely,

$$\left[\frac{\text{Max} (\Delta x, \Delta y)}{\pi_{\text{min}} \Delta \sigma_{\text{min}}} \frac{\alpha_1}{\alpha_2} \right]^2$$

Typically, this value is very large compared to unity (partly because vertical zone size is much smaller than the horizontal zone), resulting in no or very slow convergence. Other investigators, while following such formulation, have been plagued by the same problems in the past. We, therefore, made use of Line-Over-Relaxation in which the λ values in a given vertical column are calculated simultaneously rather than successively. Because only terms involving second or lower derivatives with respect to σ appear in Eq. (5.8), the implicit treatment in σ -direction results a system of tridiagonal equations in the discretized space, one for each column. These can be readily solved using the well-known Gaussian elimination procedure. This method of solution for Eq. (5.8) converges reasonably fast to yield a divergence-free solution for the velocity field, and adding very little to overall computation expense.

The implicit line relaxation method in VARMET, while making the solution insensitive convergence-wise to physical modeling parameters such as α_1/α_2 and surface slopes, shows instability for small values of α_1/α_2 ($\alpha_1^2/\alpha_2^2 < 0.01$). Since $\alpha_1/\alpha_2 \rightarrow 0$ decouples the equations in the vertical direction, a situation typical under strong stable atmospheric condition, the resulting reduction in the dimensionality of the problem can possibly explain this instability in the relaxation scheme. In any event, we have found that the addition of an explicit damping term stabilizes the solution in such cases. The form of the damping,

$$f \left(\frac{\alpha_1}{\alpha_2} \right)^2 \left(\frac{\Delta x}{\Delta \sigma} \right)^2 \frac{1}{\pi^2}$$

was chosen to be added to Eq. (5.8) based on the magnitude of the terms in the difference expressions used in the iterative scheme. It has been found that a value of $f \sim 0.05$ to 0.10 provides sufficient stabilization while retaining acceptable convergence. This may vary from problem to problem; however, no general parameterization has been developed to date.

5.2 VARMET SIMULATIONS

The procedure is applied to the wind data obtained from PASS experiment on 19 November over the limited White Sands terrain defined by the dashed lines in Figure 3.3. The coefficients α_1 and α_2 , which are believed to be stability-dependent, but the precise nature of which is yet to be evaluated, are set equal to each other. The over-relaxation parameter ω is set to a constant value of 1.7. In the east-west directions 38 grid points, and in the north-south directions 32 grid points, are employed with an equal grid interval of 25 km. The southwest corner (as shown by the dashed lines in Figure 3.3) is located at the local UTM coordinates, 337.5 km east and 3562.5 km north. In the vertical,

12 zones are used with nonuniform zone thickness defined by a geometric progression with 1.37 expansion ratio, the one nearest to the surface being approximately 30 m and the farthest one being 1000 m. The top of the computing mesh is set at a constant altitude of 4800 m MSL, and the convergence criterion for λ is set at 10^{-3} for all the simulations. The program makes use of a graphics package to prepare vector and contour plots of various quantities of interest at user-specified intervals on microfiche. A typical run on this grid takes about 80-100 iterations to converge and uses about 40 CP sec on a CDC 7600 computer, which includes the time spent in graphics.

In an effort to carry out a systematic verification over the White Sands region, we have built a simulation matrix designed to investigate the efficacy of the extrapolation technique for utilizing surface station wind data as well as the overall simulation accuracy with various numbers of data stations. Figure 5.1 defines the 10 cases that make up the matrix. In the matrix, u indicates that the actual air record (interpolated to the finite difference grid locations) was used in the wind-field initialization, s indicates that the data were used as a surface station (see below), and x indicates that the data were unused in the initialization and is thus available for comparison with the calculated results.

The use of surface stations requires some explanation, since in most applications of the model only near-surface winds will be available. In the usual treatment of such data in VARMET, the near-surface wind is extrapolated in the vertical as follows. The wind is assumed to take on an equilibrium boundary layer profile with power-law β (which may depend on terrain, surface roughness, stability, etc.) up to an arbitrary boundary layer height [0(200 m)], then a linear interpolation of wind speed and angle is used up to some assumed uniform high level winds at the top of the computational mesh. In the present calculations, this procedure was used by taking the lowest value in the

		Data Station							
		1	2	3	4	5	6	7	8
CASE	TSX	ORO	WAR	SMR	LSC	RAM	APA	HMS	
1	u	u	u	u	u	u	u	u	u
2	s	u	s	u	u	s	s	u	
3	x	u	x	u	u	x	x	u	
4	s	s	s	u	s	s	s	u	
5	x	x	x	u	x	x	s	u	
6	s	s	s	u	s	s	s	s	
7	u	x	s	u	u	s	s	u	
8	x	x	x	u	x	s	s	x	
9	x	u	x	u	x	u	x	x	
10	u	x	u	x	u	x	u	u	

u data station used, s: used as surface station, x: unused

Figure 5.1 Matrix of Verification Simulations for 11/19/74.

upper air record (usually ~200 m above ground) and extrapolating within a 200 m AGL boundary layer with $\beta = 1/7$ and extrapolated above the boundary layer using an assumed average value for the high level wind. It should be mentioned that the 200 m value for the boundary layer thickness is typical of what would be assumed if nothing were known about the wind profile so that it does not presuppose knowledge of the upper air records. Also, the values of the upper level wind speed/direction were taken as a rough average of all the upper air soundings, but an equally representative value could be determined from the gradient wind approximation to synoptic weather data in the general case. Thus, it is not believed that this choice will bias the results.

Cases 2, 4, and 6 in the test matrix were chosen to compare overall flow results utilizing 4, 6 and 7 stations taken as surface stations, respectively. Case 1, of course, used all of the upper air records and represents the "best estimate" of the wind field for the 19 November 1974 event and therefore serves as a basis for comparison for the other cases. Wind field vector and speed contour plots are presented for Cases 1, 2, 4, and 6 in Figures 5.2 through 5.5, respectively, for the near surface (15 m AGL) flow. The heavy arrows in each vector plot correspond to the original data at each station interpolated to the 15 m AGL level. Comparison of the results shows very good qualitative and quantitative correspondence of the flow in each case. Even Case 6, which uses only one actual upper air record (station SMR) and seven surface station prescriptions, compares well with the Case 1 baseline result, especially in terms of magnitude of wind speed, throughout the solution region.

It should be reiterated that the surface station prescription used the single element of the raw data record that corresponded to ~200 m AGL. In the data record for RAM, there was substantial variation in the data below this level. Thus, it is not surprising that the simulations using surface stations miss some details of

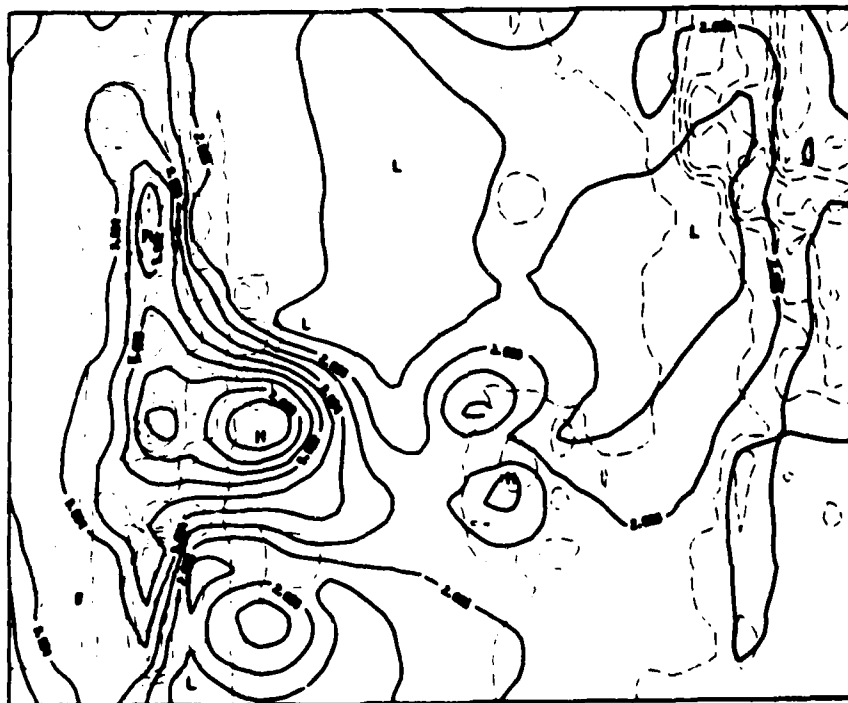
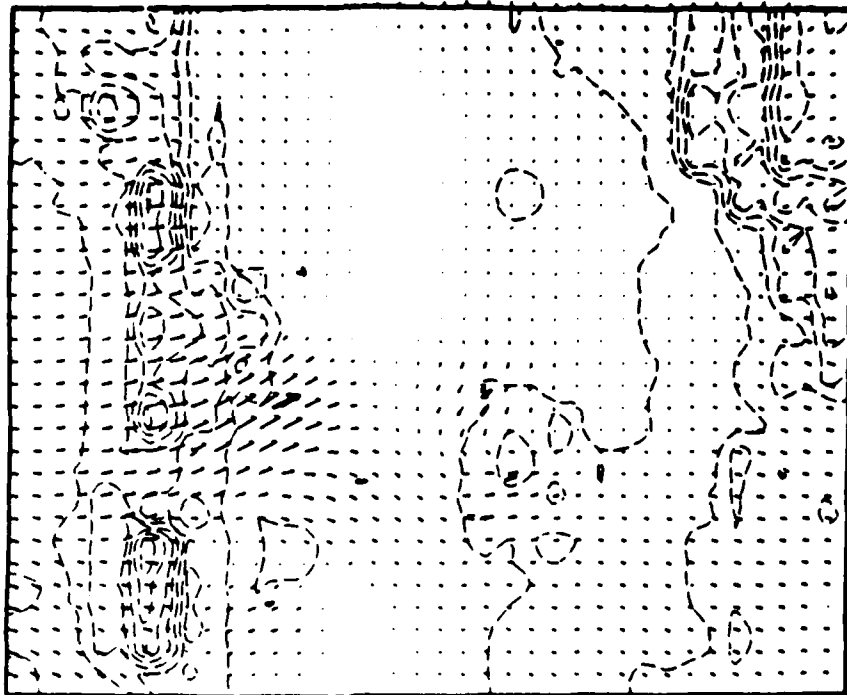


Figure 5.2 Near-Surface Wind Field Velocity Vector and Speed Contour Plots (15 m AGL), Case 1 (all stations used as upper air records).

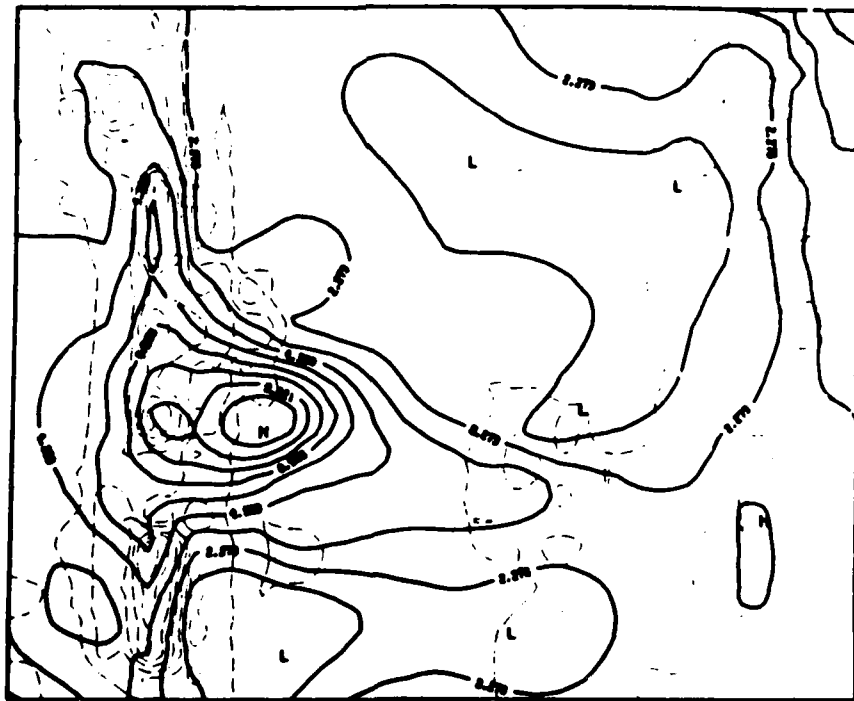
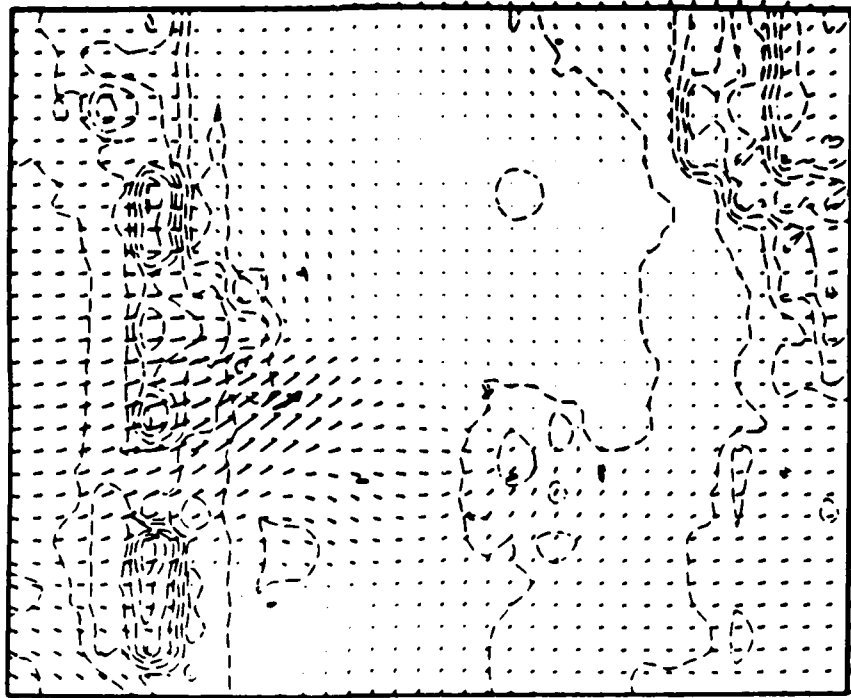


Figure 5.3 Near-Surface Wind Field Velocity Vector and Speed Contour Plots (15 m AGL), Case 2 (stations TSX (1), WAR (3), RAM (6), and APA (7) used as surface stations in initialization).

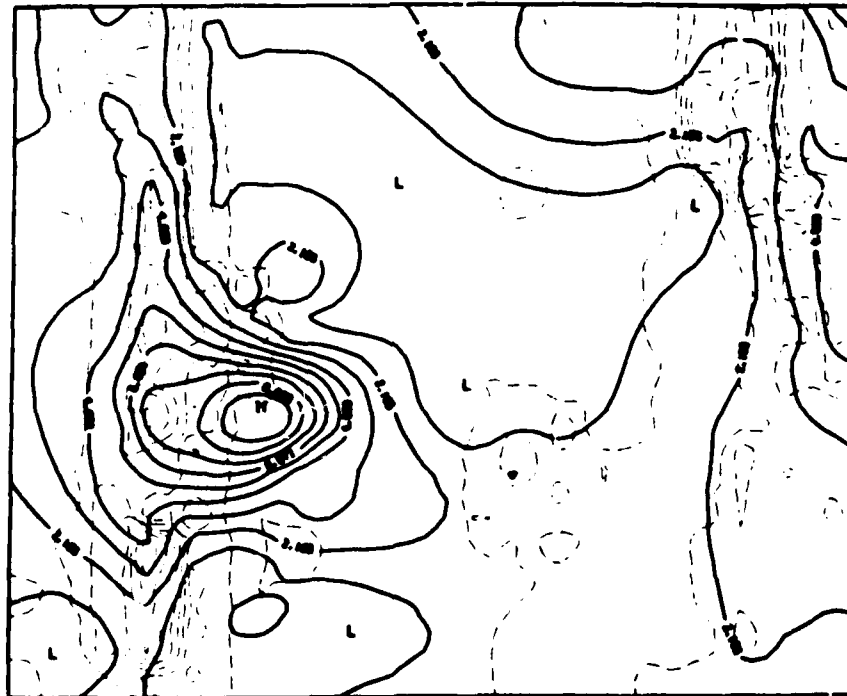
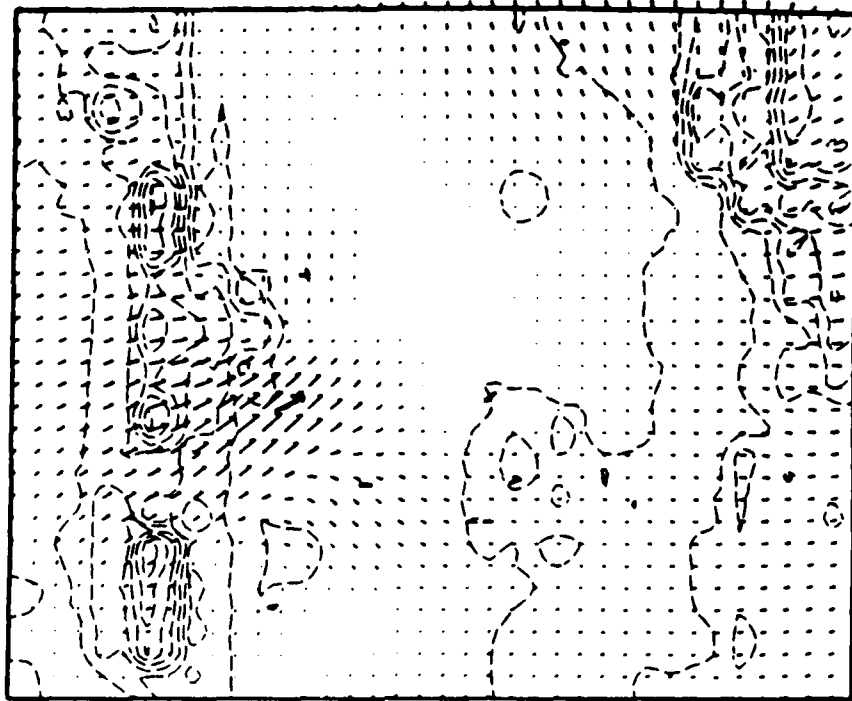


Figure 5.4 Near Surface Wind Field Velocity Vector and Speed Contour Plots (15 m AGL), Case 4 (all stations except SMR (4) and HMS (8) used as surface stations in initialization).

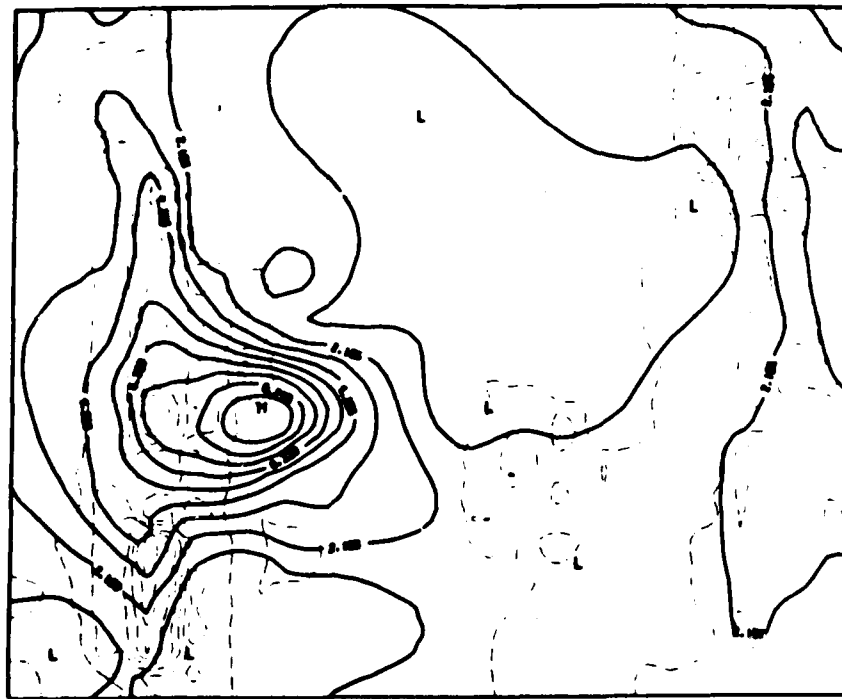
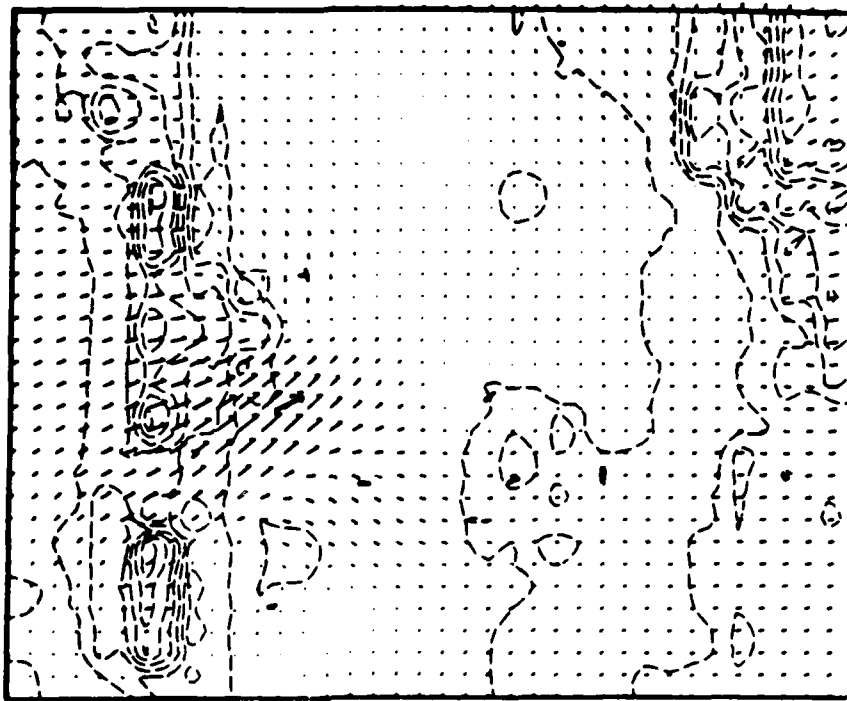


Figure 5.5 Near Surface Wind Field Velocity Vector and Speed Contour Plots (15 m AGL), Case 6 (all stations except SMR (4) used as surface stations in initialization).

the near-surface flow shown in the Case 1 result, for example, the eddy-like structure in the valley encompassing the nearby stations ORO (westerly flow) and RAM (easterly flow) and the reverse flow indicated at station WAR. These items notwithstanding, the simulated results with the surface station prescription, used in lieu of the detailed upper air records, compare very well with the baseline flow that utilizes all the upper air records.

The other cases in the matrix can be used to verify the accuracy of the model predictions at unused data stations. Results of wind speed scatter plots (q_{calc} vs. q_{obs}) are thus presented for Cases 1, 3, 5, 9, and 10 in Figures 5.6 through 5.10, respectively. In each figure, the results at 15 m, 250 m, 500 m, and 1000 m AGL are compared with the corresponding upper air record data. In Case 1 (Figure 5.6), of course, all the data were used in the initialization process, so it is not surprising that the calculated wind speeds compare so well with the observed wind speeds. It is presented, however, to show that there is little "drift" from the initialized values, at least in regions of flat terrain, which characterizes all of the data stations. It also indicates the optimum degree of comparison that can be expected for the unused data stations.

The scatter plots of the unused data stations indicate substantial scatter in the predictions and show that Case 5 (Figure 5.8), which utilizes only two upper air records in the initialization, compares as well to the observations as the other cases that utilize more initialization stations. In each case, the simulations show a clear tendency to overpredict the wind speeds in the valley (where all the data stations occur). However, the winds in the high speed areas (mountainous regions) are in relatively good correspondence for each case. This tendency to overpredict the winds can be traced, at least in part, to the uniquely high (not present in the other records) and low level winds at station SMR. This is substantiated by the Case 10 simulation, which is the only case that does not use SMR in the initialization. As shown in Figure 5.10,

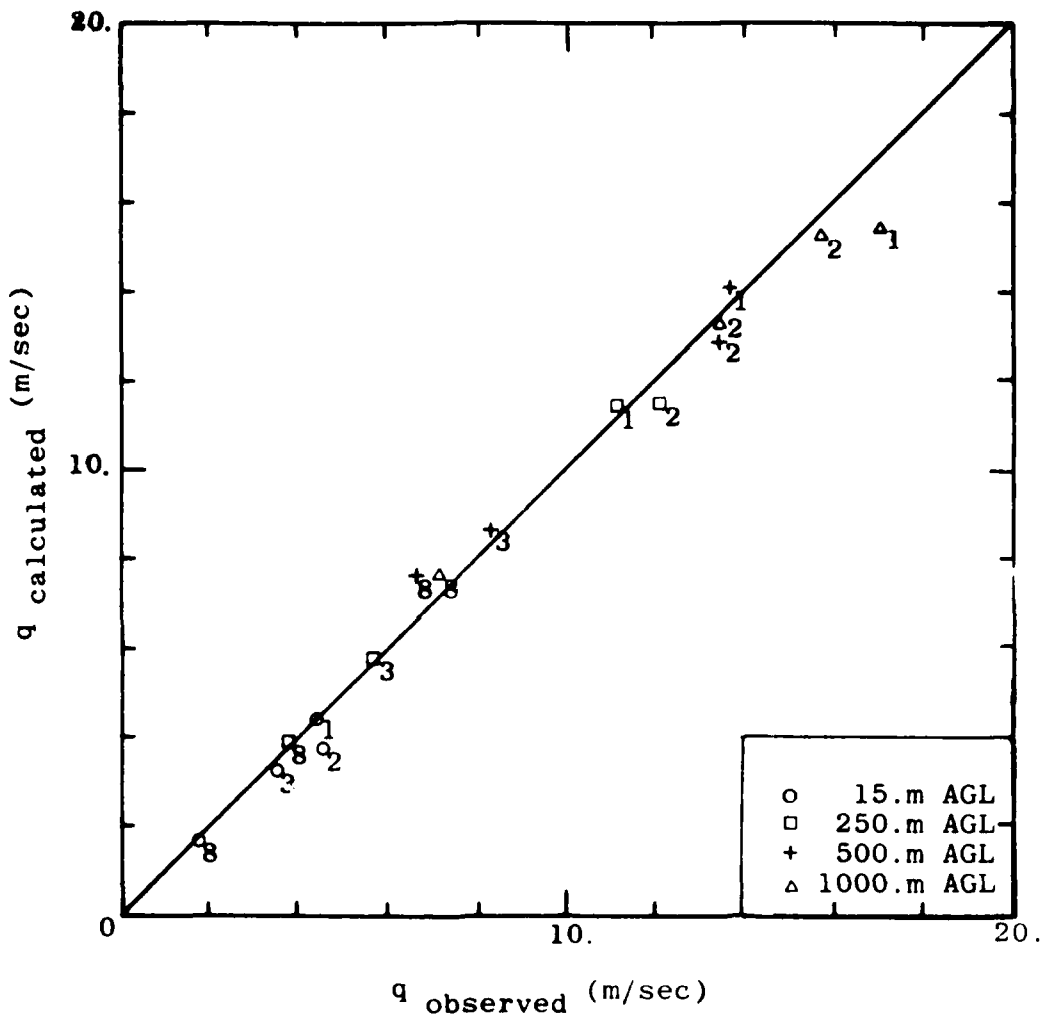
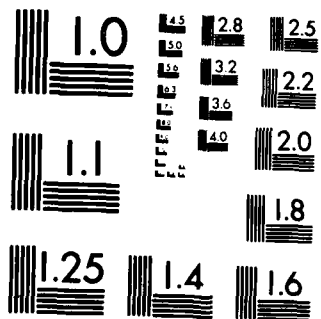


Figure 5.6 Comparison of Calculated to Observed Wind Speeds: WSMR, 11/19/74, Case 1 (all data stations used in initialization).

M-2



MICROCOPY RESOLUTION TEST CHART
NATIONAL BUREAU OF STANDARDS 1963-A

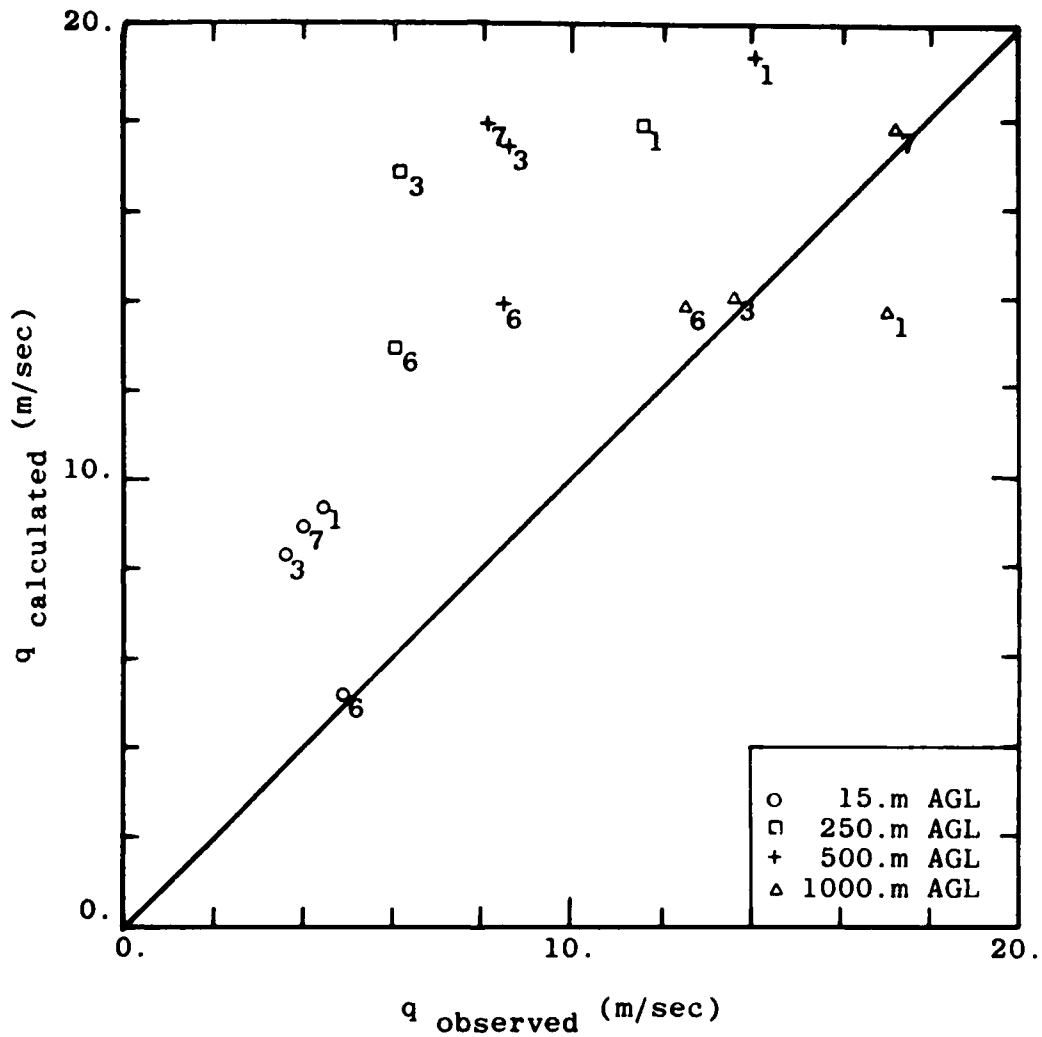


Figure 5.7 Comparison of Calculated to Observed Wind Speeds: WSMR, 11/19/74, Case 3 (station TSX (1), WAR (3), RAM (6), APA (7) not used in initialization).

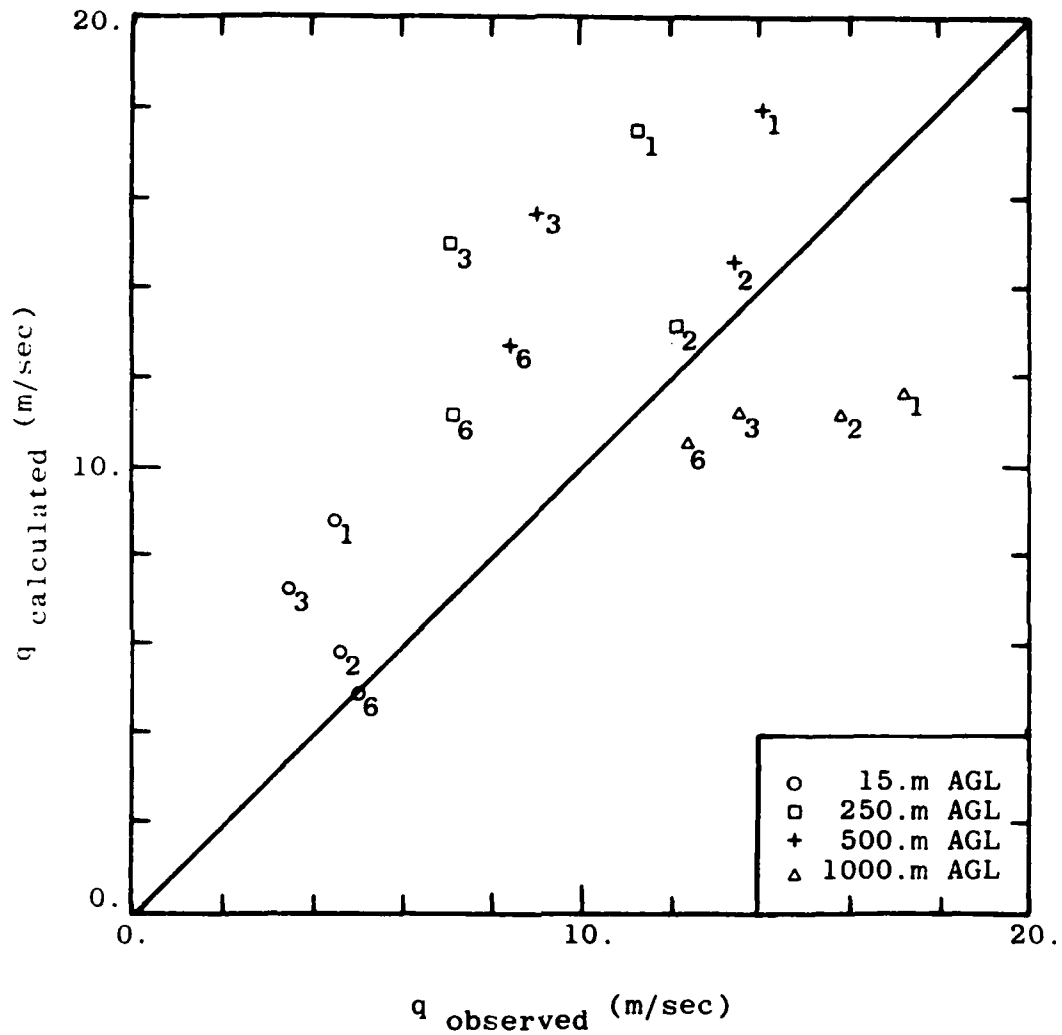


Figure 5.8 Comparison of Calculated to Observed Wind Speeds: WSMR, 11/19/74, Case 5 (stations TSX (1), ORO (2), WAR (3), RAM (6) not used in initialization).

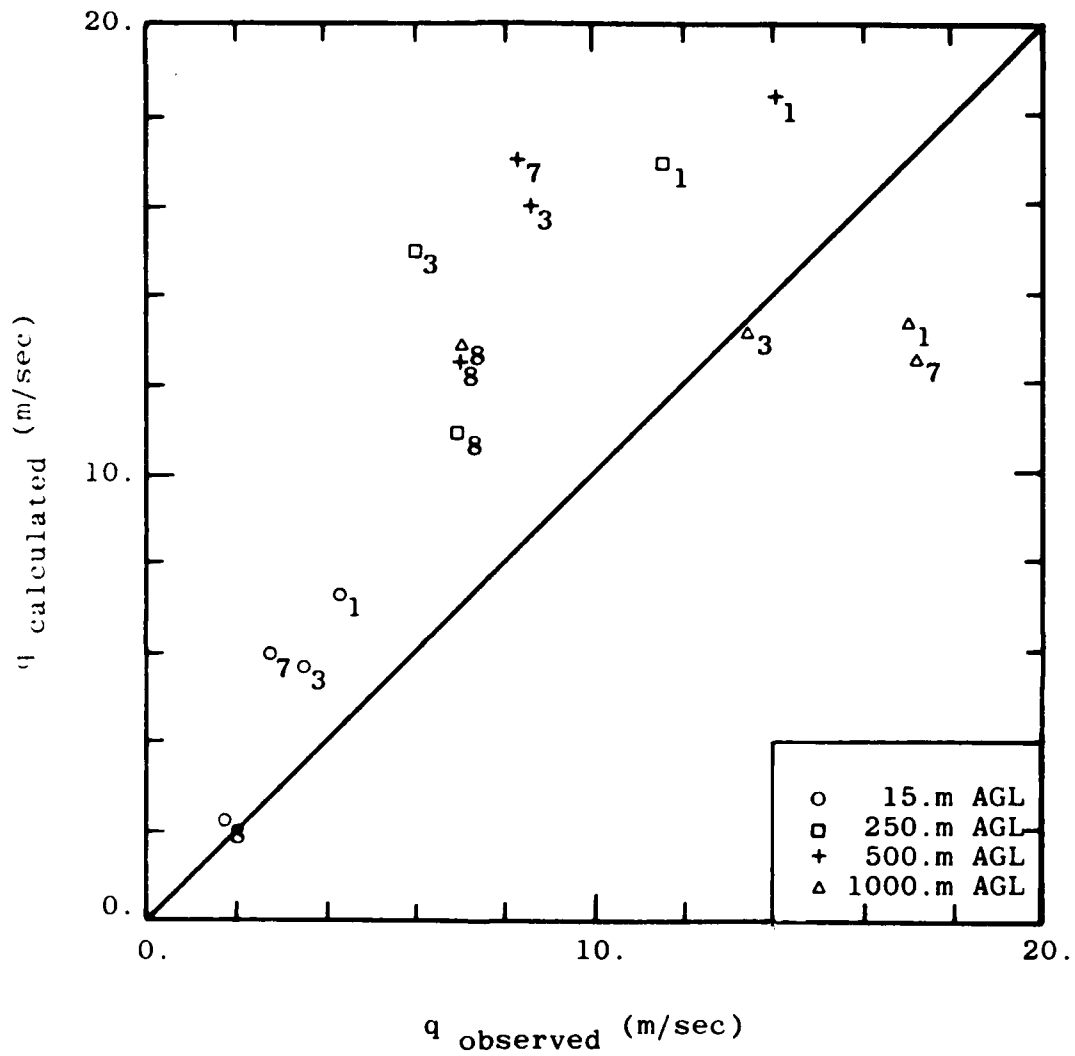


Figure 5.9 Comparison of Calculated to Observed Wind Speeds: WSMR, 11/19/74, Case 9 (stations TSX (1), WAR (3), APA (7), HMS (8) not used in initialization).

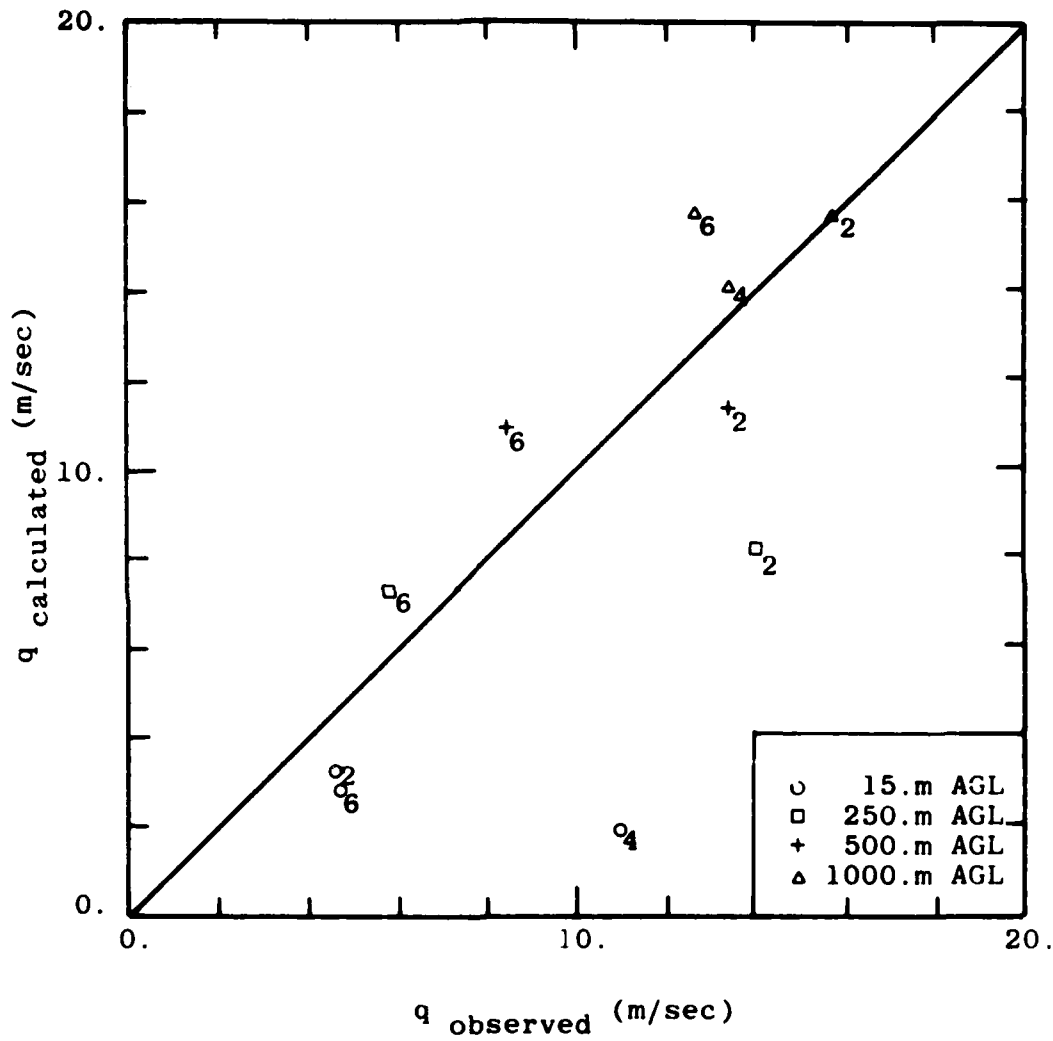


Figure 5.10 Comparison of Calculated to Observed Wind Speeds: WSMR, 11/19/74, Case 10 (stations ORO (2), SMR (4), RAM (6) not used in initialization).

the predicted results for Case 10 are quite good (lower speeds) for all stations except SMR. Unfortunately, for this choice of a comparison matrix, all other cases used SMR in the initialization.

The comparisons presented here provide clear verification of the initialization procedure for surface station data indicating that the effect of the vertical structure at the initialization stations is not of overriding importance, especially in relation to the prediction of the magnitude and extent of high wind speed areas. Moreover, they have shed some light on the accuracy of the results as influenced by the number of initialization stations and indicate that anomalous data (station SMR) can have a biasing effect on the simulation results.

6. SUMMARY AND CONCLUSION

The objective of this study is to identify, develop, and test improved simulation techniques for mesoscale meteorology. The emphasis is placed on flow over terrain features with the goal of obtaining one or more computer models that are at the same time reasonably accurate, easy to use, and economical of computing expense. This has been achieved in the study; in fact, one code was adapted for this study, and two other codes were developed from fundamentals.

The primitive equation SIGMET code was adapted from a previous version. This model, with an advanced prescription of boundary layer turbulence, radiation, soil/air interaction, and moisture treatment was used to simulate atmospheric events over the White Sands Region for selected days in the period November - December 1974. The results compared favorably with the PASS data obtained during the same period in the region.

An extensive survey which included a review of recent literature on orographic flow and discussion, with several experts in mesoscale modeling, was undertaken in Phase I of the study in order to recommend a simplified physics model for further development and testing. This survey has been reported in detail in the Phase I report (Patnaik, Freeman; 1977). The two models that emerged as a result of this survey are VARMET and LINMET. The formulation of VARMET is based on the objective analysis approach to wind field synthesis. The model uses terrain conformal coordinate for accurate representation of terrain effects. The degree of success, using the code, depends heavily on the number and location of the data stations that are used to initialize the calculation. For data-rich regions the VARMET simulations are very close to real events, whereas, for data-sparse regions, the simulations are rather poor.

A formulation containing more fundamental principles than VARMET, but less sophisticated than SIGMET, resulted in the code LINMET.

It is based on the 3-D, steady-state, linearized, inviscid Navier-Stokes equations. Calculations using LINMET are not very expensive, but it does simulate realistic flow features based on very little data. Unfortunately, only limited experiments have been carried out using LINMET, which are reported in this study.

A considerable amount was learned about orographic flow and mesoscale modeling in this study. Advantages and shortcomings of various classes of models were identified and understood. The linear code LINMET, in particular, showed very promising features which warrant further investigation in the future. Addition of a boundary layer treatment and a terrain conformal coordinate system (as in SIGMET and VARMET) to LINMET will improve its performance considerably while keeping the computational effort to a minimum; this would then prove to be a viable alternative to SIGMET. It is also possible to include certain aspects of nonlinearity to LINMET following the work of Smith, 1977.

REFERENCES

- Anthes, R.A., 1972: The Development of Asymmetries in a Three-Dimensional Numerical Model of the Tropical Cyclone. Mon. Wea. Rev., 100, 461.
- Asselin, R., 1972: Frequency Filter for Time Integration. Mon. Wea. Rev., 100, 487-490.
- Katayama, A., 1974: "A Simplified Scheme for Computing Radiative Transfer in the Troposphere", Technical Report No. 6, Dept. of Meteorology, UCLA.
- Klemp, J.B., and D.K. Lilly, 1975: The Dynamics of Wave-Induced Downslope Winds. J. Atmos. Sci., 32, 302-339.
- Mellor, G.L., and T. Yamada, 1974: A Hierarchy of Turbulence Closure Models for Planetary Boundary Layers. J. Atmos. Sci., 31, 1791-1806.
- Patnaik, P.C., and B.E. Freeman, 1977: "Improved Simulations of Mesoscale Meteorology: Phase I". Report No. SAI-77-915LJ, Science Applications, Inc., La Jolla, California.
- Patnaik, P.C., 1979. "Improved Simulations of Mesoscale Meteorology: Phase II". Report No. SAI-78-948LJ, Science Applications, Inc., La Jolla, California.
- Sasaki, Y., 1970: Some Basic Formalisms in Numerical Variational Analysis. Mon. Wea. Rev., 98, 875-883.
- Sherman, C.A., 1977: A Mass-Consistent Model for Wind Fields Over Complex Terrain. J. Appl. Meteor., 17, 312-318.
- Smith, T.B., and S.M. Howard, 1972: Methodology for Treating Diffusivity. Meteorology Research Inc., Report MRI72FR-1030, Altadena, California 91001.
- Smith, R.B., 1977: The Steepening of Hydrostatic Mountain Waves. J. Atmos. Sci., 34, 1634-1654.
- Yamada, T., and G.L. Mellor, 1975: A Simulation of the Wangara Atmospheric Boundary Layer Data. J. Atmos. Sci., 32, 2309-2329.

APPENDIX A
SIGMET ORGANIZATION

A.1 SIGMET ORGANIZATION

SIGMET is written in modular form, through the use of subroutines, with each module representing an aspect of the physical model. There is thus a close correspondence between the subroutine structure and the individual physical processes being simulated. The logical flow of the program is controlled by subprogram MAIN and proceeds through the subroutines as indicated in the summary flowchart of Figure A.1.

The numerical time and 3-D space dependent solution of the system of equations proceed sequentially through the subroutines indicated in the flow diagram. The solution state is advanced forward in time in a step-by-step fashion by the execution of the subroutines and thereby mimicks the actual evolution of the atmospheric properties. One computational cycle advances all of the state variables by a small increment corresponding to the intensity of the physical processes calculated at the time in question. The increment in time represented by one cycle is quite small so that the rates of change of the atmospheric variables may be considered constant over the interval. Thus, beginning with an initial condition state, the desired solution evolves iteratively in response to physical processes and applied boundary conditions.

Within each cycle, a sequence of computational steps is performed to advance the solution through one time interval. These steps are performed in the subroutines indicated in Figure A.1 and in the order shown. Because of the solution's explicit nature, the order of execution of some of these routines is not important; the order has been arranged primarily for programming simplicity and for reducing the amount of computer storage required to contain the current values of the state variables. Because of the sequential nature of the solution it is not necessary to store these variables

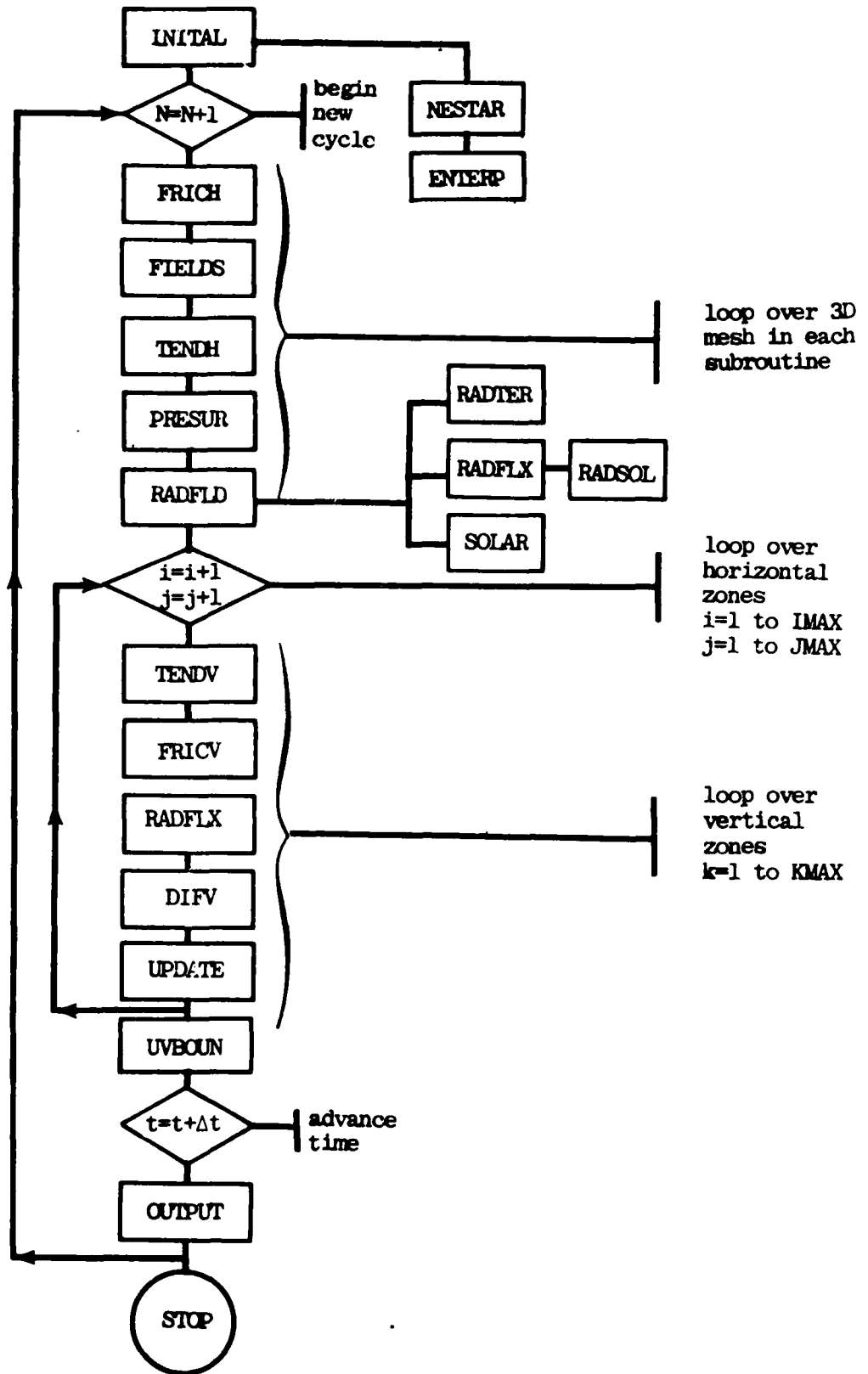


Figure A.1 SIGMET Logical Flow Diagram (all subroutines controlled and called by MAIN).

as a function of time. Only instantaneous values are required to continue the solution, and information regarding the solution state at any time is provided by periodic edits of these values.

A.2 SUBROUTINE DESCRIPTION

The subroutines that affect the numerical solution are now described in some detail. This includes a description of the function and operation of each subroutine as well as some additional explanatory comments concerning the physical model and finite difference technique. A spatially staggered mesh is utilized in the model (Figure A.2) that is referenced in the description to follow.

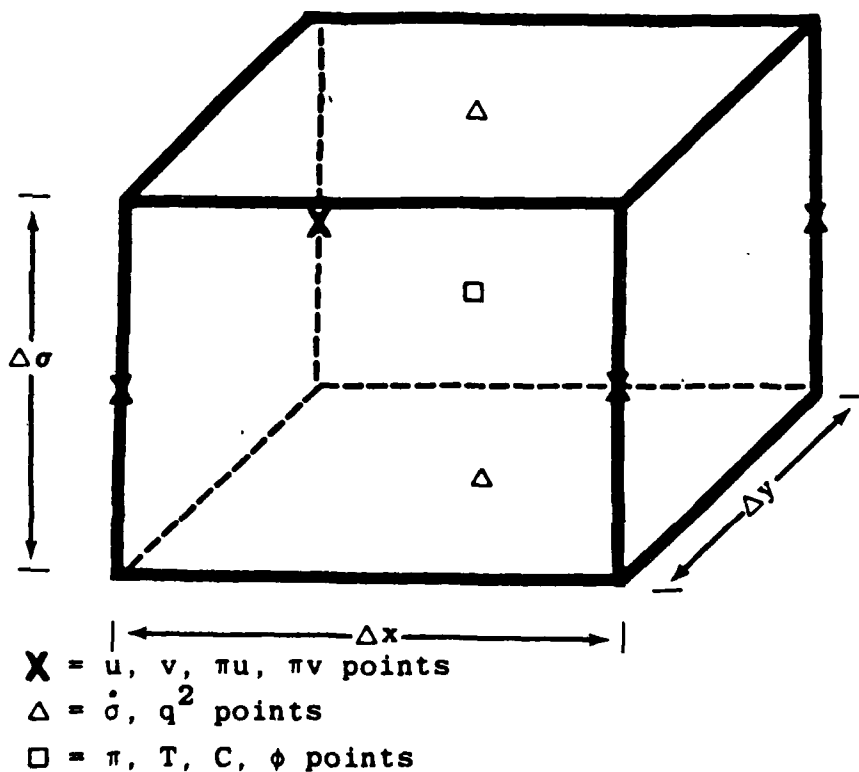


Figure A.2 A Three-Dimensional Grid Element.

INITAL

The INITAL subroutine processes data, as provided by data cards, so that all information required for subsequent normal execution of a computation cycle is available. The data cards provide values for the following quantities:

- spatial increments of the horizontal and vertical distance
- time intervals
- number of cycles of calculation
- terrain-height array
- latitude and longitude of the region
- number of parameters characterizing the terrain such as volumetric fractions of clay, sand, and organic material in the terrain, roughness height, vegetation fraction, etc.
- a number of parameters characterizing the solar and terrestrial radiation through the atmosphere
- tables in pressure coordinates describing the vertical profiles of the ambient values of horizontal velocity components, temperature and amount of water vapor in the atmosphere
- initial surface temperature
- initial surface wetness and
- indicators controlling the output of information

Options are provided so that some of the read-in quantities can be overwritten and suitable data generated internally in INITAL. For example, the vertical coordinate σ can be generated using a log-linear formula or a geometric progression series resulting in smooth nonuniform distribution of σ levels. Another example is the ambient temperature table can be constructed using a temperature near the surface, two lapse rates, and an inversion pressure height. The surface temperature can be defined using the temperature table, and the surface pressure and the water vapor concentration can be calculated from relative humidity values instead of being read-in directly.

The initial data are processed so that they are acceptable to the other subroutines of SIGMET. In some cases, this involves conversion of units from those in which the input data are commonly available to those consistent with the formulation. In addition, a number of auxiliary quantities are formed that are used during the calculation but do not change with time. Precalculation of these quantities saves computing time. In other cases, the data are interpolated to provide values at locations specified by the computational grid. This second function is performed in a subroutine called NESTAR, which forms such quantities as the pressure thickness (of the part of the atmosphere for which calculation is performed), the horizontal velocity components, the temperature, and the initial water vapor concentration. These quantities are assigned to the appropriate storage arrays.

NESTAR

In NESTAR a pressure surface is calculated corresponding to a prespecified constant boundary-layer height above the local terrain. Above this surface, the values of the horizontal velocity components are interpolated from the tables; below the surface, the values are computed from a power-law profile. Temperature and moisture are interpolated from this table at all levels. All the interpolation is done by calling the subroutine function ENTERP. Subroutine NESTAR also defines initial values of the turbulent kinetic-energy arrays using the properties of the ambient atmosphere and the "level 2" formulation of Yamada-Mellor turbulence prescription.

FRICH

The FRICH subroutine performs two functions: horizontal diffusion coefficients are calculated as functions of the local state variables, and (using these calculations) the turbulent horizontal diffusion taking place in one time interval is calculated. The result of these steps is to evaluate the contribution of horizontal diffusion to the rates of change of all of the primary variables.

The horizontal diffusion coefficients are obtained from Smith and Howard (1972) and are incorporated into FRICH in the form of tables. Entries of the main table are values of the diffusion coefficient as a function of altitude for each of the standard stability categories according to the AEC classification. A factor accounting for the dependence on stability of the ratio of horizontal-to-vertical-diffusion coefficient is also applied.

Because the horizontal diffusion is a slow process, the calculation can be performed explicitly without regard for the time interval. Consequently, the second task of the FRICH subroutine is to perform a calculation of the increment to the primary variables, u , v , θ , and C , resulting from horizontal diffusion. Numerical stability of this diffusion calculation applied to the leapfrog method requires that a special treatment of the time centering be used. If this term were the only one being calculated, a typical equation would be evaluated as follows:

$$\frac{\phi_{ij}^{n+1} - \phi_{ij}^{n-1}}{2\Delta t} = \tag{A.1}$$

$$K_H \left[\frac{\phi_{i+1,j}^{n-1} - 2\phi_{ij}^{n-1} + \phi_{i-1,j}^{n-1}}{\Delta x^2} + \frac{\phi_{i,j+1}^{n-1} - 2\phi_{ij}^{n-1} + \phi_{i,j-1}^{n-1}}{\Delta y^2} \right],$$

which has the stability requirement

$$\Delta t \leq \frac{1}{4K_H} \left(\frac{1}{\frac{1}{\Delta x^2} + \frac{1}{\Delta y^2}} \right). \tag{A.2}$$

The time centering of the right-hand term is not permitted, because such a scheme is numerically unstable. Because of the large horizontal-space increments, the stability condition given by Eq. (A.2) is considerably less stringent than that for gravity waves to be discussed below.

FIELDS

The FIELDS subroutine is executed after FRICH at the beginning of each cycle to calculate auxiliary quantities, including the two components of horizontal velocity, temperature, and moisture. These quantities are obtained from the primary variables, πu , πv , $\pi \theta$, and πC , where $\pi = P_s - P_t$ is the pressure thickness of the computational region, and θ is the potential temperature. By placing this subroutine after FRICH, storage of u , v , θ , and C at two time levels is avoided. FRICH uses the old values of these variables for stability and then FIELDS updates them to current time.

TENDH

In TENDH, the contribution of horizontal advection (the process of moving a particular property of the material from one zone to another by the horizontal-velocity components) to the rate of change is calculated. This process depends only on the horizontal components of velocity as indicated by the following advection equation:

$$\frac{\partial \pi \phi}{\partial t} = - \frac{\partial \pi u \phi}{\partial x} - \frac{\partial \pi v \phi}{\partial y} . \quad (\text{A.3})$$

The terms in Eq. (A.3) are evaluated explicitly in conservative form. The difference equation is consistent with the leapfrog time differencing and staggered spatial grid of Figure (A.2). In finite difference notation, the advection terms are written:

$$\begin{aligned} \overline{\pi U}_t^t &= - \left(\overline{U^x} \overline{\pi u^{xy}} \right)_x - \left(\overline{U^y} \overline{\pi v^{xy}} \right)_y \\ \overline{\pi \phi}_t^t &= - \left(\overline{u^y} \overline{\pi \phi^x} \right)_x - \left(\overline{v^x} \overline{\pi \phi^y} \right)_y , \end{aligned} \quad (\text{A.4})$$

where $U = (u, v)$ and $\phi = (\theta, C)$. The particular form of the differencing is dictated by the desire for a relatively simple conservative form that is accurate to second order and is computationally

stable. The advection terms are evaluated at the midlevel of the three time levels of the leapfrog scheme, thereby assuring second-order time accuracy.

Stability analysis indicates that Eq. (A.4) is stable with no damping when the following inequality is observed:

$$\Delta t \leq \frac{1}{\frac{u}{\Delta x} + \frac{v}{\Delta y}} \quad . \quad (A.5)$$

Typically, this stability condition is much less restrictive than the gravity-wave condition.

Boundary conditions at the lateral mesh surfaces are also incorporated into the TENDH routine. These conditions account for the ambient atmospheric properties that enter the calculational region from upwind and the removal of the disturbed quantities from the mesh at the downwind boundary. These boundary conditions are implemented by prescribing ambient values on the surfaces that have a wind component directed into the mesh and by extrapolating values from the mesh interior to the boundary on those surfaces that have wind components directed out of the computational region.

PRESUR

In the PRESUR subroutine, pressure gradient effects are taken into account, and rates of change of the horizontal-velocity components corresponding to them are formed. In the leapfrog equations, centered as indicated in Figure A.2, the pressure gradients can be calculated to second-order accuracy in both space and time without greatly complicating the equations. The calculation is performed explicitly (i.e., the gradient is evaluated from known quantities evaluated at the current cycle). Corresponding to this explicit formulation, an explicit stability condition exists, which severely limits the time interval. This gravity-wave-propagation condition is, in fact, the most restrictive of all the time-interval

constraints and typically limits the time interval to a few seconds. The stability condition is given by

$$\Delta t \leq \frac{\min(\Delta x, \Delta y)}{2\sqrt{gH}}, \quad (\text{A.6})$$

where H is the effective thickness of the computational region, and g is the acceleration of gravity.

The terms of interest in the PRESUR subroutine give rise to a rate of change of the horizontal-velocity components. The differential equations are

$$\begin{aligned} \frac{\partial \pi u}{\partial t} &= -\pi \left(\frac{\partial \phi}{\partial x} + \frac{\sigma}{\rho} \frac{\partial \pi}{\partial x} \right) \\ \frac{\partial \pi v}{\partial t} &= -\pi \left(\frac{\partial \phi}{\partial y} + \frac{\sigma}{\rho} \frac{\partial \pi}{\partial y} \right), \end{aligned} \quad (\text{A.7})$$

where $\phi = gz = \frac{\pi}{g} \int_{\sigma}^1 \frac{d\sigma}{\rho} + gz_s$ is the geopotential, and z_s is the surface altitude.

The above terms are approximated by the difference equations

$$\begin{aligned} \overline{\pi u}_t &= -\overline{\pi}^{xy} \left[\frac{\sigma}{\rho^{xy}} \overline{\pi}_x^y + \overline{\phi}_x^y \right] \\ \overline{\pi v}_t &= -\overline{\pi}^{xy} \left[\frac{\sigma}{\rho^{xy}} \overline{\pi}_y^x + \overline{\phi}_y^x \right]. \end{aligned} \quad (\text{A.8})$$

The terms on the right-hand side of Eq. (A.8) are evaluated from quantities available at the current time and involve centered spatial differences, which result in second-order accuracy in both space and time.

The calculation in PRESUR is carried out in two steps: first, the geopotential height is formed by integration of the hydrostatic

equation; second, the contribution of pressure terms to the momentum's rate of change is formed. A correction term, formed on the first time cycle is applied to each term throughout the calculation. As seen in Eq. (A.7), the pressure gradient is the sum of several terms. When terrain is present, each term is large and should cancel each other when the atmosphere is at rest. However, because of the finite difference approximation, these terms do not cancel exactly, giving rise to a spurious acceleration. The correction term eliminates this error, thereby increasing the accuracy of the dynamical calculation.

RADFLD

This subroutine is accessed to account for the solar and terrestrial radiation through the atmosphere. Because the amount of time spent in terrestrial radiation is about one-third of the total computational time, this subroutine is called only at a pre-set interval to update the radiation fluxes. At other times an extrapolation procedure is used to approximate the radiation fluxes.

RADFLD calls subroutine SOLAR, which determines various sun related quantities such as: solar constant for current earth-sun distance, current declination of the sun, current hour angle, zenith angle, normal insolation, and other miscellaneous quantities. RADFLD then computes the amount of water vapor in a given vertical column, taking into account the amount above the column that is outside the mesh (calculated using QEFFG). Subroutine RADTER, which determines the contribution to atmospheric heating from longwave radiation, is then called. The prescription used is that of Katayama (1974) as included in the 3-level UCLA GCM. The equations of radiative transfer are solved subject to the following boundary conditions: downward IR flux is zero at the top of the mesh, and the upward flux at the earth's surface is blackbody at the surface temperature. The solution utilizes a bulk transmission function defined as the product of water vapor and carbon dioxide transmission functions. Absorption by ozone is neglected

and the transmission function is assumed linear. RADSOL is then called from RADFLX, which calculates the radiant flux within the atmosphere due to solar insolation. A one-dimensional model is used, which takes into account: absorption of solar radiation by water vapor and the Rayleigh scattering by air molecules.

TENDV

As indicated in Figure A.1, several subroutines occur within a do-loop ranging over all of the horizontal zones. These subroutines form quantities in which the coupling is in the vertical direction and are easily and efficiently calculated a column at a time.

The first of the calculations in the TENDV subroutine takes care of the vertical advection and the rate of change of the surface pressure. The vertical advection terms contain the vertical velocity ($\dot{\sigma}$), which is the effective velocity of the fluid with respect to the σ -coordinate. This quantity is obtained by employing the mass conservation equation subsequent to the calculation of the pressure-tendency rate.

The first calculation is that of the rate of change of pressure. This quantity is obtained by summing the pressure equation over all of the vertical zones. The as-yet-unknown- $\dot{\sigma}$ terms drop out of the equation in this procedure

$$\bar{\pi}_t^t = - \sum_k (\bar{\pi}u_x^y + \bar{\pi}v_y^x) \Delta\sigma_k, \quad (\text{A.9})$$

where the horizontal velocity divergence is formed from quantities known at the current time. These terms are centered in time and space, so that the pressure tendency is second-order accurate.

The second calculation in the TENDV subroutine is that of $\dot{\sigma}$. This calculation employs the following equation in a sequential fashion.

$$\dot{\sigma}_{k+1} = \dot{\sigma}_k - \left(\overline{\pi}_t^t + \overline{\pi u}_x^y + \overline{\pi v}_y^x \right) \frac{\Delta \sigma_k}{\pi} \quad . \quad (\text{A.10})$$

The first term $\dot{\sigma}$ (k=1) is zero from the top-boundary condition. The $\dot{\sigma}$ values obtained in this step are used subsequently to evaluate the effects of vertical advection on all of the primary variables. This calculation can be considered to be an explicit one; since the velocities entering Eqs. (A.9) and (A.10) are known quantities at the current cycle.

TENDV calculates the contribution of vertical advection to u , v , θ , and C using the following relations respectively:

$$\overline{\pi u}_t^t = - \delta \left(\frac{\dot{\sigma} \overline{xy}}{\dot{\sigma}} \frac{\overline{\pi u}}{\pi u} \right) / \Delta \sigma$$

$$\overline{\pi v}_t^t = - \delta \left(\frac{\dot{\sigma} \overline{xy}}{\dot{\sigma}} \frac{\overline{\pi v}}{\pi v} \right) / \Delta \sigma$$

(A.11)

$$\overline{\pi \theta}_t^t = - \delta \left(\frac{\dot{\sigma}}{\dot{\sigma}} \frac{\overline{\pi \theta^\sigma}}{\pi \theta^\sigma} \right) / \Delta \sigma$$

$$\overline{\pi C}_t^t = - \delta \left(\frac{\dot{\sigma}}{\dot{\sigma}} \frac{\overline{\pi C^\sigma}}{\pi C^\sigma} \right) / \Delta \sigma \quad .$$

Finally, Coriolis contributions to the horizontal momentum equations are calculated in a straightforward manner:

$$\frac{\partial \pi u}{\partial t} = f (\pi v - \pi v_g)$$

(A.12)

$$\frac{\partial \pi v}{\partial t} = - f (\pi u - \pi u_g) \quad .$$

The components for the geostrophic velocity u_g and v_g are evaluated by interpolation from the ambient velocity table.

FRICV

In preparation for the calculation of the vertical diffusion resulting from turbulence, the boundary-layer diffusivities are calculated in the FRICV subroutine. They will be used subsequently in DIFV to add the effects of turbulent transport to the tendency equations. The eddy diffusivities for momentum and heat are calculated according to the '2½ level' prescription of Mellor and Yamada (1974). In this formulation, a system of algebraic equations involving the local Richardson number, turbulent kinetic energy, and the local shear is solved in order to evaluate the eddy diffusivities. The turbulent kinetic energy is described by a differential equation, which amounts to solving a tridiagonal system of equations in finite difference space. This is done in FRICV by calling subroutine TRIDG. Kinetic energy is the only quantity that is completely updated to future-time level in FRICV.

RADFLX

The subroutine RADFLD, which updates the radiation fluxes, is not called every time step for computational economy; instead, subroutine RADFLX is used to update the fluxes by performing a linear extrapolation on radiative fluxes saved at two earlier time steps. Except during sunrise and sunset hours, this procedure has been found to work well.

DIFV

This important subroutine serves several functions:

- The vertical turbulent diffusion calculation is performed using the diffusion coefficients formed in the preceding subroutine FRICV.
- The heat balance equation at the soil surface is solved efficiently and accurately to take into account phenomena taking place on and near the ground surface. An option also is provided for water/land surface.

As previously discussed, the vertical turbulent diffusion is a vigorous process, which acts across the small zone thickness corresponding to the vertical zoning. An explicit treatment of this diffusion would require that an additional numerical stability inequality be observed in the determination of the time interval. This diffusion-stability criterion would be very restrictive and would cause the time interval to be limited to even smaller values than determined by the other criteria discussed above.

In order to avoid such a costly restriction of the time interval, a numerical formulation of the terms involving vertical diffusion that is not subject to the stability criterion was implemented. Such a formulation is that of partial implicitization, in which a linear system of simultaneous equations is solved. While the method required to evaluate these equations is somewhat more complicated (as described below) than that for the explicit formulation, the computational penalty is minimal. The solution is formed cellwise column by column and makes use of diffusivities calculated previously for the column of cells in question. This solution sequence dictates that the vertical calculations of the FRICV and DIFV subroutines be performed in the innermost loop of the flowchart as indicated in Figure A.1.

The terms of the differential equation that are evaluated in DIFV are

$$\frac{\partial \pi \phi}{\partial t} = \frac{g^2}{\pi^2} \frac{\partial}{\partial \sigma} (\rho^2 K_V \frac{\partial \pi \phi}{\partial \sigma}) + \dot{\phi} \quad , \quad (A.13)$$

where $\phi = (u, v, h, C)$, and $\dot{\phi}$ is a symbolic representation of the other terms in the governing equations, which have been evaluated explicitly in the subroutines discussed above. The difference formulation evaluates the diffusion terms at the advanced time of the three levels of the leapfrog scheme. This formulation has been shown to be unconditionally stable against numerical error

growth. Taking into account the variation in vertical cell size with height, the difference equation corresponding to Eq. (A.13) is:

$$\frac{\pi\phi_k^{n+1} - \pi\phi_k^{n-1}}{2\Delta t} = \frac{g^2}{\pi\Delta\sigma} \left[\frac{(\rho^2 K_V)_+}{\Delta\sigma_+} (\pi\phi_{k+1}^{n+1} - \pi\phi_k^{n+1}) - \frac{(\rho^2 K_V)_-}{\Delta\sigma_-} (\pi\phi_k^{n+1} - \pi\phi_{k-1}^{n+1}) \right]. \quad (A.14)$$

In Eq. (A.14), the subscript (k) indicates the vertical index, the superscript (n) indicates the time index, and the subscripts (+) and (-) designate quantities to be evaluated at the interface of the zone having larger and smaller k-indices, respectively. All of the indices indicating horizontal position, which are not involved with these terms, have been suppressed.

Eq. (A.14) is a system of linear equations for the unknown quantities $\pi\phi_k^{n+1}$, which is tridiagonal (the matrix of the coefficients of $\pi\phi_k^{n+1}$ contains nonzero elements only on the main diagonal and the bordering diagonals immediately above and below the main diagonal). This system of equations is closed with boundary conditions at the top and bottom of the computational region. At the top of the mesh, zero turbulent flux is assumed. At the bottom, the velocity at the surface is matched to a wall layer solution, and the temperature boundary value at the surface is assumed to be known.

The formulation of the surface-heat balance in DIFV takes into account: 1) the sensible and latent heat fluxes to incorporate the logarithmic dependence of wind speed on height, 2) the heat flux into soil, 3) the evaporation and condensation of moisture from the soil surface, and 4) simultaneous solution of the heat balance, atmospheric temperature and water vapor equations, and the soil temperature equation. The soil moisture is defined by a wetness parameter.

UPDATE

Subroutine UPDATE updates all the primary variables to the advanced time level. In addition, a frequency filter to the time integration (Asselin 1972) is applied at each time step in order to remove the high-frequency noise from the solution. The filter also helps to damp the $2\Delta t$ oscillations inherent in leapfrog time differencing by averaging the solution over three consecutive time steps. If the superscript (n) denotes the time level and (\sim) denotes smoothed variable, then the filter is defined by the following operator:

$$\tilde{\phi}^n = \phi^n + \frac{1}{2}\alpha \left(\tilde{\phi}^{n-1} - 2\phi^n + \phi^{n+1} \right) . \quad (\text{A.15})$$

Note that the filter is applied only to old quantities (ϕ^n) after the new quantities (ϕ^{n+1}) are calculated. The parameter $\alpha = 0$ corresponds to no filtering, and $\alpha = 1$ corresponds to a heavily biased filter. A value of $\alpha = 0.5$ completely suppresses $2\Delta t$ oscillations.

UVBOUN

Values of velocity at external positions on the computational mesh have not been supplied in the previous subroutines and are added in the UVBOUN subroutine. These quantities are obtained in accordance with whether the wind velocity is directed into or out of the computational region at the boundary location in question. If the wind is directed inward, a specified boundary value of velocity is utilized. On the other hand, if the wind is directed out of the mesh, the boundary values of the wind components are obtained by extrapolation from the interior of the mesh.

OUTPUT

The OUTPUT subroutine controls the manipulation of several forms of data that flow from the computer to peripheral devices. This output may take the form of printer edits, tape dumps, printer plots, or film plots. The user determines the frequency and mode of data output by specifying parameters in the INITAL subroutine. These parameters specify how many cycles of calculation are to elapse between the successive edits of a specified type.

The printer edits provide the user with a record of the progress of the calculation in terms of the values of selected variables. These variables are chosen to provide maximum information about the quantities of greatest interest during the normal course of the calculation. More complete data output is obtained by requesting the so-called "debug" edits. These edits contain a large amount of information on intermediate quantities, which are normally not edited. They would be too expensive to print, too time consuming to inspect, and too cumbersome to archive. The debug edits find their greatest use in diagnosing abnormal behavior of a calculation by providing detailed information on the suspected quantities.

The tape dumps are transfers to mass storage of all of the variables required to start the calculation. This feature is provided to enable the user to reinitiate a calculation, to change data part way through a calculation, or to edit information about a calculation selectively or in greater detail. These dumps can be stored compactly for a long period of time and thus constitute a convenient and permanent record of completed calculations.

The printer plots provide the user with various graphical representations of the data. This form of output is invaluable in evaluating the results of the calculation. The printer plots are made during the calculation and provide greater user overview of the calculation's progress and insight into the behavior and accuracy of the results.

The most important and impressive form of plot is on microfiche. Contour plots of velocity magnitude, temperature, moisture, turbulent kinetic energy, vector plot of the horizontal velocity vectors at different σ levels, contour and prospective plots of the terrain, etc., can be generated at any frequency through calls to other plot routines from OUTPUT. The plot routines are, however, machine and computer center specific and would require modifications to utilize this capability.

A.3 USAGE AND INPUT

As might be imagined, the SIGMET code that implements all of the methods and models described above is quite sophisticated and requires knowledge and experience with such techniques to operate in a useful manner. It is being continually updated in terms of its physical and numerical methods to enhance its usefulness and efficiency. It, however, remains quite expensive to run, presently requiring on the order of 10's of minutes on a CDC 7600 computer for a typical 3-D mesoscale simulation of approximately 1-hour real-time duration. It also makes extensive use of computer storage; in its present configuration, it requires 151.5_gK words to load and 130.5_gK words of small core memory to execute as well as 404.0_gK words of large core memory (LCM). In this configuration, it can perform a calculation with a finite difference grid design of (25 x 21 x 15) zones in the x,y, and z directions respectively. The sample calculation in the next section provides coding changes of array sizes required for performing a slightly larger calculation. It is recommended that similar changes be made for a smaller calculation to minimize computational costs. Because of the extensive storage and time requirements, it goes without saying that conservative computing practice be followed when exercising the SIGMET code.

Most input variables required for a SIGMET calculation are read through two NAMELIST records: OUTPT and START. This input uses standard CDC NAMELIST format. The variables to be included in each record are listed with a functional description in Section A.5.

Variables in record OUTPT control execution and variables in START provide numerous parameters for numerical and physical description of a calculation. For an initial run, both records should be read, and for a restart run (ISTART = 1), when previously generated dump tape is used to initialize the calculation, only record OUTPT is read. SIGMET automatically generates a dump tape on logical Unit 8 for any run.

A typical input deck for an initial run is provided in the next section and has the following form:

```
NAMELIST  OUTPT           : (see A.5)
NAMELIST  START          : (see A.5)
UADAT     : (80 character field contain-
            ing upper air data description)
TRDAT     : (80 character field contain-
            ing terrain data description)
((HM(I,J), I=1, IE), J=1, JE) : terrain data in format
                                8F 10.0)
```

As suggested in the above input list, terrain data must be provided for each finite difference cell starting at the southwest corner (I,J) = (1,1) for each row in turn proceeding in an easterly (I=1, IE) direction. These data are read according to the following coding in subroutine INITAL:

```
DO 180 J = 1, JE
  READ (5,615) (HM(I,J), I = 1, IE)
180 CONTINUE
615 FORMAT (8F10.0)
```

As mentioned above, a restart run requires only the input contained in NAMELIST OUTPT to control execution as well as a dump tape of a previous run mounted on logical Unit 7.

A concrete example of the input for an initial run is now provided in the next section.

A.4 SAMPLE CALCULATION

The setup and example output for a sample SIGMET calculation are presented in this section for demonstration purposes. The test problem is the flow over a three-dimensional Gaussian Hill with a prevailing uniform westerly wind in a neutrally stratified (lapse rate = $-0.01 \text{ }^{\circ}\text{K/m} = -\text{GAM}$) atmosphere.

Table A.1 below lists the coding changes that are required to run this problem with the present code configuration. These changes include alteration in the array dimensions for various parameters and a code update to calculate the hill terrain directly, rather than read the terrain data from cards. All other input parameters are defined from NAMELIST as described below. It is noted that the radiation arrays (RADTN, RADTO, RADSN, RADSO) are dimension to 1, since radiation is neglected in this test case (IRAD = 0). This results in a substantial reduction in computer

Table A.1 Code Updates for Gaussian Hill Sample Case .

```

*IDENT GAUSS
*DELETE COMMON.2,COMMON.12
COMMON/ARRAY1/UA(25,25,15),VA(25,25,15),CA(24,24,15),TA(24,24,15)
COMMON/ARRAY2/UB(25,25,15),VB(25,25,15),CB(24,24,15),TB(24,24,15)
COMMON/ARRAY3/U(25,25,15),V(25,25,15),C(24,24,15),T(24,24,15)
COMMON/ARRAY4/UTEN(25,25,15),VTEN(25,25,15),CTEN(25,25,15),
      TTEN(25,25,15)
COMMON/ARRAY5/PHI(24,24,15),PHIPIX(24,24,15),PHIPIY(24,24,15)
COMMON/ARRAY6/QA(24,24,16),QB(24,24,16),HDIFB(24,24,15)
COMMON/ARRAY7/PSA(24,24),PSB(24,24),PTEN(24,24),HM(24,24),
      PUA(25,25),PUB(25,25),PCUT(25,25),CONVAR(25,25)
COMMON/ARRAY8/TH(24,24),TC(24,24),STEMP(24,24),CC(24,24),
      CW(24,24),HRATE(24,24),IJCOLM(24,24)
*DELETE COMMON.15,COMMON.18
COMMON/RADIAT/RADTN(1,1,1),RADTO(1,1,1),RADSN(1,1,1),RADSO(1,1,1)
COMMON/SCRACH/FACTOR(24,16),FACTOL(24,16),SDOTR(24,16),
      SDOTL(24,16)
*DELETE COMEQV.4,COMEQV.6
DIMENSION COM1(36030),COM2(36030),COM3(36030),COM4(37500),
      COM5(25920),COM6(27072),COM7(4804),COM8(4032),
      COM9(256),COM10(4),COM11(1536),COM12(96),
*DELETE INITAL.172,INITAL.176
      SICC=3000.0
      DO 180 J=1,JZ
      DO 180 I=1,IE
      XI=(I-12.5)*DX
      YI=(J-12.5)*DY
      HM(I,J)=1000.0*EXP(-(XI**2+YI**2)/SICC**2)
180 CONTINUE

```

core storage requirements. Further relief could be obtained by deleting the plotting subroutines (CONTUR, PLOTTER, AND VELVER) and adding the dummy subroutines MODESG and EXITG, since microfiche plots are not to be generated (IFILM = 0). This step should be implemented if SIGMET is to be run at a computer facility where the identical plotting package is not available.

The following are the NAMELIST input parameters and description caption input for this sample calculation :

```
$OUTPT
  NCYCLS=5,      IEDIT=5,      IOUT=0,      IPLOT=0,      ISTART=0,
  KBEG=15,      KBGPL=15,     IFILM=0,
$END

$START
  GMTMHR=7.25,  KMAX=15,      DELTAT=1.6,  DLAT=0.0,
  ANGLE=0.0,   DLONG=106.4,  PTOP=650.0,  PBOT=1000.,
  W=0.0,       IRAD=0,       XORG=0.0,   XCLAY=0.0,
  XSAND=1.0,   RPDIF=0.608, CPDIF=2.0,   TRANS=1.0,
  VEG=0.0,     ZNAUT=0.1,   QEFFG=0.5,  GDEPTH=0.1,
  TDEEP=15.0,  TWATER=15.0, ZBL=200.0,  SUREM=1.0,
  IE=24,       JE=24,       DX=750.0,   DY=750.0,
  TG=576*15.0, GW=576*0.2,  HRATE=576*0.0, IJCOLM=576*0,
  GAM=0.01,    GAM1=0.005,  PINV=500.0,  TNPRS=15.0,
  NPRES=21,    DAYBEG=1.0,  ZBOT=0.0,   ALPH=0.0,
  PPRES=600.,620.,640.,660.,680.,700.,720.,740.,760.,780.,800.,
  820.,840.,860.,880.,900.,920.,940.,960.,980.,1000.,
  UPRES=21*10.0, VPRES=21*0.0, CPRES=21*0.0, THETA=21*270.,
  RELHM=21*0.0, CX3=0.013882, CX4=1.2,
$END
```

SIMULATED INITIAL CONDITIONS 3-D GAUSSIAN HILL

If this were a usual SIGMET run in which terrain data were to be input via cards, the above input would be followed by terrain data cards in an 8F 10.0 format.

The above completes the coding changes and data input for the sample case. Table A.2 is a reproduction of the raw computer output for this calculation. The numbers and tables provided there are relatively self explanatory. For illustration and check-out purposes, only the first two pages of output for the initial conditions and for the results at the end of the 5-cycle run are provided.

Table A.2 Sample Output (Initial Condition).

XXXX X XXXX X X XXXX XXXXX
 X X X XX XX X X
 XXXX X X X X X X X X X
 X X X X X X X X X X X
 XXXX X XXXX X X XXXX X

INITIAL CONDITIONS

CONSTANTS

GRAVITY:	7.3500E+00	BLAT:	0.1000E+02	FTVP:	6.5000E+01	IRAD:	0.0000E+00	IBIT:	0.0000E+02		0.0000E+00
DELTA:	1.0000E+00	BLORC:	0.0000E+00	FRUV:	1.0000E+02	ZBL:	0.0000E+00	IPLOT:	0.0000E+00		0.0000E+00
PCYELS:	1.0000E+00	ARCL:	0.0000E+00	FRIV:	0.0000E+01	TRIS:	0.0000E+00	ISTART:	1.0000E+01		0.0000E+00
PFNS:	21	VRG:	0.0000E+00	RFIF:	0.0000E+01	XSAND:	0.0000E+00	ALPH:	5.7000E-01		0.0000E+00
IC:	0.0000E+02	XX:	7.5000E+02	CRIF:	2.0000E+00	TRANS:	0.0000E+00	IFIL:	1.0000E+00		0.0000E+00
CAP:	1.0000E-02	IE:	26	KMAX:	15	VEG:	0.0000E+00	RELA:	0.0000E+00		0.0000E+00
TDRP:	2.0016E+02	ZRADT:	1.0000E-01	QFFC:	5.0000E-24	CHPTR:	0.0000E+00	ZROT:	1.0000E-01		0.0000E+00
		TRATR:	2.0016E+02	JF:		DY:	0.0000E+00	CAH:	7.5000E+02		5.0000E-03

SIMULATED INITIAL CONDITIONS

K	PPRS	UPRS	VPRS	TPRS	CPZR	R.E.	TETA
1	0.0000E+01	1.0000E+01	0.0000E+00	-2.5000E+01	0.0000E+00	0.00	2.7000E+02
2	0.2000E+01	1.0000E+01	0.0000E+00	-2.2614E+01	0.0000E+00	0.00	2.7000E+02
3	0.4000E+01	1.0000E+01	0.0000E+00	-2.0276E+01	0.0000E+00	0.00	2.7000E+02
4	0.6000E+01	1.0000E+01	0.0000E+00	-1.7988E+01	0.0000E+00	0.00	2.7000E+02
5	0.8000E+01	1.0000E+01	0.0000E+00	-1.5750E+01	0.0000E+00	0.00	2.7000E+02
6	1.0000E+01	1.0000E+01	0.0000E+00	-1.3575E+01	0.0000E+00	0.00	2.7000E+02
7	1.2000E+01	1.0000E+01	0.0000E+00	-1.1468E+01	0.0000E+00	0.00	2.7000E+02
8	1.4000E+01	1.0000E+01	0.0000E+00	-9.3616E+00	0.0000E+00	0.00	2.7000E+02
9	1.6000E+01	1.0000E+01	0.0000E+00	-7.3368E+00	0.0000E+00	0.00	2.7000E+02
10	1.8000E+01	1.0000E+01	0.0000E+00	-5.3858E+00	0.0000E+00	0.00	2.7000E+02
11	2.0000E+01	1.0000E+01	0.0000E+00	-3.5234E+00	0.0000E+00	0.00	2.7000E+02
12	2.2000E+01	1.0000E+01	0.0000E+00	-1.7560E+00	0.0000E+00	0.00	2.7000E+02
13	2.4000E+01	1.0000E+01	0.0000E+00	6.6797E-01	0.0000E+00	0.00	2.7000E+02
14	2.6000E+01	1.0000E+01	0.0000E+00	2.3598E+00	0.0000E+00	0.00	2.7000E+02
15	2.8000E+01	1.0000E+01	0.0000E+00	4.4207E+00	0.0000E+00	0.00	2.7000E+02
16	3.0000E+01	1.0000E+01	0.0000E+00	6.2520E+00	0.0000E+00	0.00	2.7000E+02
17	3.2000E+01	1.0000E+01	0.0000E+00	8.0547E+00	0.0000E+00	0.00	2.7000E+02
18	3.4000E+01	1.0000E+01	0.0000E+00	9.8299E+00	0.0000E+00	0.00	2.7000E+02
19	3.6000E+01	1.0000E+01	0.0000E+00	1.1579E+01	0.0000E+00	0.00	2.7000E+02
20	3.8000E+01	1.0000E+01	0.0000E+00	1.3302E+01	0.0000E+00	0.00	2.7000E+02
21	4.0000E+01	1.0000E+01	0.0000E+00	1.5000E+01	0.0000E+00	0.00	2.7000E+02

3-B GAUSSIAN BILL

1-	2	3	4	5	6	7	8	9	10	11	12	13	14	15	16	17	18	19	20
1	0	0	0	0	0	0	0	0	0	0	0	0	0	0	0	0	0	0	0
21	0	0	0	0	0	0	0	0	0	0	0	0	0	0	0	0	0	0	0
J=24	0	0	0	0	0	0	0	0	0	0	0	0	0	0	0	0	0	0	0
J=23	0	0	0	0	0	0	0	0	0	0	0	0	0	0	0	0	0	0	0
J=22	0	0	0	0	0	0	0	0	0	0	0	0	0	0	0	0	0	0	0
J=21	0	0	0	0	0	0	0	0	0	0	0	0	0	0	0	0	0	0	0
J=20	0	0	0	0	0	0	0	0	0	0	0	0	0	0	0	0	0	0	0
J=19	0	0	0	0	0	0	0	0	0	0	0	0	0	0	0	0	0	0	0
J=18	0	0	0	0	0	0	0	0	0	0	0	0	0	0	0	0	0	0	0
J=17	0	0	0	0	0	0	0	0	0	0	0	0	0	0	0	0	0	0	0

Table A.2 Sample Output (Initial Condition).
(continued)

PCVT MARKS ON ZEL	1	2	3	4	5	6	7	8	9	10	11	12	13	14	15	16	17	18	19	20
J=16	0	14	33	70	131	216	318	404	458	458	404	318	216	131	70	33	14	0	0	0
J=15	0	0	48	102	191	318	458	588	666	666	588	458	318	191	102	48	0	0	0	0
J=14	0	0	62	131	248	404	588	755	855	855	755	588	404	248	131	62	0	0	0	0
J=13	0	0	70	149	278	438	646	855	969	969	855	646	438	278	149	70	0	0	0	0
J=12	0	0	70	149	278	438	646	855	969	969	855	646	438	278	149	70	0	0	0	0
J=11	0	0	62	131	248	404	588	755	855	855	755	588	404	248	131	62	0	0	0	0
J=10	0	0	48	102	191	318	458	588	666	666	588	458	318	191	102	48	0	0	0	0
J=9	0	0	33	70	131	216	318	404	458	458	404	318	216	131	70	33	0	0	0	0
J=8	0	0	20	43	80	131	191	248	278	278	248	191	131	80	43	20	0	0	0	0
J=7	0	0	11	23	43	70	102	131	149	149	131	102	70	43	23	11	0	0	0	0
J=6	0	0	5	11	20	33	48	62	70	70	62	48	33	20	11	5	0	0	0	0
J=5	0	0	2	4	8	14	20	26	29	29	26	20	14	8	4	2	0	0	0	0
J=4	0	0	1	2	3	5	7	10	11	11	10	7	5	3	2	1	0	0	0	0
J=3	0	0	0	1	1	2	3	3	3	3	3	3	3	3	3	3	1	0	0	0
J=2	0	0	0	0	0	1	1	1	1	1	1	1	1	1	1	1	0	0	0	0
J=1	0	0	0	0	0	0	0	0	0	0	0	0	0	0	0	0	0	0	0	0

A.5 GLOSSARY OF INPUT VARIABLES

The set of input variables required to define a SIGMET simulation is presented in the following table. Variables are input in standard CDC namelist format in either NAMELIST /OUTPT/ or NAMELIST /START/ as indicated.

NAMELIST /OUTPT/

<u>Variable</u>	<u>Description</u>
ISTART:	Starting parameter = 0 for initial run > 0 for restart runs. For restart runs save tape should be mounted on logical Unit 7
IEDIT:	Frequency of edit cycle
IPLOT:	Frequency of printer plot
IOUT:	Frequency of debug edit cycle
IFILM:	Frequency of film plot
NCYCLS:	Total number of time cycles
KBEG:	Starting edit level (if IEDIT is nonzero printer edit is provided level by level for all variables from K = KBEG to KMAX)
KBGPL:	If IFILM is nonzero plots on horizontal slices K=KBGPL to KMAX are to be prepared

NAMELIST /START/

<u>Variable</u>	<u>Description</u>
KMAX:	No. of vertical levels
IE:	No. of computational zones in x-direction
JE:	No. of computational zones in y-direction
DX:	Grid size in x-direction in meters
DY:	Grid size in y-direction in meters
DELTAT:	Time step size in seconds

VariableDescription

$\left\{ \begin{array}{l} \text{GAM} \\ \text{TNPRS} \\ \text{GAM1} \\ \text{PINV} \end{array} \right\}$	By assigning a non-negative value to GAM, the measured profile of temperature (TPRES) can be replaced by one with TNPRS (in °C) at ground decreasing with altitude at lapse rate GAM (in °C per meter). An inversion layer can be simulated by having a smaller lapse rate GAM1 (in °C/meter) starting at a level where pressure is PINV (in millibar).
ANGLE:	x-axis rotation measured counter clockwise from East in degrees
ZBOT:	Ground elevation (AGL) of measurement location if available
TG:	A two-dimensional array at least IE x JE long representing ground temperature is °C. If measured values for TG are not available, they can be extrapolated from the measurement of temperature in the atmosphere. This is done by setting the value of GDEPTH negative.
GW:	A two dimensional array at least IE x JE long representing ground moisture expressed as fraction of the saturated humidity of air near the ground
HRATE:	A two-dimensional array at least IE x JE long representing external ground heat source, if any
TWATER:	Temperature in °K of water body, if any, present in the region of simulation
TDEEP:	Temperature in °K of underground soil assumed constant everywhere
$\left\{ \begin{array}{l} \text{XORG} \\ \text{XCLAY} \\ \text{XSAND} \end{array} \right\}$	Composition of soil in the region of simulation, in fraction by mass of organic materials, clay and sand, respectively
VEG:	Vegetated fraction of the total surface area
ZNAUT:	Roughness length in meters typical to the terrain over the region
DLAT:	Latitude in degrees of region of simulation
DLONG:	Longitude in degrees of region of simulation
Q:	One-dimensional array of at least KMAX +1 long for σ values
CX1, CX2:	Two parameters specifying the log-linear distribution of σ levels
CX3, CX4:	Two parameters specifying σ values according to a geometric progression series
	Note: If one of two parameters is zero, σ values are not computed and preset values (read through Q) are used.

<u>Variable</u>	<u>Description</u>
GTMHR	Gmt hour (in fraction notation) corresponding to initial simulation time
DAYBEG:	Julian day of initial simulation
PTOP:	Pressure in millibar corresponding to the top level of the model
PBOT:	Standard sea level pressure in millibar
{ UPRES VPRES TPRES CPRES }	Ambient (usually obtained from soundings) values of horizontal wind in meter/sec or in mi/h, temperature °C, humidity in kg/kg. These are one-dimensional arrays of length 30 each.
PPRES:	One-dimensional array of size 30 representing pressure in millibar where UPRES, VPRES, etc., are measured
NPRES:	No. of entries of UPRES, VPRES, etc. (≤ 30)
THETA:	A one-dimensional array of at least NPRES length representing angle in degrees of wind vector measured clockwise from north. If the measurement is available in magnitude/direction format, UPRES should contain the magnitude in meters per sec and THETA the direction. If component measurements are to be entered, UPRES should contain the East-West component, and VPRES should contain the North South component, both in miles per hour, and all THETA should be set at zero.
RELHM:	An array of at least NPRES elements representing values of relative humidity at NPRES levels of the atmosphere. Expressed as percentage of saturated value for air at given temperature. If any of RELHM is nonzero, the measurement CPRES is replaced by new values calculated from RELHM and TPRES.
ALPH:	Time smoothing parameter to damp out high frequency temporal oscillations, $0 \leq \text{ALPH} \leq 1$
ZBL:	Boundary layer height in meters above which an interpolated value from UPRES, VPRES is used for initializing the velocity field. Below ZBL a power law profile is used.
IRAD:	Frequency of cycles when radiation subroutines are called. If zero, radiation contribution is completely ignored.
{ W TRANS SUREM QEFFG }	Radiation parameters
GDEPTH:	Length scale in meters required for solution of ground temperature

Variable

Description

IJCOLM:

A two-dimensional array of size IE x JE, each element corresponding to a given vertical column. A nonzero value will result in printout of a column ($1 \leq K \leq KMAX$) of flow variables every IOU cycles.

APPENDIX B
LINMET ORGANIZATION

B.1 LINMET ORGANIZATION

The 3-D steady linear code LINMET, to calculate stratified flow over terrain was developed during the contract. This code, in essence, solves the Scorer's equation for the Fourier transform of the perturbation vertical velocity and then computes the perturbation to all three components of the velocity. As indicated in the flow diagram (Table B.1), the various specific tasks are done through calls to different subroutines from the main program. The code is written in FORTRAN IV ensuring portability to any computer. An exception is the DPLT subroutine that makes use of machine dependent plotting routines available at Lawrence Berkeley computing facility. This is the only subroutine that has to be deleted or replaced for adaptation to other machines.

B.2 SUBROUTINE DESCRIPTION

In the following, we give a short description of each of the subroutines in LINMET.

INPUT SUBROUTINE

The INPUT subroutine processes data provided through NAMELIST data cards, so that all information required for subsequent normal execution of a problem simulation are available. These data cards provide values for the following quantities:

- spatial step sizes both in horizontal and vertical direction
- powers of two, which define the number of grids in the horizontal directions
- the number of grids in the vertical direction
- height of the computing mesh
- editing and plotting parameters
- option switch for self-prescribed standard data

The terrain height data are normally read from a disk file. INPUT selects a limited area from the entire terrain data and then performs a boundary smoothing to remove boundary related errors

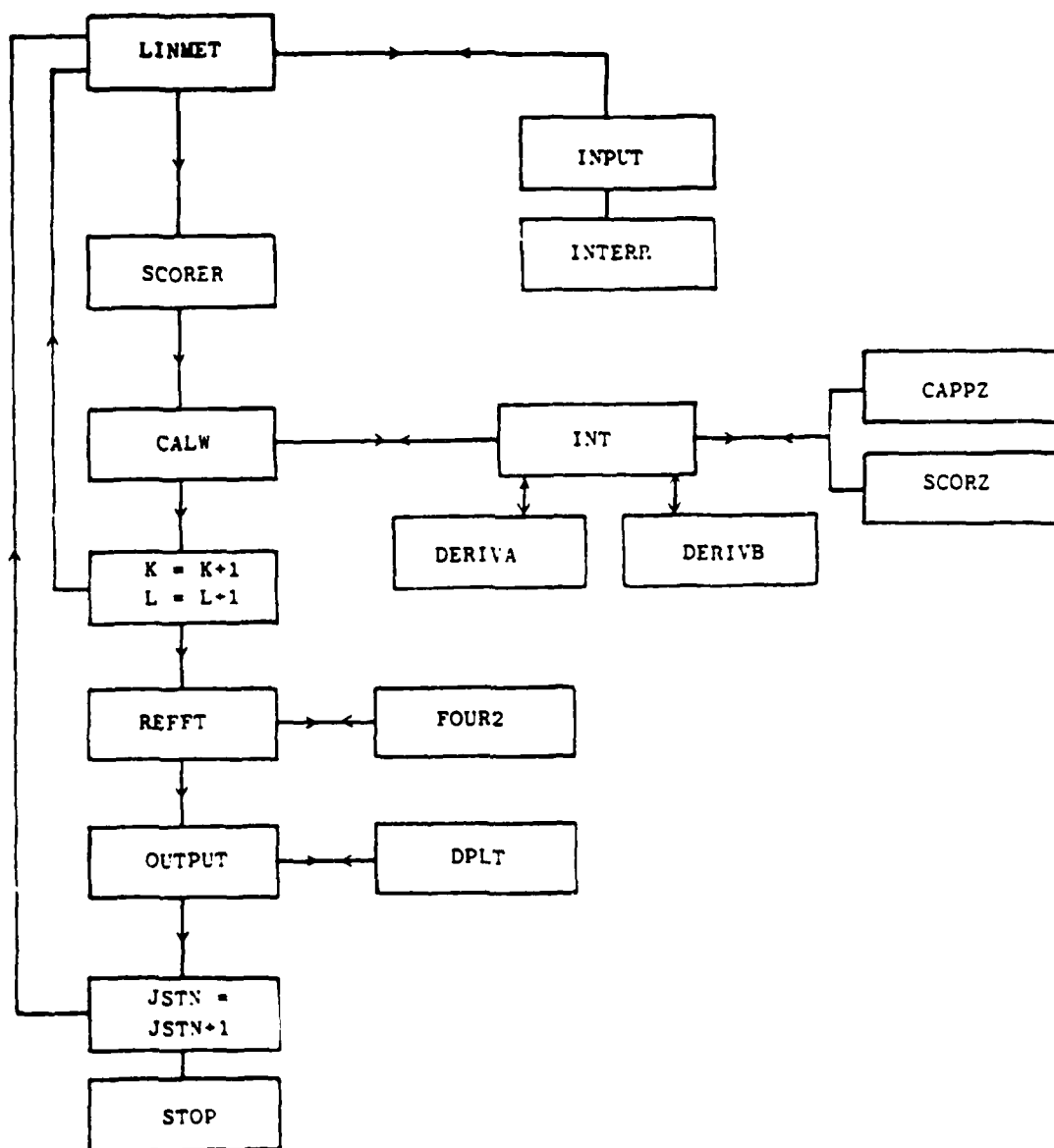


TABLE B.1 LINMET Logical Flow Diagram.

arising from periodic boundary condition. It then computes the Fourier transform of the smoothed terrain data for later use. It also computes the constant vertical mesh with the average terrain height as the lowest level and the top of the computing mesh as the highest level. Through a switch, INPUT is capable of providing self-prescribed meteorological and terrain data that can be used for checking out various aspects of the code.

INTERR SUBROUTINE

The meteorological data read in subroutine INPUT are not necessarily at the levels of the vertical mesh. INTERR interpolates these data to the levels of the vertical grid and stores them in arrays. It also computes the derived quantities from these data arrays and stores them for later use.

SCORER SUBROUTINE

This subroutine is called from the main program in a loop covering all the wave numbers. SCORER first computes the multipliers in the Fourier plane, which are related to various finite difference operations in the physical plane. It then computes the Scorer parameter and the wave vector and stores them in arrays. In doing so it checks for critical levels, if any, and thereby sets up the domain of integration (from ground to critical level, if any, or top of the computing region). It also sets up a switch to avoid integration for certain modes for which the solution is trivial.

CALW SUBROUTINE

This subroutine controls the other subroutines that integrate the Scorer's equation to solve for the perturbation vertical velocity. It first distinguishes between two categories based on the behavior of the Scorer's equation at the top boundary. It then sets up the initial values of the functions corresponding to the top boundary before calling the integration routines. The

integrated function and its derivatives are stored for each vertical level. The latter is required to compute the horizontal perturbation velocity from the vertical perturbation velocity. Once the integration is complete, the bottom boundary condition is utilized to give the actual vertical perturbation velocity in the Fourier plane. Before returning to the main routine, CALW calculates the other perturbation components as well.

INT SUBROUTINE

Subroutine INT, which is called from CALW, performs a step-by-step solution of a system of first-order differential equations (initial values problem) by sixth-order Adams-Moulton Predictor Corrector method, with starting procedure based on Rosser's formula. It employs double precision arithmetic and uses variable step size to satisfy a preset error criterion, but steps are forced to land on multiples of a specified print interval. Before INT is called, another subroutine (INTO) must be called, which initializes various constants used by INT.

DERIVA, DERIVB SUBROUTINES

These subroutines are called from INT to provide derivatives of the function at given vertical height. DERIVA subroutine supplies the derivatives for Case A integration, and DERIVB does the same for Case B. These subroutines are declared in EXTERNAL statements in CALW, because their names appear as dummy parameters in calls to INT routine.

CAPPZ SUBROUTINE

This subroutine function provides the value of the modified wave vector at any altitude by interpolation from the wave vector table that was set up by SCORER. This is frequently called from DERIVA/DERIVB subroutines that must supply derivatives to INT at a great many subdivisions within a vertical grid to satisfy the error criterion.

SCORZ SUBROUTINE

This subroutine function is identical in structure to CAPPZ. It supplies interpolated values of the Scorer's parameter at any altitude to DERIVA/DERIVB.

REFFT SUBROUTINE

Once the perturbation components are calculated for all wave numbers and for all vertical levels, this subroutine is called from the main program. REFFT calls FOUR2 at each vertical level to perform the inverse Fourier transform. The results are stored in three-dimensional arrays.

FOUR2 SUBROUTINE

This is a fast and efficient Fourier transform routine employing Cooley-Tukey algorithm and capable of handling multi-dimensional data. The dimension of the data is required to be an integral power of two. Switches are provided so that the same routine can handle real, complex, and half-complex data and do both Fourier synthesis and analysis.

OUTPUT SUBROUTINE

The OUTPUT subroutine controls the manipulation of two forms of data that flow from the computer to peripheral devices. These outputs are in the form of printer edits or film plots. Both are activated through switches read from data cards. Printer edit provides the three perturbation velocity components along each horizontal slice starting from the top. Film plots include for each horizontal slice a vector plot and two contour plots: one for the magnitude of the horizontal velocity vector and the other for vertical velocity component. On the background of each frame, the contour of the terrain is provided.

DPLT SUBROUTINE

This subroutine prepares the graphic output on film by making use of various plotting subroutines available through IDDS graphic package at Lawrence Berkeley Laboratory. In the event of adaptation of this code to a different computer, the contents of this subroutine should be thoroughly reviewed, and changes should be made to utilize the available plotting routines. If plots are not required, the whole subroutine can be replaced by a dummy subroutine by the same name.

B.3 A SAMPLE LINMET RUN

The deck setup and the output from a typical LINMET run are included here for demonstration. The test problem over a grid of 32 x 4 x 10 is initialized by self-prescribed standard data provided in INPUT (by setting IDUMDAT=1 in NAMELIST data). This self-prescribed data consist of terrain heights corresponding to a two-dimensional Gaussian mountain (no variation on y-direction), a uniform westerly wind of 10 meters/second, and a linear temperature profile corresponding to a constant lapse rate with $T = 288^{\circ}\text{K}$ at sea level.

Table B.2 lists the change cards required to modify the existing version of the code for this test run. Notice that the references to all plotting routines in DPLT are deleted, since plots were not requested for this run. Table B.3 lists the input data cards. Notice that with the option of IDUMDAT=1, the meteorological data are not required. Following Table B.3 is the reproduction of the raw computer output for this run.

Table B.2 List of Change Cards Required for the Demonstration Run.

IDENT	TEST
*****	*IDENT TEST
	*DELETE COMMON.15,COMMON.18 COMMON/TERRAIN/TOPO(41,51),H(32,4) COMMON/FIELDS/U(34,4,20),V(34,4,20),W(34,4,20) COMMON/FFTALL/UTRANZ(2,17,4),VTRANZ(2,17,4),WTRANZ(2,17,4), ZTRANZ(2,17,4),N(2)
	*DELETE COMMON.20 DIMENSION REFFTU(32,4),REFFTV(32,4),REFFTW(32,4),HH(32,4)
	*DELETE DPLT,4,DPLT,218

Table B.3 NAMELIST Input Data for the Demonstration Run.

\$START	
DX	= .1E+04,
DY	= .1E+04,
MPOW	= 5,
NPOW	= 2,
NZ	= 20,
ZTOP	= .5E+04,
NSTN	= 1,
MBEGPR	= 18,
MBEGPL	= 18,
IEDIT	= 1.
IFILM	= 0.
IDUMDAT	= 1.
\$END	

Copy available to DTIC does not
 permit fully legible reproduction.

Table B.4 Computer Output for the Demonstration Run.

TERRAIN DATA IN METERS														
1	2	3	4	5	6	7	8	9	10	11	12	13	14	15
10	17	18	19	20	21	22	23	24	25	26	27	28	29	30
31	32													
1	10.3	20.7	46.0	71.3	105.4	209.6	282.1	367.9	465.0	569.0	676.6	778.6	1.040.0	939.4
	940.5	1000.0	900.5	860.0	778.0	676.6	569.0	465.0	367.9	282.1	209.6	151.0	105.4	71.3
	46.0	29.7												
2	15.3	29.7	46.0	71.3	105.4	209.6	282.1	367.9	465.0	569.0	676.6	778.6	1.040.0	939.4
	940.5	1000.0	900.5	860.0	778.0	676.6	569.0	465.0	367.9	282.1	209.6	151.0	105.4	71.3
	46.0	29.7												
3	10.3	29.7	46.0	71.3	105.4	209.6	282.1	367.9	465.0	569.0	676.6	778.6	1.040.0	939.4
	940.5	1000.0	900.5	860.0	778.0	676.6	569.0	465.0	367.9	282.1	209.6	151.0	105.4	71.3
	46.0	29.7												
0	10.3	29.7	46.0	71.3	105.4	209.6	282.1	367.9	465.0	569.0	676.6	778.6	1.040.0	939.4
	940.5	1000.0	900.5	860.0	778.0	676.6	569.0	465.0	367.9	282.1	209.6	151.0	105.4	71.3
	46.0	29.7												
ZBUT AVERAGE TERRAIN HEIGHTS 440.99														

STATION ID- DUMMY RELEASE TIME- 0 UTMX= 0.00 UTMZ= 0.00 2451E 0.00														
Z	X	Y	U	V	Y	Y	Y	Y	Y	Y	Y	Y	Y	Y
0000312E+03 0	0	0	1000000E+02 0	1000000E+02 0	20350007E+03 0	29110049E+03 0	27070111E+03 0	1000000E+02 0						
0000005E+03 0	0	0	1000000E+02 0	1000000E+02 0	20350007E+03 0	29110049E+03 0	27070111E+03 0	1000000E+02 0						
0200033E+00 0	0	0	1000000E+02 0	1000000E+02 0	20350007E+03 0	29110049E+03 0	27070111E+03 0	1000000E+02 0						
1000740E+00 0	0	0	1000000E+02 0	1000000E+02 0	20350007E+03 0	29110049E+03 0	27070111E+03 0	1000000E+02 0						
1000731E+00 0	0	0	1000000E+02 0	1000000E+02 0	20350007E+03 0	29110049E+03 0	27070111E+03 0	1000000E+02 0						
10000795E+00 0	0	0	1000000E+02 0	1000000E+02 0	20350007E+03 0	29110049E+03 0	27070111E+03 0	1000000E+02 0						
21200272E+00 0	0	0	1000000E+02 0	1000000E+02 0	20350007E+03 0	29110049E+03 0	27070111E+03 0	1000000E+02 0						
2360575E+00 0	0	0	1000000E+02 0	1000000E+02 0	20350007E+03 0	29110049E+03 0	27070111E+03 0	1000000E+02 0						
26000227E+00 0	0	0	1000000E+02 0	1000000E+02 0	20350007E+03 0	29110049E+03 0	27070111E+03 0	1000000E+02 0						
28000700E+00 0	0	0	1000000E+02 0	1000000E+02 0	20350007E+03 0	29110049E+03 0	27070111E+03 0	1000000E+02 0						
30000100E+00 0	0	0	1000000E+02 0	1000000E+02 0	20350007E+03 0	29110049E+03 0	27070111E+03 0	1000000E+02 0						
3320035E+00 0	0	0	1000000E+02 0	1000000E+02 0	20350007E+03 0	29110049E+03 0	27070111E+03 0	1000000E+02 0						
3500313E+00 0	0	0	1000000E+02 0	1000000E+02 0	20350007E+03 0	29110049E+03 0	27070111E+03 0	1000000E+02 0						
38002613E+00 0	0	0	1000000E+02 0	1000000E+02 0	20350007E+03 0	29110049E+03 0	27070111E+03 0	1000000E+02 0						
40002091E+00 0	0	0	1000000E+02 0	1000000E+02 0	20350007E+03 0	29110049E+03 0	27070111E+03 0	1000000E+02 0						
4201156E+00 0	0	0	1000000E+02 0	1000000E+02 0	20350007E+03 0	29110049E+03 0	27070111E+03 0	1000000E+02 0						
45201043E+00 0	0	0	1000000E+02 0	1000000E+02 0	20350007E+03 0	29110049E+03 0	27070111E+03 0	1000000E+02 0						
47000523E+00 0	0	0	1000000E+02 0	1000000E+02 0	20350007E+03 0	29110049E+03 0	27070111E+03 0	1000000E+02 0						
5000000E+00 0	0	0	1000000E+02 0	1000000E+02 0	20350007E+03 0	29110049E+03 0	27070111E+03 0	1000000E+02 0						

Table B.4 (cont'd) Computer Output for the Demonstration Run.

3000.02	10.000	0.000	257.196	6971.094	.95E+03	0.	0.	-.10E-01	0.	0.	-.10E-10	.95E-00	.37E-00
2000.27	10.000	0.000	250.505	72134.085	.97E+03	0.	0.	-.10E-01	0.	0.	-.10E-17	.80E-04	.36E-00
2000.52	10.000	0.000	261.995	74000.072	.90E+03	0.	0.	-.10E-01	0.	0.	-.10E-17	.95E-00	.30E-00
2300.37	10.000	0.000	264.394	76042.760	.10E+04	0.	0.	-.10E-01	0.	0.	-.10E-17	.62E-04	.35E-00
2120.03	10.000	0.000	266.794	79196.637	.10E+04	0.	0.	-.10E-01	0.	0.	-.10E-17	.92E-00	.34E-00
1000.00	10.000	0.000	269.193	81550.534	.11E+04	0.	0.	-.10E-01	0.	0.	-.10E-17	.91E-04	.34E-00
1000.73	10.000	0.000	271.593	83904.921	.11E+04	0.	0.	-.10E-01	0.	0.	-.10E-17	.90E-00	.33E-00
1000.70	10.000	0.000	273.992	86250.309	.11E+04	0.	0.	-.10E-01	0.	0.	-.10E-17	.89E-04	.33E-00
1100.00	10.000	0.000	276.392	88612.196	.11E+04	0.	0.	-.10E-01	0.	0.	.12E-16	.88E-00	.32E-00
920.09	10.000	0.000	278.791	90966.083	.11E+04	0.	0.	-.10E-01	0.	0.	.12E-16	.88E-04	.31E-00
000.94	10.000	0.000	281.191	93319.970	.12E+04	0.	0.	-.10E-01	0.	0.	-.10E-17	.87E-00	.31E-00
400.99	10.000	0.000	283.590	95673.857	.12E+04	0.	0.	-.10E-01	0.	0.	-.10E-17	.86E-00	.31E-00
CASE 4	00 2	L0 2	L0 1	INTEGRATION	CARRIED FROM	02	1	TO 20	00.	0F	STEPS	TAKEN	95
CASE 4	00 2	L0 2	L0 2	INTEGRATION	CARRIED FROM	02	1	TO 20	00.	0F	STEPS	TAKEN	95
CASE 4	00 2	L0 3	L0 3	INTEGRATION	CARRIED FROM	02	1	TO 20	00.	0F	STEPS	TAKEN	95
CASE 4	00 3	L0 1	L0 4	INTEGRATION	CARRIED FROM	02	1	TO 20	00.	0F	STEPS	TAKEN	95
CASE 4	00 3	L0 2	L0 1	INTEGRATION	CARRIED FROM	02	1	TO 20	00.	0F	STEPS	TAKEN	95
CASE 4	00 3	L0 3	L0 2	INTEGRATION	CARRIED FROM	02	1	TO 20	00.	0F	STEPS	TAKEN	95
CASE 4	00 3	L0 4	L0 3	INTEGRATION	CARRIED FROM	02	1	TO 20	00.	0F	STEPS	TAKEN	95
CASE 4	00 4	L0 1	L0 2	INTEGRATION	CARRIED FROM	02	1	TO 20	00.	0F	STEPS	TAKEN	95
CASE 4	00 4	L0 2	L0 3	INTEGRATION	CARRIED FROM	02	1	TO 20	00.	0F	STEPS	TAKEN	95
CASE 4	00 4	L0 3	L0 4	INTEGRATION	CARRIED FROM	02	1	TO 20	00.	0F	STEPS	TAKEN	95
CASE 4	00 5	L0 1	L0 1	INTEGRATION	CARRIED FROM	02	1	TO 20	00.	0F	STEPS	TAKEN	95
CASE 4	00 5	L0 2	L0 2	INTEGRATION	CARRIED FROM	02	1	TO 20	00.	0F	STEPS	TAKEN	95
CASE 4	00 5	L0 3	L0 3	INTEGRATION	CARRIED FROM	02	1	TO 20	00.	0F	STEPS	TAKEN	95
CASE 4	00 5	L0 4	L0 4	INTEGRATION	CARRIED FROM	02	1	TO 20	00.	0F	STEPS	TAKEN	95
CASE 4	00 6	L0 1	L0 1	INTEGRATION	CARRIED FROM	02	1	TO 20	00.	0F	STEPS	TAKEN	95
CASE 4	00 6	L0 2	L0 2	INTEGRATION	CARRIED FROM	02	1	TO 20	00.	0F	STEPS	TAKEN	95
CASE 4	00 6	L0 3	L0 3	INTEGRATION	CARRIED FROM	02	1	TO 20	00.	0F	STEPS	TAKEN	95
CASE 4	00 6	L0 4	L0 4	INTEGRATION	CARRIED FROM	02	1	TO 20	00.	0F	STEPS	TAKEN	95
CASE 4	00 7	L0 1	L0 1	INTEGRATION	CARRIED FROM	02	1	TO 20	00.	0F	STEPS	TAKEN	95
CASE 4	00 7	L0 2	L0 2	INTEGRATION	CARRIED FROM	02	1	TO 20	00.	0F	STEPS	TAKEN	95
CASE 4	00 7	L0 3	L0 3	INTEGRATION	CARRIED FROM	02	1	TO 20	00.	0F	STEPS	TAKEN	95
CASE 4	00 7	L0 4	L0 4	INTEGRATION	CARRIED FROM	02	1	TO 20	00.	0F	STEPS	TAKEN	95
CASE 4	00 8	L0 1	L0 1	INTEGRATION	CARRIED FROM	02	1	TO 20	00.	0F	STEPS	TAKEN	95
CASE 4	00 8	L0 2	L0 2	INTEGRATION	CARRIED FROM	02	1	TO 20	00.	0F	STEPS	TAKEN	95
CASE 4	00 8	L0 3	L0 3	INTEGRATION	CARRIED FROM	02	1	TO 20	00.	0F	STEPS	TAKEN	95
CASE 4	00 8	L0 4	L0 4	INTEGRATION	CARRIED FROM	02	1	TO 20	00.	0F	STEPS	TAKEN	95
CASE 4	00 9	L0 1	L0 1	INTEGRATION	CARRIED FROM	02	1	TO 20	00.	0F	STEPS	TAKEN	95
CASE 4	00 9	L0 2	L0 2	INTEGRATION	CARRIED FROM	02	1	TO 20	00.	0F	STEPS	TAKEN	95
CASE 4	00 9	L0 3	L0 3	INTEGRATION	CARRIED FROM	02	1	TO 20	00.	0F	STEPS	TAKEN	95
CASE 4	00 9	L0 4	L0 4	INTEGRATION	CARRIED FROM	02	1	TO 20	00.	0F	STEPS	TAKEN	95
CASE 4	00 10	L0 1	L0 1	INTEGRATION	CARRIED FROM	02	1	TO 20	00.	0F	STEPS	TAKEN	95
CASE 4	00 10	L0 2	L0 2	INTEGRATION	CARRIED FROM	02	1	TO 20	00.	0F	STEPS	TAKEN	95
CASE 4	00 10	L0 3	L0 3	INTEGRATION	CARRIED FROM	02	1	TO 20	00.	0F	STEPS	TAKEN	95
CASE 4	00 10	L0 4	L0 4	INTEGRATION	CARRIED FROM	02	1	TO 20	00.	0F	STEPS	TAKEN	95

Table B.4 (cont'd) Computer Output for the Demonstration Run.

CASE 4	4011	L 1	INTEGRATION	CARRIED	FROM	2	1	TO	20	NU.	OF	STEPS	TAKEN	95
CASE 4	4011	L 2	INTEGRATION	CARRIED	FROM	2	1	TO	20	NU.	OF	STEPS	TAKEN	95
CASE 4	4011	L 3	INTEGRATION	CARRIED	FROM	2	1	TO	20	NU.	OF	STEPS	TAKEN	95
CASE 4	4011	L 4	INTEGRATION	CARRIED	FROM	2	1	TO	20	MI.	OF	STEPS	TAKEN	95
CASE 4	4012	L 1	INTEGRATION	CARRIED	FROM	2	1	TO	20	NU.	OF	STEPS	TAKEN	95
CASE 4	4012	L 2	INTEGRATION	CARRIED	FROM	2	1	TO	20	MI.	OF	STEPS	TAKEN	95
CASE 4	4012	L 3	INTEGRATION	CARRIED	FROM	2	1	TO	20	NU.	OF	STEPS	TAKEN	95
CASE 4	4012	L 4	INTEGRATION	CARRIED	FROM	2	1	TO	20	MI.	OF	STEPS	TAKEN	95
CASE 4	4013	L 1	INTEGRATION	CARRIED	FROM	2	1	TO	20	NU.	OF	STEPS	TAKEN	95
CASE 4	4013	L 2	INTEGRATION	CARRIED	FROM	2	1	TO	20	MI.	OF	STEPS	TAKEN	95
CASE 4	4013	L 3	INTEGRATION	CARRIED	FROM	2	1	TO	20	NU.	OF	STEPS	TAKEN	95
CASE 4	4013	L 4	INTEGRATION	CARRIED	FROM	2	1	TO	20	MI.	OF	STEPS	TAKEN	95
CASE 4	4014	L 1	INTEGRATION	CARRIED	FROM	2	1	TO	20	NU.	OF	STEPS	TAKEN	95
CASE 4	4014	L 2	INTEGRATION	CARRIED	FROM	2	1	TO	20	MI.	OF	STEPS	TAKEN	95
CASE 4	4014	L 3	INTEGRATION	CARRIED	FROM	2	1	TO	20	NU.	OF	STEPS	TAKEN	95
CASE 4	4014	L 4	INTEGRATION	CARRIED	FROM	2	1	TO	20	MI.	OF	STEPS	TAKEN	95
CASE 4	4015	L 1	INTEGRATION	CARRIED	FROM	2	1	TO	20	NU.	OF	STEPS	TAKEN	95
CASE 4	4015	L 2	INTEGRATION	CARRIED	FROM	2	1	TO	20	MI.	OF	STEPS	TAKEN	95
CASE 4	4015	L 3	INTEGRATION	CARRIED	FROM	2	1	TO	20	NU.	OF	STEPS	TAKEN	95
CASE 4	4015	L 4	INTEGRATION	CARRIED	FROM	2	1	TO	20	MI.	OF	STEPS	TAKEN	95
CASE 4	4016	L 1	INTEGRATION	CARRIED	FROM	2	1	TO	20	NU.	OF	STEPS	TAKEN	95
CASE 4	4016	L 2	INTEGRATION	CARRIED	FROM	2	1	TO	20	MI.	OF	STEPS	TAKEN	95
CASE 4	4016	L 3	INTEGRATION	CARRIED	FROM	2	1	TO	20	NU.	OF	STEPS	TAKEN	95
CASE 4	4016	L 4	INTEGRATION	CARRIED	FROM	2	1	TO	20	MI.	OF	STEPS	TAKEN	95
CASE 4	4016	L 5	INTEGRATION	CARRIED	FROM	2	1	TO	20	MI.	OF	STEPS	TAKEN	95
CASE 4	4016	L 6	INTEGRATION	CARRIED	FROM	2	1	TO	20	MI.	OF	STEPS	TAKEN	95

Table B.4 (cont'd) Computer Output for the Demonstration Run.

J#	ELEVATION ABOVE MEAN TERRAIN ^{00 METERS}																															
	21	22	23	24	25	26	27	28	29	30	31	32	13	14	15	16	17	18	19	20												
J# 0	0.00	0.00	0.00	0.00	0.00	0.00	0.00	0.00	0.00	0.00	0.00	0.00	0.00	0.00	0.00	0.00	0.00	0.00	0.00	0.00	0.00	0.00										
J# 3	0.00	0.00	0.00	0.00	0.00	0.00	0.00	0.00	0.00	0.00	0.00	0.00	0.00	0.00	0.00	0.00	0.00	0.00	0.00	0.00	0.00	0.00										
J# 2	0.00	0.00	0.00	0.00	0.00	0.00	0.00	0.00	0.00	0.00	0.00	0.00	0.00	0.00	0.00	0.00	0.00	0.00	0.00	0.00	0.00	0.00										
J# 1	0.00	0.00	0.00	0.00	0.00	0.00	0.00	0.00	0.00	0.00	0.00	0.00	0.00	0.00	0.00	0.00	0.00	0.00	0.00	0.00	0.00	0.00										

J#	ELEVATION ABOVE MEAN TERRAIN ^{00 METERS}																															
	21	22	23	24	25	26	27	28	29	30	31	32	13	14	15	16	17	18	19	20												
J# 0	0.00	0.00	0.00	0.00	0.00	0.00	0.00	0.00	0.00	0.00	0.00	0.00	0.00	0.00	0.00	0.00	0.00	0.00	0.00	0.00	0.00	0.00										
J# 3	0.00	0.00	0.00	0.00	0.00	0.00	0.00	0.00	0.00	0.00	0.00	0.00	0.00	0.00	0.00	0.00	0.00	0.00	0.00	0.00	0.00	0.00										
J# 2	0.00	0.00	0.00	0.00	0.00	0.00	0.00	0.00	0.00	0.00	0.00	0.00	0.00	0.00	0.00	0.00	0.00	0.00	0.00	0.00	0.00	0.00										
J# 1	0.00	0.00	0.00	0.00	0.00	0.00	0.00	0.00	0.00	0.00	0.00	0.00	0.00	0.00	0.00	0.00	0.00	0.00	0.00	0.00	0.00	0.00										

J#	ELEVATION ABOVE MEAN TERRAIN ^{00 METERS}																															
	21	22	23	24	25	26	27	28	29	30	31	32	13	14	15	16	17	18	19	20												
J# 0	0.00	0.00	0.00	0.00	0.00	0.00	0.00	0.00	0.00	0.00	0.00	0.00	0.00	0.00	0.00	0.00	0.00	0.00	0.00	0.00	0.00	0.00										
J# 3	0.00	0.00	0.00	0.00	0.00	0.00	0.00	0.00	0.00	0.00	0.00	0.00	0.00	0.00	0.00	0.00	0.00	0.00	0.00	0.00	0.00	0.00										
J# 2	0.00	0.00	0.00	0.00	0.00	0.00	0.00	0.00	0.00	0.00	0.00	0.00	0.00	0.00	0.00	0.00	0.00	0.00	0.00	0.00	0.00	0.00										
J# 1	0.00	0.00	0.00	0.00	0.00	0.00	0.00	0.00	0.00	0.00	0.00	0.00	0.00	0.00	0.00	0.00	0.00	0.00	0.00	0.00	0.00	0.00										

J#	ELEVATION ABOVE MEAN TERRAIN ^{00 METERS}																															
	21	22	23	24	25	26	27	28	29	30	31	32	13	14	15	16	17	18	19	20												
J# 0	0.00	0.00	0.00	0.00	0.00	0.00	0.00	0.00	0.00	0.00	0.00	0.00	0.00	0.00	0.00	0.00	0.00	0.00	0.00	0.00	0.00	0.00										
J# 3	0.00	0.00	0.00	0.00	0.00	0.00	0.00	0.00	0.00	0.00	0.00	0.00	0.00	0.00	0.00	0.00	0.00	0.00	0.00	0.00	0.00	0.00										
J# 2	0.00	0.00	0.00	0.00	0.00	0.00	0.00	0.00	0.00	0.00	0.00	0.00	0.00	0.00	0.00	0.00	0.00	0.00	0.00	0.00	0.00	0.00										
J# 1	0.00	0.00	0.00	0.00	0.00	0.00	0.00	0.00	0.00	0.00	0.00	0.00	0.00	0.00	0.00	0.00	0.00	0.00	0.00	0.00	0.00	0.00										

Copy available to DTIC does not permit fully legible reproduction

APPENDIX C
VARMET ORGANIZATION

C.1 VARMET ORGANIZATION

VARMET is written in modular form to enhance the reading of the code and to facilitate structural changes or additions. The code is divided into three phases as shown in Figure C.1. The initialization phase defines the problem parameters, generates the computational mesh, and specifies the estimated flow field. The adjustment phase computes a nondivergent flow field based on the estimated field determined in the initialization phase, and the the output phase edits the flow field variables and saves the final solution on tape. Figure C.2 is a flowchart showing the logical flow of the Fortran code in addition to summarizing the subroutine functions.

C.2 SUBROUTINE DESCRIPTIONS

CARDS SUBROUTINE

CARDS interprets free-form input card data, loading blank common according to the position of a variable within the common block. CARDS performs a function similar to a namelist statement, but unlike namelist, it is machine independent. Section C.3 describes the CARDS input form accepted by subroutine CARDS.

CNWAD SUBROUTINE

CNWAD adjusts the estimated flow field in conformal space. The estimated wind components are first transformed from real to conformal space. The velocity potential is then determined based on the transformed wind components through successive line over-relaxation algorithm. Once the potential field is known the non-divergent velocity field is computed. Finally, an inverse transformation is applied to determine the final values of the velocity components in real space.

CONTROLLING ROUTINE

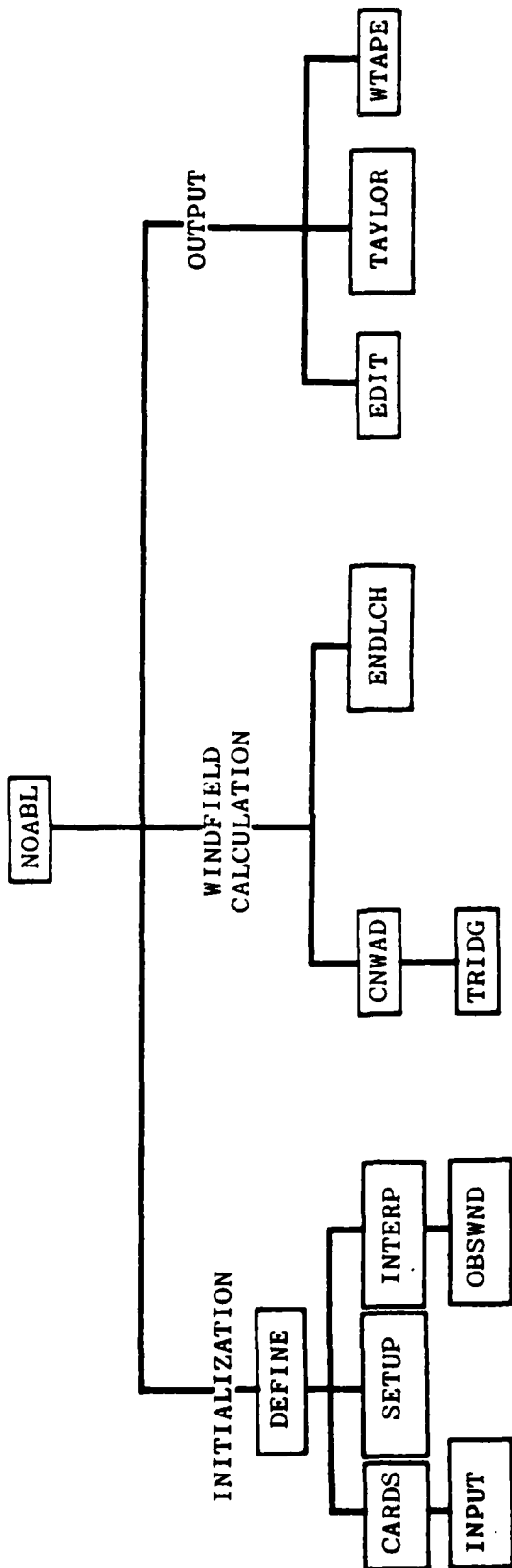


Figure C.1 Grouping of Related functions.

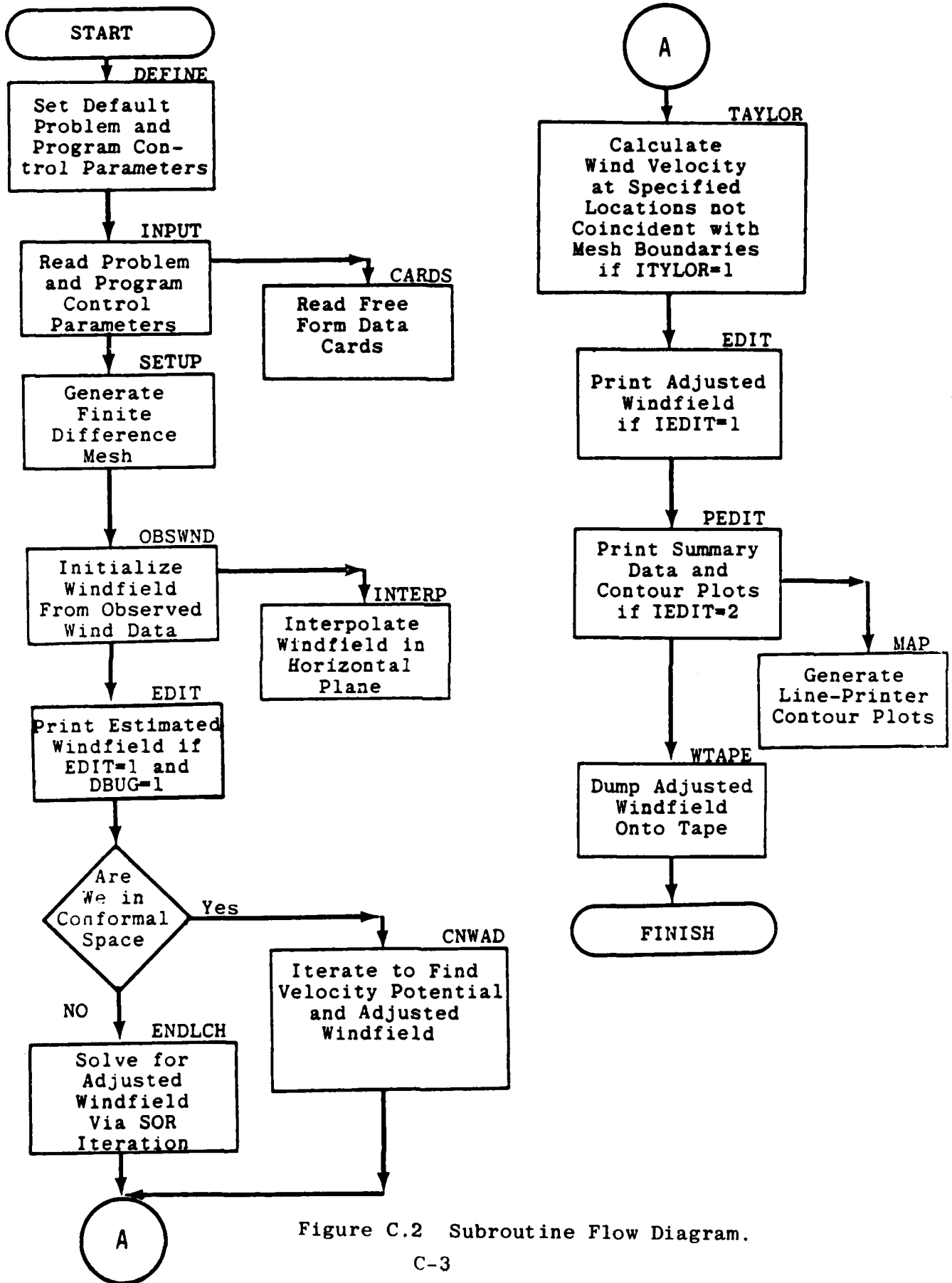


Figure C.2 Subroutine Flow Diagram.

DEFINE SUBROUTINE

DEFINE zeroes common area and sets default values of program and problem control parameters. A list of default values is given in C.4.

EDIT SUBROUTINE

EDIT generates line printer output of the flow field variables. A control flag may be set to bypass this capability if the data are processed by a separate program developed to produce vector and contour plots of the calculated wind field or if output produced by subroutine PEDIT is preferred. EDIT may be called from two locations in the program flow (see Figure C.2). EDIT prints for each cell (i,j,k) the velocity components (u,v,w), the local divergence, and velocity potential in blocks corresponding to horizontal planes. All or part of the computational domain may be printed by appropriately setting IMN, IMX, JMN, JMX, KMN, and KMX.

ENDLCH SUBROUTINE

ENDLCH adjusts the estimated flow field in real space through an SOR iteration to obtain the divergence-free wind field. The effects of topography and, to some extent, atmospheric stability are accounted for in the iteration. Boundary conditions are imposed only along the terrain boundary where the normal velocity is taken to be zero. Velocities at the lateral and upper boundary surfaces are determined by the iteration procedure.

INPUT SUBROUTINE

Terrain, surface winds, mesh parameters, and program control data are entered through subroutine INPUT. INPUT utilizes subroutine CARDS to initialize the mesh parameter, program control, and surface winds data. Terrain data may be entered through an input tape, data cards, or data statement.

INTERP SUBROUTINE

INTERP generates the horizontal distribution of the estimated wind field. The observed data at a given level above the terrain are interpolated using a $1/r^2$ weighting factor to obtain the set of velocity components corresponding to the appropriate cell faces for that level.

MAP SUBROUTINE

MAP generates line printer contour plots of the terrain, velocity components, wind speed, divergence, and velocity potential. For three-dimensional domains, contour plots are defined for the distribution of a variable on a horizontal plane. When the two-dimensional option is chosen, the contour plots represent the distribution in the 2-D plane of the computation.

OBSWND SUBROUTINE

OBSWND initializes the estimated flow field. Surface data from one or more observation stations and/or upper-air data from one observation station are interpolated to define the discrete field of estimated velocity components throughout the mesh.

PEDIT SUBROUTINE

PEDIT provides a summary edit of mesh parameters and calls subroutine MAP to provide contour line printer plots of the flow variables. PEDIT may be used in place of subroutine EDIT to reduce the volume of output or if detailed numbers are not required.

SETUP SUBROUTINE

Subroutine SETUP initializes the finite difference mesh according to mesh spacing and domain size information provided by INPUT. SETUP assumes constant zoning in both the x and y directions. For real space calculations, zoning in the vertical direction is also assumed constant. In the conformal mode, either constant or

variable zoning may be used. Variable zoning may be generated in one of two ways. A log-linear distribution is available that assumes a minimum zone size at the surface and expands the zoning with increasing altitude according to a logarithmic formula. In lieu of this expansion, a geometric increase in zone size may be chosen. Again, the model assumes a minimum zone size at the terrain surface and expands subsequent zones in the vertical by a constant factor, γ computed in SETUP based on DZMIN, KMAX, and ZDIST. To avoid large truncation errors, γ should be kept in the range $1.0 < \gamma < 1.3$.

TAYLOR SUBROUTINE

TAYLOR interpolates a wind speed and direction at a specified number of points within the mesh using a second-order TAYLOR expansion about the points of interest. TAYLOR has no effect on the solution of the adjusted wind field and is only used for editing purposes.

TRIDG SUBROUTINE

TRIDG inverts the tridiagonal matrix composed of the coefficients defined by the finite difference approximation to the governing equation for the velocity potential along a column (i,j). TRIDG is a special adaptation of the Gaussian Elimination Procedure.

WTAPE SUBROUTINE

Subroutine WTAPE dumps the common block onto tape after the estimated and adjusted wind fields are calculated. The common block contains all the pertinent zoning information and field variable arrays.

C.3 DESCRIPTION OF INPUT DATA

VARMET requires several types of input data to initialize a run. Control flags are used to guide the simulation along one of many paths present in the code. Mesh parameters are necessary to describe the problem geometry. Terrain data are needed to define the bottom boundary of the computational domain, and observed wind data are required to determine an estimated wind field throughout the domain.

Free-form input-card data comprising the control flags, mesh parameters, and surface/upper air wind observations are read by subroutine CARDS. Hollerith headings for specified locations within the mesh where wind speed and direction data are to be edited (see below) are read from cards during the initialization phase. Terrain data are read from cards or tape or initialized via a data statement in subroutine INPUT. The format structure of terrain data may need to be modified in INPUT to conform to the specific data tapes being processed.

The Input Variable Glossary in Section C.4 contains the necessary input parameters read by subroutine CARDS. These variables comprise the start or initial simulation deck. VARMET has the capability to process one or more wind simulation cases in a single run. If operating in this mode, additional blocks of free-form data are included behind the start deck and serve to modify only those parameters that change from simulation to simulation. A detailed description of the general card input form and data block arrangement is described below.

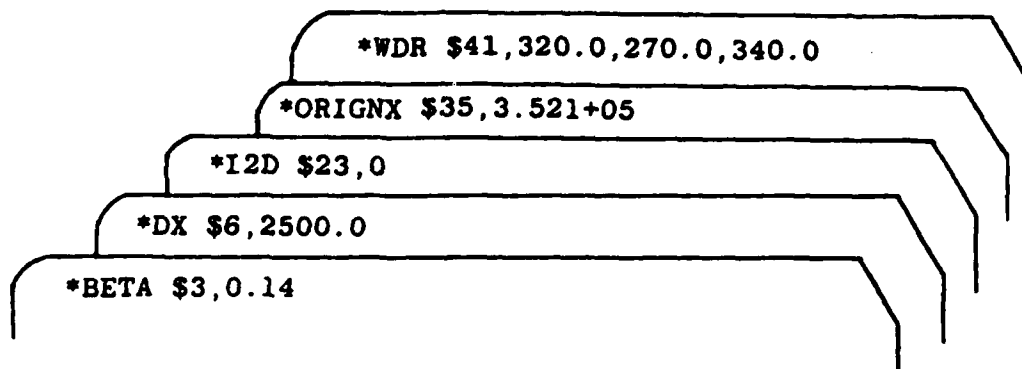
FORMAT OF THE INPUT DATA CARDS

The input data cards found in the glossary are read by subroutine CARDS according to the following format:

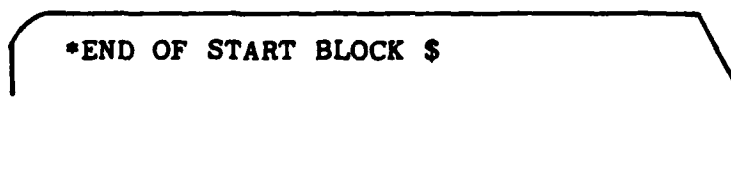
1. An asterisk is entered in column 1.
2. After the asterisk any form of a Hollerith label (normally the variable name) may be entered.
3. A dollar sign is entered.

4. The location in Blank Common is entered followed by a comma.
5. The numerical value of the variable is entered;
 - a. if the variable is integer, enter the value as integer.
 - b. if the variable is real, enter the value in floating point or E-format.
 - c. if the variable is logical, enter a 1 for true, 0 for false.
 - d. if an array is being input, either enter each element individually (as in a-c above), or enter multiple elements on one card.

Example:



To end a block of data, the field following the dollar sign is left blank. For example:



The start deck should contain values for each of the variables listed in the glossary that differ from their preassigned value specified in subroutine DEFINE. If more than one simulation will be processed, additional decks for each subsequent simulation must be included. These additional decks should contain only those variables that need modifying. In most cases the modifications will include at a minimum the redefinition of the date and time of the simulation and of the observed wind station data. An example of a multisimulation deck setup is given in Figure C.3.

It is often desirable to edit wind speed and direction data at specified locations within the computational domain that do not necessarily coincide with a mesh boundary. This capability is provided by subroutine TAYLOR. TAYLOR computes and edits wind information along a vertical column for up to 25 specific locations within the area of interest. Hollerith headings (of up to four characters) may be provided via data cards for these locations. These cards must appear after the first simulation deck and before the terrain data deck as shown in Figure C.3. This Hollerith information must be entered in a 20A4 format. Default numerical headings will be provided if these cards are not present.

Terrain data (assumed to be in meters) may be initialized in one of three ways as discussed above. Data on tape are read from unit 8 (8F10.8 format). Data on cards are read from a terrain data deck directly following the start deck (10F8.1 format). Whether the terrain data are on cards or tape, the first terrain height data point is assumed to be located in the southwest corner of the grid and ordered such that the elements in each row are read from west to east, and the rows are read from south to north. The terrain data statement option exists for 2-D problems in which the volume of terrain data is minimal and may be "hardwired" for a specific terrain configuration.

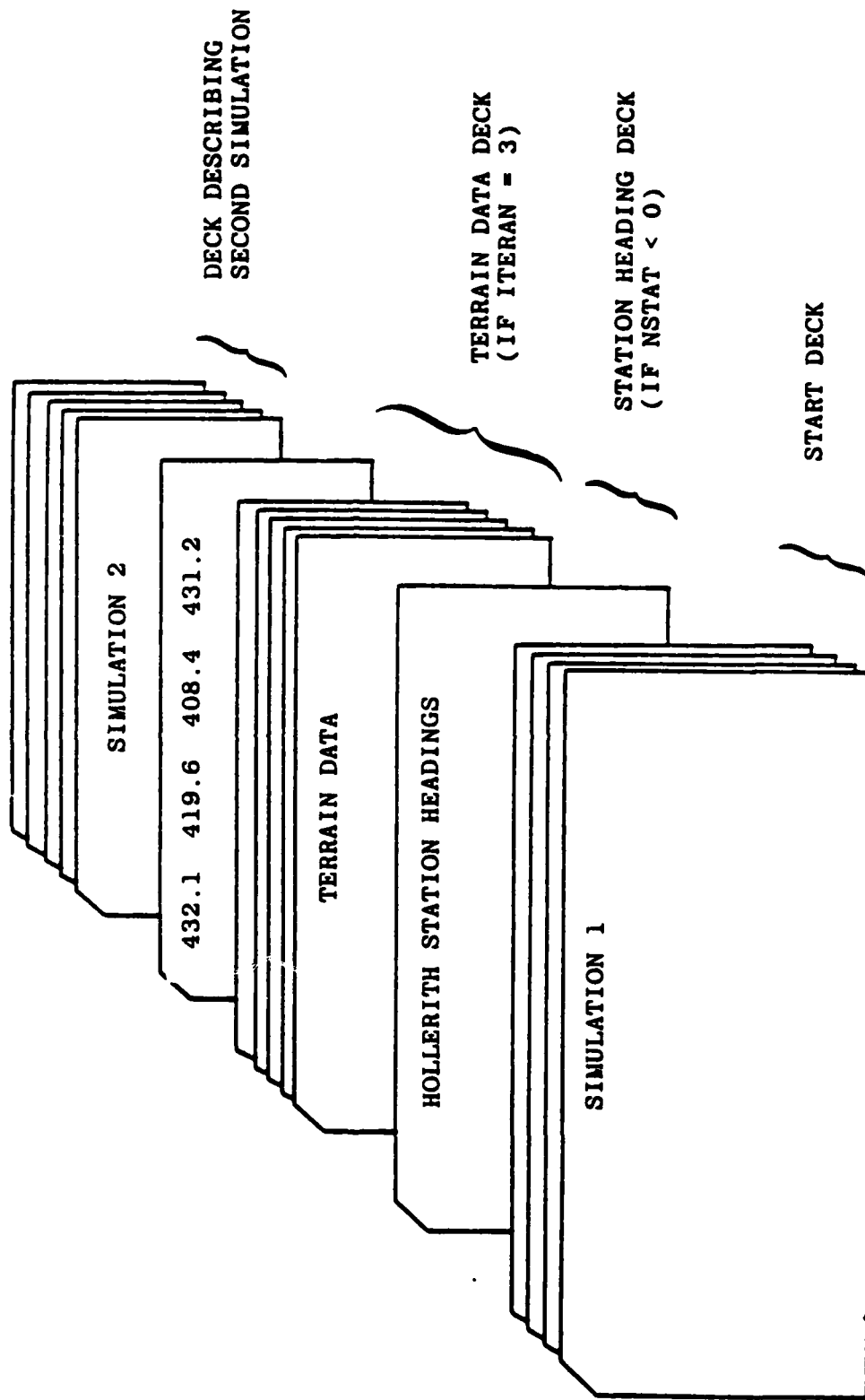


Figure C.3 Free-Form Input Deck Setup.

C.4 GLOSSARY OF INPUT VARIABLES

<u>VARIABLE</u>	<u>LOCATION</u>	<u>TYPE</u>	<u>DEFAULT</u>	<u>DEFINITION</u>
ALFA1	1	Real	0.70710678	Defines horizontal transmissivity $\tau_h = 1.0/(2.0*ALFA1**2)$
ALFA2	2	Real	0.70710678	Defines vertical transmissivity $\tau_v = 1.0/(2.0*ALFA2**2)$
ATOP	343	Real		Wind direction at top of mesh (degrees)
BETA	3	Real	0.1429	Exponent of power law profile
DEBUG	5	Integer	0	Debug flag 0: no debug edit 1: turn on debug edits
DMP	39	Real	0.0	Damping factor for conformal simulations of highly stable flow; suggest: $DMP \sim .05 + .1$ for $\tau_v < .01$
DX	6	Real	2000.0	Constant zone size in x-direction (east) (m)
DY	7	Real	2000.0	Constant zone size in y-direction (north) (m)
DZ	8	Real		Constant zone size in z-direction (vertical) (m). Set for real space runs only
DZMIN	9	Real	30.0	Minimum vertical zone size (m). Specified when ISIG = 3
EPSLN	10	Real	0.1	min $\Delta\phi_{ijk}$ + conformal space min Div _{ijk} + real space
I2D	23	Integer	0	Space dimension flag 0: 3-D space (x,y,z or σ) 1: 2-D space (x,y or σ)

<u>VARIABLE</u>	<u>LOCATION</u>	<u>TYPE</u>	<u>DEFAULT</u>	<u>DEFINITION</u>
IDAY	11	Integer	1	Day of month being simulated
IEDIT	12	Integer	0	Edit flag 0: no edit of flow variables 1: edit flow variables 2: generate line printer contour plots 3: generate summary edit plus line printer contour plots
IHOUR	13	Integer	1	Hour of day being simulated
IMAX	14	Integer	30	Maximum number of cells in x-direction (east)
IMN	15	Integer	1	Minimum column in I-direction to be edited
IMX	16	Integer	30	Maximum column in I-direction to be edited
IPATH	17	Integer	2	Geometry flag 1: real space 2: conformal space
ISIG	18	Integer	3	Vertical zoning flag (conformal space only) 1: log linear distribution 2: constant zoning 3: geometric progression
ITERAN	19	Integer	3	Terrain data source flag 1: read terrain data from tape (unit 8) [8F10.8 format] 2: initialize terrain data from data statement 3: read terrain data from cards [10F8.1 format]
ITMAX	40	Integer	100	Maximum allowable number of iterations

<u>VARIABLE</u>	<u>LOCATION</u>	<u>TYPE</u>	<u>DEFAULT</u>	<u>DEFINITION</u>
ITYLOR	20	Integer	0	Special edit flag 0: no special edit 1: interpolate adjusted field to define wind speed and direction at specified locations within the mesh
IWIND	21	Integer	1	Wind data type flag 1: surface wind data only, input wind speed and direction 2: surface wind data only, input wind components 3: surface wind data and one upper air station, input wind speed and direction 4: surface wind data and one upper air station, input wind components
IYEAR	22	Integer	1	Simulation year
JMAX	24	Integer	30	Maximum number of cells in y-direction (north)
JMN	25	Integer	1	Minimum column in J-direction to be edited
JMX	26	Integer	30	Maximum column in J-direction to be edited
KMAX	27	Integer	15	Maximum number of cells in vertical direction
KMN	28	Integer	1	Minimum row to be edited
KMX	29	Integer	15	Maximum row to be edited
MONTH	30	Integer	1	Month of simulation
MPS	31	Integer	1	Windspeed units flag 0: input is mi/h 1: input is m/sec 2: input is knots

<u>VARIABLE</u>	<u>LOCATION</u>	<u>TYPE</u>	<u>DEFAULT</u>	<u>DEFINITION</u>
NDAYS	32	Integer	1	Number of separate simulations to be performed
NPTS	33	Integer	1	Number of wind observation stations -1: initialization with upper air data only
NSTAT	291	Integer	0	Number of stations where wind speed and wind direction are to be computed for editing purposes. If NSTAT is negative 4 character Hollerith station I.D.'s are to be entered via card input (see Section 4.1)
NUA	345	Integer	2	Number of upper air reporting levels
OMEG	34	Real	-1.0	Over relaxation parameter set to -1.0 in DEFINE, used initially as a flag -1.0: OMEG is calculated >0 : OMEG was entered through cards
ORIGNX ORIGNY	35,36	Real	0.0,0.0	Position of grid origin (m)
QTOP	342	Real	999.0	Wind speed at top of mesh, if QTOP=999.0 wind speed at top of mesh is assumed equal to that at top of boundary layer (m/sec, mi/h, knots)
ZBL	344	Real	200.0	Boundary layer height (AGL) (m)
ZDIST	38	Real	2*[Range of Terrain Heights]	Height of top boundary with respect to minimum terrain altitude (m)
UAMSL	396	Real Array		Array of upper level heights (MSL) corresponding to reported upper level winds (m)
WDR	41	Real Array		Array of observed surface wind direction or V-components (degrees, m/sec, mi/h, or knots)
WDRUA	371	Real Array		Array of observed upper air wind direction or V-components read from lowest level to highest level (degrees, m/sec, mi/h, or knots)

<u>VARIABLE</u>	<u>LOCATION</u>	<u>TYPE</u>	<u>DEFAULT</u>	<u>DEFINITION</u>
WSPD	91	Real Array		Array of observed surface windspeeds or U-components (m/sec, mi/h, or knots)
WSPDUA	346	Real Array		Array of observed upper air wind speeds or U-components read from lowest level to highest level (m/sec, mi/h, or knots)
XO	141	Real Array		Array of X-positions of observed wind velocities (m)
XSTA	292	Real Array		X-locations of each of NSTAT stations (m)
YO	191	Real Array		Array of Y-positions of observed wind velocities (m)
YSTA	317	Real Array		Y-locations of each of NSTAT stations (m)
ZO	241	Real Array		Array of Z-positions (AGL) of observed wind velocities (m)

C.5 SAMPLE CALCULATION

To facilitate familiarization with the code, it is useful to discuss a sample problem. The test case chosen is a 3-D Gaussian Hill in the presence of a westerly wind as shown in Figure C.4. Input conditions must include control flag specifications, zoning requirements, terrain height data, and the initial velocity profile.

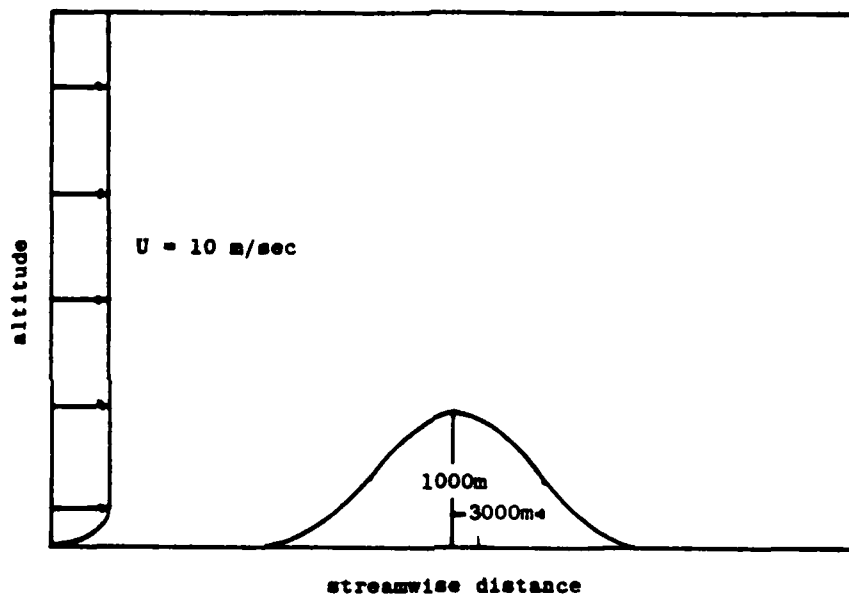


Figure C.4 Simulation Geometry for Gaussian Hill Sample Problem.

The simulation was run in the conformal mode with variable sigma spacing defined by a geometric progression assuming a minimum zone size at the surface equal to 0.013882 and an expansion factor, $\gamma = 1.2$. Horizontal zoning was taken to be 750 m in both the x and y directions. The Gaussian Hill terrain height data follows from

$$z(x,y) = 1000.00 \text{ EXP} - \left[\frac{(x-x_0)^2 + (y-y_0)^2}{(3000)^2} \right] \quad (\text{C.1})$$

where $x_0 = y_0 = 9375.0$. A total of 25 zones was used in both the x and y directions, with 15 zones specified in the vertical. The velocity profile was defined by a 0.14 power-law up to 200 m and was held constant and equal to 10 m/sec above 200 m. The top of the mesh was taken to be 3000 m, and a neutral atmosphere was assumed.

Given these problem specifications and the glossary of input variables, the input deck structure may be defined. Figure C.5 represents the start deck and shows the use of the free-form variable format defined in earlier sections. The values of the terrain height array are given by Eq. (C.1) and are tabulated in Figure C.6. The overall deck structure is shown in Figure C.7.

```

*ZO      $241,200.0
*WSPD    $91,10.0
*WCR     $41,270.0
*JMN     $25.12
*JMX     $26.13
*IMN     $15.1
*IMX     $16.25
*KMN     $28.1
*KMX     $29.13
*IEDIT   $12.1
*DX      $6,750.0
*DY      $7,750.0
*IMAX    $14.25
*JMAX    $24.25
*KMAX    $27.12
*ZDIST   $38,1500.0
*DZMIN   $9.50.0
*OMEG    $34,1.78
*END OF DATA $

```

Figure C.5 Input Deck Structure.

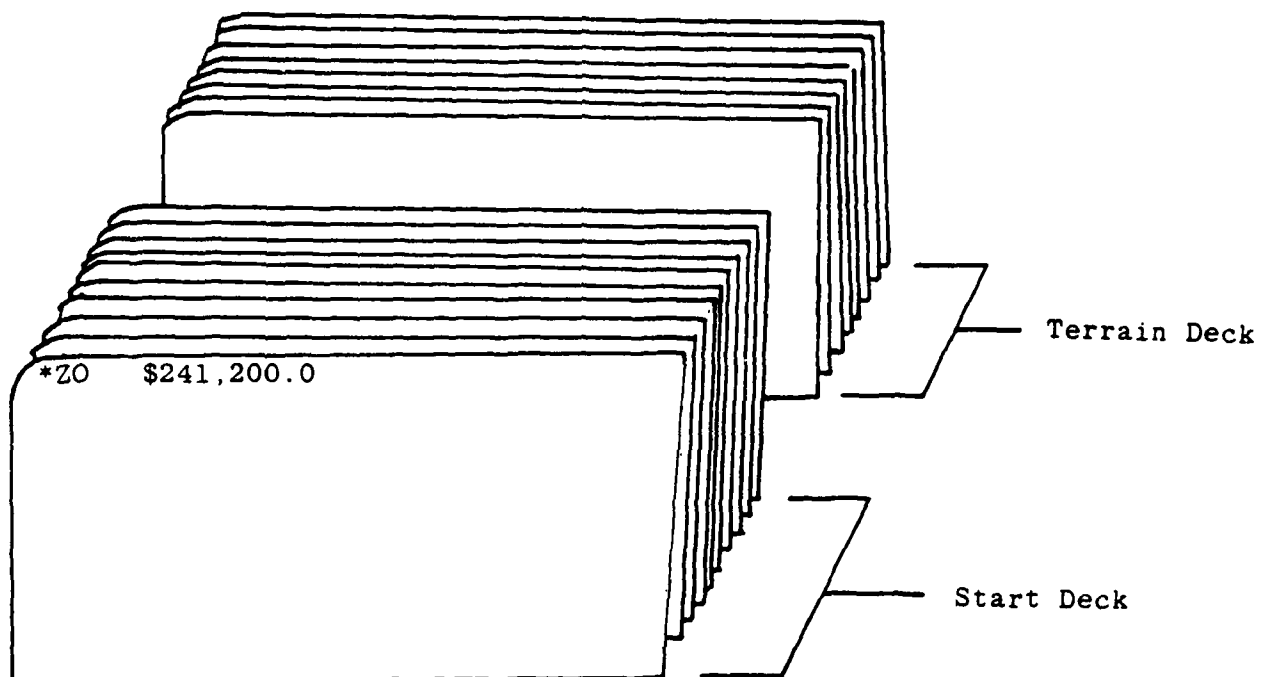


Figure C.7 Sample Problem Deck Structure.

Using the input deck structure shown in Figure C.5 and the terrain data from Figure C.6, VARMET first calculates the finite difference mesh arrays (Figure C.8) and the initial flow profile (Figure C.9). These data are printed in subroutines SETUP and OBSWND, respectively, and are useful in verifying the initial conditions. Given the initial wind field, the velocity adjustment phase is entered. Here the velocity potential field is first calculated. Figure C.10 indicates the iteration by iteration reduction in the maximum potential residual. Once the velocity-potential field is known, adjustments to the initial velocity field are made. The final velocities, potentials, and divergences are then printed in subroutine EDIT. An example of the line-printer output is shown in Figure C.11 and represents only a few columns about the hill peak. Here U,V,W are the velocity potential and DIV the local divergence. This edit is arranged so that field variables are edited from the top of the mesh down. The value 999.0 or 999 indicates that an edit of a variable would be, not applicable.

MESH PARAMETERS

LOCATION OF ORIGIN (METERS)
 ORIGNX= 0. ORIGNY= 0. ORIGNZ= 1.5230E-05
 DX= 7.5000E+02 DY= 7.5000E+02 ZDIST= 3.0000E+03
 MAXIMUM HEIGHT OF TERRAIN (METERS)= 1.0000E+03

X-ARRAY (METERS)

1	3.7500E+02	2	1.1250E+03	3	1.8750E+03	4	2.6250E+03
5	3.3750E+03	6	4.1250E+03	7	4.8750E+03	8	5.6250E+03
9	6.3750E+03	10	7.1250E+03	11	7.8750E+03	12	8.6250E+03
13	9.3750E+03	14	1.0125E+04	15	1.0875E+04	16	1.1625E+04
17	1.2375E+04	18	1.3125E+04	19	1.3875E+04	20	1.4625E+04
21	1.5375E+04	22	1.6125E+04	23	1.6875E+04	24	1.7625E+04
25	1.8375E+04						

Y-ARRAY (METERS)

1	3.7500E+02	2	1.1250E+03	3	1.8750E+03	4	2.6250E+03
5	3.3750E+03	6	4.1250E+03	7	4.8750E+03	8	5.6250E+03
9	6.3750E+03	10	7.1250E+03	11	7.8750E+03	12	8.6250E+03
13	9.3750E+03	14	1.0125E+04	15	1.0875E+04	16	1.1625E+04
17	1.2375E+04	18	1.3125E+04	19	1.3875E+04	20	1.4625E+04
21	1.5375E+04	22	1.6125E+04	23	1.6875E+04	24	1.7625E+04
25	1.8375E+04						

Z-ARRAY (METERS)

1	2.7326E+03	2	2.2425E+03	3	1.8340E+03	4	1.4937E+03
5	1.2100E+03	6	9.7363E+02	7	7.7666E+02	8	6.1251E+02
9	4.7572E+02	10	3.6173E+02	11	2.6673E+02	12	1.8757E+02
13	1.2161E+02	14	6.6634E+01	15	2.0823E+01		

SIGMAF ARRAY

1	8.6325E-06	2	1.7824E-01	3	3.2677E-01	4	4.5054E-01
5	5.5369E-01	6	6.3964E-01	7	7.1127E-01	8	7.7096E-01
9	8.2070E-01	10	8.6215E-01	11	8.9670E-01	12	9.2548E-01
13	9.4947E-01	14	9.6946E-01	15	9.8612E-01	16	1.0000E+00

DSIGMAF ARRAY

1	1.7823E-01	2	1.4853E-01	3	1.2377E-01	4	1.0314E-01
5	8.5954E-02	6	7.1623E-02	7	5.9690E-02	8	4.9742E-02
9	4.1451E-02	10	3.4543E-02	11	2.8786E-02	12	2.3988E-02
13	1.9990E-02	14	1.6658E-02	15	1.3882E-02	16	1.3882E-02

SIGMAC ARRAY

1	8.9125E-02	2	2.5251E-01	3	3.8866E-01	4	5.0212E-01
5	5.9666E-01	6	6.7546E-01	7	7.4111E-01	8	7.9583E-01
9	8.4143E-01	10	8.7942E-01	11	9.1109E-01	12	9.3748E-01
13	9.5946E-01	14	9.7779E-01	15	9.9306E-01		

DSIGMAC ARRAY

1	1.6338E-01	2	1.6338E-01	3	1.3615E-01	4	1.1346E-01
5	9.4549E-02	6	7.8791E-02	7	6.5659E-02	8	5.4716E-02
9	4.5397E-02	10	3.7997E-02	11	3.1664E-02	12	2.6387E-02
13	2.1909E-02	14	1.8324E-02	15	1.5270E-02		

Figure C.8 Mesh Parameters for Gaussian Hill Sample Calculation.

SIGMA	U	V
8.9125E-02	9.9915E+00	7.0296E-07
2.3251E-01	9.9758E+00	1.8900E-06
3.8266E-01	9.9629E+00	2.8763E-06
5.0212E-01	9.9519E+00	3.6963E-06
5.9666E-01	9.9428E+00	4.3783E-06
6.7346E-01	9.9353E+00	4.9456E-06
7.4111E-01	9.9290E+00	5.4177E-06
7.9522E-01	9.9238E+00	5.8107E-06
8.4143E-01	9.9194E+00	6.1378E-06
8.7942E-01	9.9158E+00	6.4102E-06
9.1109E-01	9.9127E+00	6.6371E-06
9.3743E-01	9.9106E+00	6.7964E-06
9.5946E-01	9.9092E+00	6.8963E-06
9.7779E-01	9.9085E+00	6.9296E-06
9.9295E-01	9.9084E+00	6.9661E-06

Figure C.9 Sample Problem Initial Flow Profile.

ITERATION NUMBER=	1	MAXIMUM RESIDUAL=	2.9277E+03
ITERATION NUMBER=	2	MAXIMUM RESIDUAL=	1.1301E+03
ITERATION NUMBER=	3	MAXIMUM RESIDUAL=	7.2749E+02
ITERATION NUMBER=	4	MAXIMUM RESIDUAL=	5.9778E+02
ITERATION NUMBER=	5	MAXIMUM RESIDUAL=	4.5310E+02
ITERATION NUMBER=	6	MAXIMUM RESIDUAL=	3.4207E+02
ITERATION NUMBER=	7	MAXIMUM RESIDUAL=	2.7558E+02
ITERATION NUMBER=	8	MAXIMUM RESIDUAL=	2.2652E+02
ITERATION NUMBER=	9	MAXIMUM RESIDUAL=	1.9634E+02
ITERATION NUMBER=	10	MAXIMUM RESIDUAL=	1.6942E+02
ITERATION NUMBER=	11	MAXIMUM RESIDUAL=	1.4340E+02
ITERATION NUMBER=	12	MAXIMUM RESIDUAL=	1.2144E+02
ITERATION NUMBER=	13	MAXIMUM RESIDUAL=	1.0130E+02
ITERATION NUMBER=	14	MAXIMUM RESIDUAL=	8.3566E+01
ITERATION NUMBER=	15	MAXIMUM RESIDUAL=	6.8235E+01
ITERATION NUMBER=	16	MAXIMUM RESIDUAL=	5.5228E+01
ITERATION NUMBER=	17	MAXIMUM RESIDUAL=	4.4508E+01
.	.	.	.
.	.	.	.
.	.	.	.
ITERATION NUMBER=	84	MAXIMUM RESIDUAL=	2.6144E-02
ITERATION NUMBER=	85	MAXIMUM RESIDUAL=	2.3560E-02
ITERATION NUMBER=	86	MAXIMUM RESIDUAL=	2.1232E-02
ITERATION NUMBER=	87	MAXIMUM RESIDUAL=	1.9134E-02
ITERATION NUMBER=	88	MAXIMUM RESIDUAL=	1.7243E-02
ITERATION NUMBER=	89	MAXIMUM RESIDUAL=	1.5539E-02
ITERATION NUMBER=	90	MAXIMUM RESIDUAL=	1.4003E-02
ITERATION NUMBER=	91	MAXIMUM RESIDUAL=	1.2619E-02
ITERATION NUMBER=	92	MAXIMUM RESIDUAL=	1.1372E-02
ITERATION NUMBER=	93	MAXIMUM RESIDUAL=	1.0242E-02
ITERATION NUMBER=	94	MAXIMUM RESIDUAL=	9.2352E-03
ITERATION CONVERGED			
ITER= 94	RESIDUAL=	9.2352E-03	

Figure C.10 Maximum Residual in Potential Field.

J=	I=	13	I=	14	Y(J)=	9.375E+03	X(I)=	1.012E+04	DX=	7500.00	DY=	7500.00	SICMA	Z	IFLAG
K	N				U	V	W	PHI	DIV						
1	39	1.1201E+01	3.9267E-02	1.4231E-09	9.0729E+02	0.1041E-04	2.7326E+03	8.9125E-02						999	
2	39	1.1251E+01	4.4469E-02	1.5000E-01	9.5780E+02	9.0391E-04	2.2425E+03	2.5251E-01						999	
3	39	1.1343E+01	5.3591E-02	2.9031E-01	1.0393E+03	1.0610E-03	1.8340E+03	3.8856E-01						999	
4	39	1.1462E+01	6.5782E-02	4.2977E-01	1.1398E+03	1.2865E-03	1.4937E+03	5.0212E-01						999	
5	39	1.1596E+01	8.0460E-02	5.7097E-01	1.2511E+03	1.5472E-03	1.2100E+03	5.9666E-01						999	
6	39	1.1737E+01	9.7053E-02	7.1348E-01	1.3671E+03	1.8408E-03	9.7363E+02	6.7546E-01						999	
7	39	1.1878E+01	1.1497E-01	8.5542E-01	1.4829E+03	2.1572E-03	7.7666E+02	7.4111E-01						999	
8	39	1.2016E+01	1.3359E-01	9.9431E-01	1.5952E+03	2.4702E-03	6.1251E+02	7.9503E-01						999	
9	39	1.2147E+01	1.5232E-01	1.1277E+00	1.7012E+03	2.8012E-03	4.7572E+02	8.4143E-01						999	
10	39	1.2268E+01	1.7065E-01	1.2535E+00	1.7995E+03	3.1151E-03	3.6173E+02	8.7942E-01						999	
11	39	1.2378E+01	1.8815E-01	1.3702E+00	1.8890E+03	3.4166E-03	2.6673E+02	9.1109E-01						999	
12	39	1.2479E+01	2.0327E-01	1.4770E+00	1.9694E+03	3.6845E-03	1.8757E+02	9.3748E-01						999	
13	39	1.1906E+01	2.1361E-01	1.5327E+00	2.0389E+03	3.9191E-03	1.2161E+02	9.5946E-01						999	
14	39	1.1309E+01	2.1825E-01	1.5236E+00	2.0965E+03	4.0480E-03	6.6634E+01	9.7779E-01						999	
15	39	1.0083E+01	2.2037E-01	1.4977E+00	2.1422E+03	4.0320E-03	2.0823E+01	9.9306E-01						999	
16	39	9.9900E+02	9.9900E+02	1.5037E+00	2.1868E+03	3.9900E+02	9.9900E+02	1.0000E+00						999	

J=	I=	15	I=	16	Y(J)=	9.375E+03	X(I)=	1.087E+04	DX=	7500.00	DY=	7500.00	SICMA	Z	IFLAG
K	N				U	V	W	PHI	DIV						
1	40	1.0978E+01	6.7422E-02	5.7746E-09	1.6488E+03	1.2935E-03	2.7326E+03	8.9125E-02						999	
2	40	1.1006E+01	7.6210E-02	2.4570E-01	1.7420E+03	1.4331E-03	2.2425E+03	2.5251E-01						999	
3	40	1.1059E+01	9.1358E-02	4.9492E-01	1.8917E+03	1.6711E-03	1.8340E+03	3.8856E-01						999	
4	40	1.1127E+01	1.1119E-01	7.2681E-01	2.0747E+03	1.9766E-03	1.4937E+03	5.0212E-01						999	
5	40	1.1199E+01	1.3450E-01	9.5597E-01	2.2753E+03	2.3273E-03	1.2100E+03	5.9666E-01						999	
6	40	1.1271E+01	1.6016E-01	1.1811E+00	2.4017E+03	2.7039E-03	9.7363E+02	6.7546E-01						999	
7	40	1.1339E+01	1.8710E-01	1.3991E+00	2.6830E+03	3.0896E-03	7.7666E+02	7.4111E-01						999	
8	40	1.1401E+01	2.1434E-01	1.6064E+00	2.8801E+03	3.4702E-03	6.1251E+02	7.9503E-01						999	
9	40	1.1453E+01	2.4103E-01	1.8003E+00	3.0620E+03	3.8348E-03	4.7572E+02	8.4143E-01						999	
10	40	1.1503E+01	2.6652E-01	1.9785E+00	3.2284E+03	4.1737E-03	3.6173E+02	8.7942E-01						999	
11	40	1.1543E+01	2.9033E-01	2.1399E+00	3.3784E+03	4.5004E-03	2.6673E+02	9.1109E-01						999	
12	40	1.1582E+01	3.1048E-01	2.2851E+00	3.5118E+03	4.8393E-03	1.8757E+02	9.3748E-01						999	
13	40	1.1015E+01	3.2386E-01	2.3476E+00	3.6260E+03	5.1549E-03	1.2161E+02	9.5946E-01						999	
14	40	1.0345E+01	3.2939E-01	2.3071E+00	3.7195E+03	5.3955E-03	6.6634E+01	9.7779E-01						999	
15	40	9.1030E+00	3.3136E-01	2.1639E+00	3.7924E+03	5.1567E-03	2.0823E+01	9.9306E-01						999	
16	40	9.9900E+02	9.9900E+02	2.2448E+00	3.8633E+03	9.9900E+02	9.9900E+02	1.0000E+00						999	

J=	I=	16	I=	16	Y(J)=	9.375E+03	X(I)=	1.162E+04	DX=	7500.00	DY=	7500.00	SICMA	Z	IFLAG
K	N				U	V	W	PHI	DIV						
1	41	1.0630E+01	8.0370E-02	8.2313E-09	2.1301E+03	1.3823E-03	2.7326E+03	8.9125E-02						999	
2	41	1.0624E+01	9.0303E-02	2.9936E-01	2.2490E+03	1.5110E-03	2.2425E+03	2.5251E-01						999	

Figure C.11 Edit of Flow Field for Columns Adjacent to Hill Peak.